UNIVERSITÄT HAMBURG

Universität Hamburg
DER FORSCHUNG | DER LEHRE | DER BILDUNG

# Analyzing and Implementing the Local Analytic Sector Subtraction Scheme for Handling Infrared Singularities at NNLO in QCD

DISSERTATION

*zur Erlangung des Doktorgrades*
*an der Fakultät für Mathematik,*
*Informatik und Naturwisschenschaften*

Fachbereich Physik
der Universität Hamburg

*vorgelegt von:*
Bakar CHARGEISHVILI
aus Tiflis, Georgien

July 8, 2024

| | |
|---|---|
| Gutachter der Dissertation: | Prof. Dr. Sven-Olaf Moch<br>Prof. Dr. Bernd Kniehl |
| Zusammensetzung der Prüfungskommission: | Dr. Adam Kardos<br>Prof. Dr. Bernd Kniehl<br>Prof. Dr. Sven-Olaf Moch<br>Prof. Dr. Günter Sigl<br>Prof. Dr. Zoltán Trócsányi |
| Vorsitzende/r der Prüfungskommission: | Prof. Dr. Günter Sigl |
| Datum der Disputation: | 03.07.2024 |
| Vorsitzender Fach-Promotionsausschusses PHYSIK: | Prof. Dr. Markus Drescher |
| Leiter des Fachbereichs PHYSIK: | Prof. Dr. Wolfgang J. Parak |
| Dekan der Fakultät MIN: | Prof. Dr.-Ing. Norbert Ritter |

UNIVERSITÄT HAMBURG

# *Zusammenfassung*

**Analyzing and Implementing the Local Analytic Sector Subtraction Scheme for Handling Infrared Singularities at NNLO in QCD**

abgelegt von Bakar CHARGEISHVILI

Diese Arbeit analysiert und implementiert das Local Analytic Sector Subtraction (LASS) Schema zur Behandlung von Infrarot-Singularitäten in Berechnungen der nächst-nächst-führenden Ordnung (NNLO) in der perturbativen Quantenchromodynamik (QCD). Die LASS-Methode bietet ein vollständig lokales und analytisches Verfahren zur Subtraktion Infrarot-Divergenzen in Beiträgen reeller Strahlung durch Aufteilung des Phasenraums in Sektoren, die einen minimalen Satz von Singularitäten enthalten. Die Schlüsselaspekte des Schemas, einschließlich der Konstruktion von Sektorfunktionen, Parametrisierung singulärer Grenzwerte, Herleitung von Subtraktionsgegenterm und analytische Integrationstechniken, werden eingehend untersucht. Ein neuartiger Ansatz unter Verwendung eines Satisfiability Modulo Theories (SMT)-Solvers und eines symbolischen Manipulationsprogramms wird entwickelt, um die für die Farbzerlegung von QCD-Amplituden erforderlichen Farbbasen automatisch zu generieren. Das vollständige LASS-Framework wird numerisch implementiert, wobei der Prozess der Elektron-Positron-Annihilation in drei Jets als Proof-of-Concept im Fokus steht. Das Grenzverhalten der Subtraktionsterme, die endlichen Reste des Doppel-Virtuell-Beitrags und die Auswirkung des technischen Cut-Parameters werden sorgfältig untersucht. Differentielle Wirkungsquerschnitte für verschiedene Ereignisformobservablen werden berechnet und zeigen die Stabilität und Effizienz der Methode. Diese Arbeit legt den Grundstein für die Entwicklung eines vollautomatischen Tools für NNLO-Berechnungen in QCD mit dem LASS-Schema.

# *Abstract*

This thesis analyzes and implements the Local Analytic Sector Subtraction (LASS) scheme for handling infrared singularities in next-to-next-to-leading order (NNLO) calculations in perturbative Quantum Chromodynamics (QCD). The LASS method provides a fully local and analytic procedure for subtracting infrared divergences in real-radiation contributions by partitioning the phase space into sectors containing a minimal set of singularities. The key aspects of the scheme, including the construction of sector functions, parametrization of singular limits, derivation of subtraction counterterms, and analytic integration techniques, are examined in detail. A novel approach combining a satisfiability modulo theories (SMT) solver and symbolic manipulation program is developed to automatically generate the color bases required for color decomposition of QCD amplitudes. The complete LASS framework is numerically implemented, with a focus on the process of electron-positron annihilation into three jets as a proof-of-concept. The limiting behavior of the subtraction terms, the finite remainders of the double-virtual contribution, and the effect of the technical cut parameter are meticulously investigated. Differential cross sections for several event shape observables are computed, showcasing the stability and efficiency of the method. This work lays the foundation for the development of a fully automated tool for NNLO calculations in QCD using the LASS scheme.

*"At dawn, when you have trouble getting out of bed, tell yourself: I have to go to work — as a human being. What do I have to complain of, if I'm going to do what I was born for — the things I was brought into the world to do? Or is this what I was created for? To huddle under the blankets and stay warm?"*

- Marcus Aurelius

*"Der Mensch kann tun was er will; er kann aber nicht wollen was er will.*
*(Man can do what he wills, but he cannot will what he wills.) "*

- Arthur Schopenhauer

# Contents

# Chapter 1

# Introduction

The pursuit of precision in theoretical predictions is one of the cornerstones of modern particle physics. As experimental measurements at particle accelerators like the Large Hadron Collider (LHC) become increasingly accurate, it is essential that theoretical calculations keep pace to allow for stringent tests of the Standard Model and the potential discovery of new physics. The required accuracy standard for fixed-order predictions is rapidly shifting towards the next–to–next–to–leading order (NNLO) in QCD. For a number of simple processes, state-of-the-art theoretical calculations have already reached the third perturbative order ($N^3LO$) in the strong coupling [1]. Entering of a new era of high-luminosity experiments is going to cause higher general demand on NNLO calculations.

One of the key challenges in performing high-precision calculations in Quantum Chromodynamics (QCD) is the handling of infrared divergences that arise from the emission of soft and collinear partons. Thus, the correct treatment of these singularities gain increasing prevalence.

The problem manifests itself already at next–to–leading order (NLO). At this level, the problem of handling infrared singularities has been solved by several general and efficient algorithms, such as phase-space slicing methods [2, 3] and subtraction schemes [4–8]. Most of these methods are implemented in widely-used multi-purpose NLO event generators [9–14].

At NNLO handling infrared divergences becomes substantially more intricate, both conceptually and practically. This increased complexity arises from various factors, including the rapid proliferation of overlapping singular regions, the necessity to consider strongly-ordered infrared limits, and the interplay between virtual poles

and phase-space singularities. Nevertheless, in recent years, significant advancements have been achieved in developing efficient methods to properly handle soft and collinear singularities at NNLO level as well.

The existing approaches to NNLO subtraction can be broadly categorized into *slicing techniques*, *non-local subtraction schemes*, and *local subtraction methods*.

The slicing methods work by separating the real radiation phase space into regions where the matrix elements are approximated (singular regions) and regions where they are evaluated exactly (non-singular regions). The approximated matrix elements in the singular regions are integrated analytically, while the non-singular regions are integrated numerically. Examples of slicing methods include those of Refs. [15, 16].

Non-local subtraction schemes define counterterms that are not strictly local in phase space, but rather factorise the real radiation matrix elements into simpler pieces that are then subtracted and integrated analytically. A notable example is the N-jettiness subtraction of Refs. [17, 18].

Local subtraction schemes construct local counterterms in all singular regions of phase space. These counterterms are then subtracted from the real radiation matrix elements, and their integrals added back analytically to cancel all infrared poles. Different approaches vary in how the local counterterms are constructed and organized. The antenna subtraction of Refs. [19, 20] builds counterterms from antenna functions. The residue-subtraction scheme of Ref. [21] constructs counterterms from residues of the matrix elements in various singular limits. Notably, it was possible to calculate the NNLO correction to hadronic production of the three jets using this method [22].

The sector decomposition methods, like that of Refs. [23–25], partition phase space into sectors containing different singular limits. Counterterms are then built separately in each sector by asymptotically expanding the matrix elements.

The nested soft-collinear subtraction of Ref. [26] uses a nested sequence of subtractions, first constructing soft counterterms, then adding collinear counterterms inside the soft regions.

While powerful, each of these methods faces increasing complexity when dealing

with complicated processes, either at the level of the analytic integration of counterterms or at the level of a numeric implementation.

Among the methods described above, recently in the category of local subtraction schemes the ***L**ocal **A**nalytic **S**ector **S**ubtraction* (LASS) has emerged as a promising approach for performing NNLO calculations in a numerically stable and efficient manner [27–29].

The LASS scheme, which currently treats only massless final-state colored particles, aims to optimize the calculation structure at all stages while preserving the full locality of the counterterms and complete universality for all hadronic final states. It provides a completely analytic expression for all required counterterms and their phase-space integrals, including finite contributions. The key advantages of this approach are:

1. It exploits the flexibility in defining local infrared counterterms by partitioning the phase space into sectors, each containing only a minimal set of soft and collinear singularities.

2. It employs flexible phase-space parametrizations that can be varied sector-by-sector and for each contribution to the local counterterms, leading to a minimal and simple set of phase-space integrals to be evaluated.

3. It yields a completely analytic subtraction formula that can be implemented within any existing numerical framework, limited only by the available computational resources and multi-loop matrix elements.

Overall, the LASS scheme presents a highly versatile and efficient framework for NNLO calculations by leveraging the key advantages outlined above. While a public implementation is not currently available, the analytic techniques and tailored phase-space parametrizations employed by this scheme have significant potential for efficient implementations. Consequently, the LASS scheme promises to drive further advancements in the field of perturbative QCD calculations, allowing for more accurate and comprehensive theoretical predictions for a wide range of hadronic final states.

In this thesis, we will analyze the theoretical foundations of the LASS method and discuss the details of its implementation. We will explore the construction of the

sector functions, the derivation of the subtraction counterterms, and the analytic integration techniques employed. Furthermore, we will discuss the application of the method to the procoess of the leptonic production of three jets and present numerical results showcasing its performance.

The thesis is organized as follows: In Chapter 2, we review the basic concepts of perturbative QCD and the challenges posed by infrared divergences. Chapter 3 introduces the Local Analytic Sector Subtraction method and its theoretical underpinnings. In Chapter 4, we provide a step-by-step guide how to perform the integration of the subtraction terms and describe important cross-checks used for the validation. Chapter 5 discusses the calculation of the color correlators and describes the novel method to derive the color basis automatically. In Chapter 6 we discuss the details of the numerical implementation. Chapter 7 presents numerical results for the leptonic production of the 3 jets, showcasing the effectiveness of the method. Finally, in Chapter 8, we conclude with a summary of our findings and an outlook on future developments and applications of the local analytic sector subtraction method.

# Chapter 2

# Theoretical background

## 2.1 Perturbative QCD

Quantum chromodynamics (QCD) is the theory that governs the interactions between quarks and gluons, the fundamental particles that make up hadrons such as protons and neutrons. This interaction is termed "strong" because at short distances, it is the most powerful of the four fundamental forces in nature. However, the actual strength of this interaction varies with the distance between the participating particles, a phenomenon known as asymptotic freedom.

In addition to the usual quantum numbers, quarks possess an intrinsic property called "color," which gives rise to the term "chromodynamics" in the theory's name. A comprehensive review of QCD is beyond the scope of this thesis, but interested readers are encouraged to consult the following literature: Ref. [30] for a historical perspective, and Refs. [31–34] for more in-depth discussions.

In the following sections, we will briefly summarize the topics relevant to the remainder of this thesis. We begin our review by constructing the Lagrangian of QCD. Quarks are Dirac fermions that come in six different flavors, and in the Standard Model (SM), they are grouped into three left-handed $\mathrm{SU}(2)$ doublets:

$$\begin{pmatrix} u \\ d \end{pmatrix}_L \qquad \begin{pmatrix} c \\ s \end{pmatrix}_L \qquad \begin{pmatrix} t \\ b \end{pmatrix}_L \tag{2.1}$$

In addition there are six right-handed $\mathrm{SU}(2)$ singlets. Quarks exhibit the same $\mathrm{SU}_L(2) \times U_Y(1)$ symmetry as leptons with respect to the electroweak interaction. One of the characteristics of quarks is that each quark flavor eigenstate is a unitary

mixing of the mass eigenstates. This is not the case for the leptons in the SM, where neutrinos are assumed to be massless. However, in the past years various neutrino oscillation experiments [35] have proved that neutrinos have non-zero masses, which means that mixing is possible in the lepton sector as well [36]. A truly distinctive feature of the quark sector is the underlying color symmetry. In the SM each quark can have three different colors and the color interaction is mediated by eight gauge bosons called gluons (g). Mathematically this means that quarks belong to the fundamental representation of the SU(3) color-group and the gluons to the adjoint one.

The Lagrangian which embodies all these features is given as follows:

$$\mathcal{L}_{\text{cl}} = \sum_{f}^{N_f} \overline{\psi}_f \left( i\gamma_\mu D^\mu - m_f \right) \psi_f - \frac{1}{4} F^a_{\mu\nu} F^{a\mu\nu} \,, \tag{2.2}$$

where the $\psi_f$ is a fermionic field of flavor $f$ and mass $m_f$, interacting with the gluon fields $A^a_\mu$, which are currently hidden in the definitions of the covariant derivative:

$$D_\mu = \partial_\mu - igA^a_\mu t^a \tag{2.3}$$

and the field strength tensor:

$$F^a_{\mu\nu} = \partial_\mu A^a_\nu - \partial_\nu A^a_\mu + g f^{abc} A^b_\mu A^c_\nu \tag{2.4}$$

and $N_f$ is the number of flavors.

In Eqs. (2.3) and (2.4) $g$ is the strong coupling, $t^a$ are generators of SU($N$) ($N = 3$ for SM QCD), connected with Gell-Mann matrices in the following way:

$$t^a \equiv \frac{\lambda^a}{2}, \qquad \text{Tr}[t^a \cdot t^b] = T_R \delta^{ab} \,, \tag{2.5}$$

with a normalization constant $T_R$, the value of which is typically chosen as $\frac{1}{2}$. In Eq. (2.4) $f^{abc}$ are structure constants, defining the Lie algebra of SU($N$):

$$[t^a, t^b] = i f^{abc} t^c \,. \tag{2.6}$$

The quadratic Casimir operator $C_r$ is given as ($r$ stands either for the fundamental or for the adjoint representation):

$$t_r^a t_r^a = C_r \mathbb{1}_{D_r \times D_r}\,, \tag{2.7}$$

where $D_r$ is the dimension of the representation. It is possible to re-express the Casimir operator in terms of $N_c$. One gets the following values for the fundamental and adjoint representations:

$$C_F = \frac{N_c^2 - 1}{2N_c}, \qquad C_A = N_c\,. \tag{2.8}$$

For the standard QCD ($N_c = 3$) we get:

$$C_F = \frac{4}{3}, \qquad C_A = 3\,. \tag{2.9}$$

The Lagrangian in Equation (2.2) is constructed in such a way that it is locally invariant under Lorentz transformations and SU($N_c$) transformations. While this property is necessary to properly describe the symmetries of the SM, it leads to issues during canonical quantization due to the large degeneracy between different sets of gluon configurations.

This problem can be addressed by introducing a gauge-fixing term to the Lagrangian:

$$\mathcal{L}_{GF} = -\frac{1}{2\xi}\left(\partial^\mu A_\mu^a\right)\left(\partial^\nu A_\nu^a\right). \tag{2.10}$$

The choice of the gauge parameter $\xi$ is arbitrary, as it only affects the overall normalization and has no influence on physical quantities. A common choice is $\xi = 1$, known as the Feynman gauge, as it often simplifies calculations. Another popular choice is the axial gauge: $n \cdot A = 0$, where $n$ is a Lorentz 4-vector. This can be further restricted, for example, to the light-cone gauge by setting $n^2 = 0$.

After fixing the covariant gauge, it is generally necessary to include the contribution from Faddeev-Popov ghost fields $\chi^a$ [37]:

$$\mathcal{L}_{FP} = g f^{abc} \overline{\chi}^a \partial^\mu \left(A_\mu^c \chi^b\right) - \overline{\chi}^a \partial^\mu \partial_\mu \chi^a. \tag{2.11}$$

The purpose of these ghost fields is to eliminate non-physical degrees of freedom remaining after gauge fixing and to restore the unitarity of scattering amplitudes. If working in a physical gauge, there is no need to include ghost contributions, as the extra degrees of freedom are automatically removed. In the path integral formulation of quantum field theory, the ghost fields appear naturally, eliminating the need for manual modification of the Lagrangian [38].

Combining all components, we obtain the following expression for the QCD Lagrangian in the general covariant gauge:

$$\begin{aligned}\mathcal{L}_{\mathrm{QCD}} = &\sum_{f}^{N_f} \overline{\psi}_f \left(i\gamma_\mu D^\mu - m_f\right) \psi_f - \frac{1}{4} F^a_{\mu\nu} F^{a\mu\nu} \\ &- \frac{1}{2\xi}\left(\partial^\mu A^a_\mu\right)\left(\partial^\nu A^a_\nu\right) + g f^{abc} \overline{\chi}^a \partial^\mu \left(A^c_\mu \chi^b\right) - \overline{\chi}^a \partial^\mu \partial_\mu \chi^a. \end{aligned} \tag{2.12}$$

Notice that, because of the non-abelian character of the SU(3) group Eq. (2.12) the term $F^a_{\mu\nu} F^{a\mu\nu}$ contains three and four different gluon fields interacting with each other. This kind of self-interaction is another distinctive feature of QCD.

It is important to note that after adding the ghost fields to the original Lagrangian ($\mathcal{L}_{\mathrm{cl}}$), it loses the property of invariance with respect to local gauge transformations. This is a significant issue because the proof of renormalizability in QCD relies on gauge symmetry.

However, this situation can be resolved by recognizing that the full $\mathcal{L}_{\mathrm{QCD}}$ is invariant under the more extended BRST (Becchi-Rouet-Stora-Tyutin) transformations [38–40]. From the BRST symmetry, it is possible to show that QCD amplitudes satisfy generalized Ward-Takahashi (Slavnov-Taylor) identities [41, 42], which guarantees the renormalizability of the theory.

Once the Lagrangian is known, it becomes possible to calculate the amplitudes of different scattering processes. These scattering amplitudes are defined in terms of the S-matrix [31, 38], which can be reduced to the n-particle Green function using the LSZ (Lehmann-Symanzik-Zimmermann) reduction formula [43]. Although it is possible to formally write the exact expression for the Green function, the actual evaluation of it for a Lagrangian like the one in Eq. (2.12) is very challenging.

Therefore, an approximative method for the calculation is necessary. In this thesis, we will employ the perturbative approach to calculate physical quantities in QCD.

Perturbation theory takes advantage of the smallness of the interaction terms, making it possible to express everything as a power series and work with fixed-order accuracy. In the case of QCD, we use the fact that the strong coupling is small and treat it as an expansion parameter. Mathematically, this means that the Lagrangian from Eq. (2.12) should be separated into two parts:

$$\mathcal{L}_{\mathrm{QCD}} = \mathcal{L}_0 + \mathcal{L}_{\mathrm{I}}, \tag{2.13}$$

where $\mathcal{L}_0$ contains only the free fields and $\mathcal{L}_{\mathrm{I}}$ contains the interaction part. This makes it possible to associate the processes with appropriate Feynman diagrams and by employing the Feynman rules of QCD calculate the amplitudes for various processes with the desired fixed-order accuracy. The Feynman rules are summarized in Fig. 2.1.

In this way, the cross-section of a typical process in QCD can be written as follows:

$$\sigma = \sigma^{\mathrm{LO}} + \alpha_s \sigma^{\mathrm{NLO}} + \alpha_s^2 \sigma^{\mathrm{NNLO}} + \dots, \tag{2.14}$$

where LO represents the leading order contribution and $\alpha_s$ is related to the strong coupling $g$ in the following way:

$$\alpha_s = \frac{g^2}{(4\pi)}. \tag{2.15}$$

The important assumption, on which expansions like the one Eq. (2.14) rely, is that each correction becomes smaller with the increasing order of the calculation. On the one hand, this is guaranteed by the smallness of the parameter $\alpha_s$, on the other hand, however, if the $\sigma^{(\mathrm{N})\dots\mathrm{LO}}$ contains a factorially growing number of Feynman diagrams, so that the predictive power of the perturbation theory might be in danger.

Another issue with the fixed-order calculation is the problem of infinities which appear in the high-order calculations. We will tackle with problem in the next subsection.

Vertex factors:

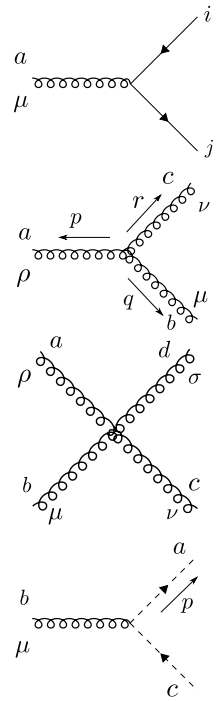


$$ig_s\gamma_\mu t^a_{ji}$$

$$-g_s f^{abc}\left[(p-q)_\nu g_{\rho\mu} + (q-r)_\rho g_{\mu\nu} + (r-p)_\mu g_{\nu\rho}\right]$$

$$\begin{aligned}
&-ig_s^2 f^{abe} f^{cde}\left(g_{\rho\nu}g_{\mu\sigma} - g_{\rho\sigma}g_{\mu\nu}\right)\\
&-ig_s^2 f^{ace} f^{bde}\left(g_{\rho\mu}g_{\nu\sigma} - g_{\rho\sigma}g_{\mu\nu}\right)\\
&-ig_s^2 f^{ade} f^{cbe}\left(g_{\rho\nu}g_{\mu\sigma} - g_{\rho\mu}g_{\sigma\nu}\right)
\end{aligned}$$

$$g_s f^{abc} p_\mu$$

Propagators:

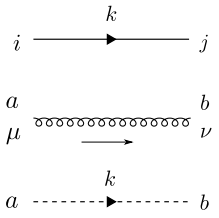


$$i\delta_{ij}\frac{(\not{k}+m)}{k^2-m^2+i\epsilon}$$

$$\frac{-i\delta_{ab}}{k^2+i\epsilon}\left[g_{\mu\nu} - (1-\xi)\frac{k_\mu k_\nu}{k^2}\right] \qquad \xi = \begin{cases}1, \text{ Feynman gauge}\\ 0, \text{ Landau gauge}\end{cases}$$

$$\frac{-i\delta_{ab}}{k^2+i\epsilon}$$

FIGURE 2.1: Feynman rules for QCD, collected from [31].

### 2.1.1 Regularization and renormalization

When calculating scattering matrices at the lowest order, finite results are obtained. As we go higher in accuracy, one has to consider virtual corrections, usually associated with numerous loops and the real corrections (emission from the initial or final state particles). To account for these terms correctly, one has to sum and integrate over intermediate states. If we express the integration in terms of the energy variable, we can encounter two types of infinities:

- One type is coming from the **low energy** limit and these infinities are called **infrared (IR)** divergences.

- The other source is the **high energy** limit, designated as **ultraviolet (UV)** divergences.

If not dealt with properly these singularities can spoil the perturbative calculations. Hence, one needs to develop some technique for properly treating them. In perturbative QFT, this is achieved by shifting the infinities from the physical quantities in the nonphysical parameters (ones which are not measurable), which the Lagrangian contains. This is accomplished in two steps: *Regularization* and *Renormalization*, which solve the problem of UV divergences. Below we outline the basic strategy and basic steps involved in each of them.

The purpose of the regularization is to localize the divergences by introducing some kind of regulator. Throughout the years, there have been numerous different schemes developed. The one which we are going to use is the *dimensional regularization* [44]. The main advantage of this scheme is that it preserves Lorentz and gauge invariance. The idea of the dimensional regularization is to change the dimensionality of the integration from a typical three+one space-time to some general $D$ dimension: $\mathrm{d}^4\ell \to \mathrm{d}^D\ell$. Because the action is by definition dimensionless,

$$S = \int \mathrm{d}^D x \mathcal{L} \qquad \Rightarrow \qquad [\mathcal{L}] = D$$

to preserve the dimension of the action, we have to introduce a new scale $\mu$, with mass dimension $[\mu] = 1$ and replace the coupling in the following way:

$$g \to \mu^{(4-D)/2} g$$

A common parametrization for $D$ is like this: $D = 4 - 2\epsilon$. Then $\epsilon$ effectively becomes a regulator of the singularities. The type of the singularities can be deduced by analyzing the source or the operation after which they appear in the results. However, there is an easier and purely mathematical method for this purpose: based on the definition of UV and IR divergences given above:

1. If for $\epsilon < 0$ the expression diverges, then it has an UV divergence
2. If for $\epsilon > 0$ the expression diverges, then it has an IR divergence

Once the expressions have been regularized, it is time to shift the infinite contributions from the measurable quantities to the nonphysical ones. This can be achieved

by adding counterterm contributions to the original Lagrangian. The "bare" Lagrangian is connected with the renormalized one in the following way:

$$\mathcal{L}(A_0, \psi_0, \chi_0, m_0, g_0\mu^\epsilon) = \mathcal{L}(A, \psi, \chi, m, g\mu^\epsilon) + \mathcal{L}_c(A, \psi, \chi, m, g\mu^\epsilon), \tag{2.16}$$

where $\mathcal{L}_c$ denotes the counterterm Lagrangian and the bare and renormalized parameters are related according to the following relations:

$$A^\mu = Z_3^{-\frac{1}{2}} A_0^\mu, \quad \psi = Z_2^{-\frac{1}{2}} \psi_0, \quad \chi = \tilde{Z}_3^{-\frac{1}{2}} \chi_0, \quad m = Z_m^{-1} m_0, \quad \xi = Z_3^{-1} \xi_0 \tag{2.17}$$

$$g_0 = g\mu^\epsilon \frac{Z_1}{Z_3^{\frac{3}{2}}} = g\mu^\epsilon \frac{\tilde{Z}_1}{\tilde{Z}_3 Z_3^{\frac{1}{2}}} = g\mu^\epsilon \frac{Z_1^F}{Z_2} = g\mu^\epsilon \frac{Z_4^{\frac{1}{2}}}{Z_3} = g\mu^\epsilon Z_g, \tag{2.18}$$

where the $Z_3$, $Z_1^F$, $\tilde{Z}_1$, $Z_4$ are 3-gluon vertex, quark-gluon-vertex, ghost-gluon-vertex and four gluon vertex counterterms. The detailed description of the method for their determination can be found in [31, 32, 38]. Each counterterm can be expanded in a power series of $\epsilon$. The expansion coefficients are chosen in a way that poles are removed from the physical quantities. The scheme, where only the poles are being absorbed in the counterterms is called a minimal subtraction (MS), if common constant factors, like $\ln(4\pi)$ and $\gamma_E$ are being absorbed as well, then such a scheme is called $\overline{\text{MS}}$.

One can represent the counterterms by means of Feynman diagrams. This is possible if we plug Eqs. (2.17) and (2.18) in the original QCD Lagrangian and observe the structure:

$$\begin{aligned}
\mathcal{L}_c = & -\frac{1}{4}(Z_3 - 1)\left(\partial_\mu A_\nu - \partial_\nu A_\mu\right)^2 + i(Z_2 - 1)\,\overline{\psi}\partial\!\!\!/\psi \\
& - (Z_2 Z_m - 1)\,\overline{\psi} m \psi + \left(\tilde{Z}_3 - 1\right)\partial_\mu \chi^\dagger \partial^\mu \chi \\
& + \frac{g}{2}\mu^\epsilon (Z_1 - 1) f^{abc}\left(\partial_\mu A_\nu^a - \partial_\nu A_\mu^a\right) A_b^\mu A_c^\nu + \left(\tilde{Z}_1 - 1\right) i g \mu^\epsilon \partial_\mu \chi^\dagger \mathcal{A}^\mu \chi \\
& - \left(Z_1^F - 1\right) g\mu^\epsilon \overline{\psi} \mathcal{A}^\mu \psi - \frac{g^2}{4}\mu^{2\epsilon}(Z_4 - 1) f^{abc} f^{ade} A_b^\mu A_c^\nu A_d^\mu A_e^\nu.
\end{aligned} \tag{2.19}$$

The Feynman rules can be readily determined from the expression above. Thus, for every process it is possible to generate corresponding counterterm diagrams, which

upon addition with the normal contribution will eliminate the UV divergences. Notice, that in Eq. (2.19) not all constants are independent. This would lead us to the inconsistent renormalization theory. In fact the aforementioned Slavnov-Taylor identities guarantee that:

$$\frac{Z_1}{Z_3} = \frac{\tilde{Z}_1}{\tilde{Z}_3} = \frac{Z_1^F}{Z_2} = \frac{Z_4}{Z_1}\,, \tag{2.20}$$

compare this with the simple Ward identity for QED $Z_1^F = Z_2$.

With these techniques at hand, we are ready to discuss the phenomenon of the running coupling, which was advertised earlier and which is of crucial importance for explaining numerous observations in QCD.

The running coupling, denoted by $\alpha(\mu)$, is a function of the energy scale $\mu$, which represents the energy or momentum transfer in a given process. The dependence of the constant on the energy scale is governed by the renormalization group equation:

$$\mu \frac{d\alpha(\mu)}{d\mu} = \beta(\alpha(\mu))\,. \tag{2.21}$$

Here, $\beta(\alpha(\mu))$ is the beta function, which describes the evolution of the coupling with respect to the energy scale. The beta function can be expressed as a perturbative series in powers of the coupling:

$$\beta(\alpha(\mu)) = -\sum_{n=0}^{\infty} \beta_n \alpha^{n+2}(\mu)\,. \tag{2.22}$$

The coefficients $\beta_n$ are determined by the specific theory and particle content. For example, in QCD, the first two coefficients are:

$$\beta_0 = \frac{11N_c - 2N_f}{12\pi} \tag{2.23}$$

$$\beta_1 = \frac{17N_c^2 - 5N_cN_f - 3C_FN_f}{24\pi^2} \tag{2.24}$$

where $N_c$ is the number of colors, $n_f$ is the number of active quark flavors, and $C_F$ is a group theory factor. Integrating the renormalization group equation, one can obtain an expression for the running coupling at a given energy scale $\mu$ in terms of a reference scale $\mu_0$ and the coupling at that scale, $\alpha(\mu_0)$.

Graphically the running coupling is shown in Figure 2.2.

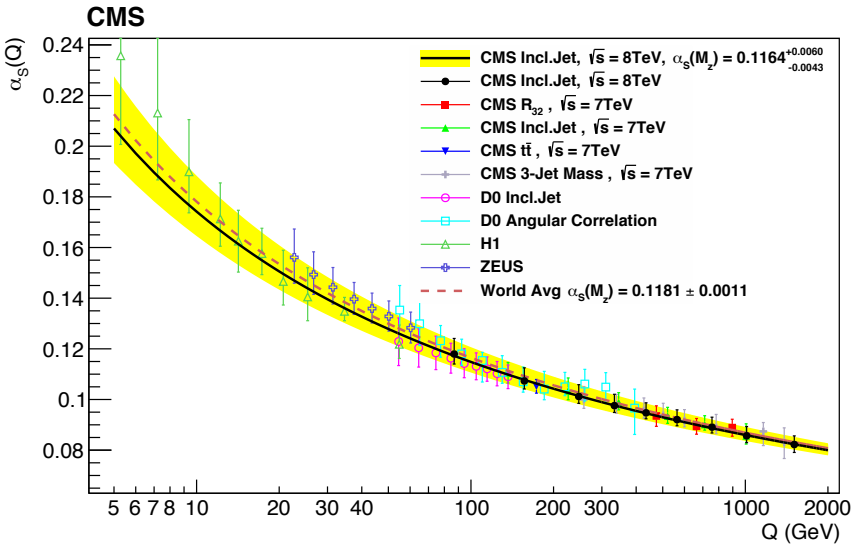


FIGURE 2.2: The running coupling $\alpha_s$ as a function of scale $Q$, taken from [45].

This behavior is called asymptotic freedom [46] and it plays the central role for explaining numerous QCD phenomena. One of them is a concept of hadrons and the parton model, which we are going to review in the next subsection.

### 2.1.2 Parton model

The parton model is a theoretical framework that describes hadrons, such as protons, as composed of point-like constituents called partons, which include quarks and gluons. This model plays a crucial role in understanding the structure of hadrons and the interactions between them in high-energy collisions. To illustrate the key concepts of the parton model, we will focus on the deep-inelastic scattering (DIS) process, where an electron scatters off a proton target, denoted as:

$$H(P) + e(k) \to e(k') + X(K)\,. \tag{2.25}$$

Here, $H$ represents the initial-state hadron (proton), $X$ denotes the collection of produced hadrons, and $k$, $k'$, $P$, and $K$ are the respective four-momenta of the particles. This summary is based on references [47–49]. To characterize the DIS process we

introduce the following set of invariants:

$$\begin{aligned} Q^2 &\equiv -q^2 \equiv -\left(k-k'\right)^2 \\ y &\equiv \frac{P\cdot q}{P\cdot k}; \quad 0 \leq y \leq 1 \\ x &\equiv x_{Bj} = \frac{Q^2}{2P\cdot q} = \frac{Q^2}{(P+q)^2+Q^2}; \quad 0 \leq x \leq 1 \end{aligned}$$

$x_{Bj}$ refers to the *Bjorken scaling variable* and one can interpret it as a longitudinal momentum fraction of the incoming parton at LO.

The cross-section of (2.25) can be represented as:

$$\mathrm{d}\sigma = \frac{\mathrm{d}^3\vec{k}'}{k'} \frac{L^{\mu\nu}\left(k,k'\right) W_{\mu\nu}(P,q)}{2sQ^4}, \tag{2.26}$$

where $L^{\mu\nu}(k,k')$ is a lepton tensor associated with the lepton vertex and it can be easily calculated using the Feynman rules:

$$L^{\mu\nu}(k,k') = \frac{e^2}{(8\pi)^2}\mathrm{Tr}(\not{k}\gamma^\mu \not{k}'\gamma^\nu)\,, \tag{2.27}$$

where $e$ is the electric charge of the electron.

By imposing the parity and current conversation rules for the hadronic tensor, we are able to write it as:

$$\begin{aligned} W_{\mu\nu}(P,q) = &-\left(g_{\mu\nu} - q_\mu q_\nu/q^2\right) W_1\left(x,Q^2\right) \\ &+\left[P_\mu - q_\mu\left(P\cdot q/q^2\right)\right]\left[P_\nu - q_\nu\left(P\cdot q/q^2\right)\right] W_2\left(x,Q^2\right)\,. \end{aligned} \tag{2.28}$$

The structure functions $W_1(x,Q^2)$ and $W_2(x,Q^2)$ are connected to more commonly used functions $F_1$ and $F_2$ in the following way:

$$F_1(x,Q^2) = -W_1(x,Q^2), \qquad F_2(x,Q^2) = (P\cdot q)W_2(x,Q^2)\,. \tag{2.29}$$

The leading order differential cross-section can be written as:

$$\frac{\mathrm{d}^2\sigma}{\mathrm{d}x\mathrm{d}y} = \frac{4\pi\alpha^2}{yQ^2}\left[\left(1+(1-y)^2\right)F_1 + \frac{1-y}{x}\left(F_2 - 2xF_1\right)\right], \tag{2.30}$$

where $\alpha$ is the fine-structure constant defined as:

$$\alpha = \frac{e^2}{4\pi\epsilon_0\hbar c}\,. \tag{2.31}$$

In this expression $\epsilon_0$ is the permitivity of free space, $\hbar$ is the reduced Planck constant and $c$ is the speed of light.

The structure functions $F_1$ and $F_2$ contained in Eq. (2.30) can be measured experimentally. In the scaling limit corresponding to $Q^2 \to \infty$ we get: $2xF_1 \to F_2$ and $F_2$ becomes independent of $Q^2$. This feature can be seen on Fig. 2.3 and it is often referred as Bjorken scaling.

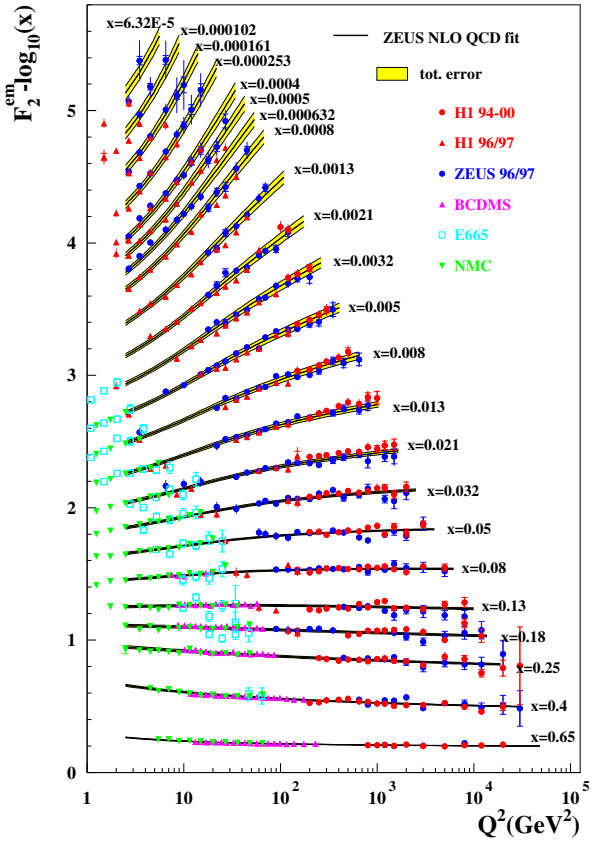


FIGURE 2.3: The structure function $F_2$ as a function of $Q^2$ for various values of $x$, taken from [50].

In the parton model, the proton is viewed as a collection of quasi-free partons, each carrying a fraction $\xi$ of the proton's momentum. The key assumption is that, at sufficiently high energies and momentum transfers, the electron scatters off an individual parton, and the scattering process can be described using perturbative QCD.

This allows us to express the hadronic cross section as a convolution of the partonic cross section, calculated perturbatively, and the parton distribution functions (PDFs), which describe the probability of finding a parton of a given type and with a particular momentum fraction inside the proton.

Thus, the differential cross-section we obtain the following result:

$$\frac{\mathrm{d}^2\hat{\sigma}}{\mathrm{d}x\mathrm{d}y} = \frac{4\pi\alpha^2}{yQ^2}\left[1+(1-y)^2\right]\frac{1}{2}e_q^2\delta(\xi-x), \tag{2.32}$$

where $e_q = Q_f e$ is a fractional charge of the quark.

Comparing this equation with Eq. (2.30) we see, that:

$$\hat{F}_1(x) \propto e_q^2\delta(\xi-x), \qquad \hat{F}_2 - 2x\hat{F}_1 = 0\,. \tag{2.33}$$

These equations are called *Callan-Gross* relations [51]. The hat on the $\sigma$ in Eq. (2.32) indicates that it is a partonic cross-section. To relate it with the hadronic cross section, we need to introduce a concept of the parton distribution function (PDF):

Let $\phi_{i/P}(\xi)\mathrm{d}\xi$ denote the probability of finding the parton of flavor $i$ inside the proton, with the momentum fraction between $\xi$ and $\xi+\delta\xi$.

With this definition the hadronic cross-section can be related to the partonic one according to:

$$\frac{\mathrm{d}^2\sigma}{\mathrm{d}x\,\mathrm{d}Q^2} = \int_x^1 \frac{\mathrm{d}\xi}{\xi}\sum_i \phi_{i/P}(\xi)\frac{\mathrm{d}^2\hat{\sigma}}{\mathrm{d}x\,\mathrm{d}Q^2}\left(\frac{x}{\xi},Q^2\right) + \mathcal{O}\left(\frac{\Lambda}{Q}\right)^p. \tag{2.34}$$

This actually means that we can separate short-distance, partonic effects, which are calculable perturbatively from long-distance effects, which have to be measured experimentally or predicted within the framework of non-perturbative QCD. Eq. (2.34) is also referred as QCD factorization theorem.

Now we outline what happens in the higher order calculations and in the next section complete detailed calculations will be shown for the Drell-Yan process.

When we carry out the calculation at the higher orders, as it was discussed already, different types of singularities appear. The UV divergences can be treated using the common renormalization scheme. However, in the final result there will still be

collinear singularities present. Assume a massless quark of momentum $p + k$ emits a gluon of momentum $k$. The corresponding propagator is given as:

$$\frac{1}{(p+k)^2} = \frac{1}{2pk} = \frac{1}{2E_q E_g(1-\cos\theta)}\,. \tag{2.35}$$

As one can see if $E_g \to 0$, or $\cos\theta \to 0$ the expression becomes singular. The first case corresponds to the soft emission, the second one to the collinear one. Within the framework of dimension regularization they appear as a $1/\epsilon$ poles. It is also possible to have a soft emission which is collinear as well, in this case one gets double poles proportional to $1/\epsilon^2$.

The soft and double poles from the real emission graphs cancel order-by-order with the respective poles from the virtual corrections. What remains are the single poles from the collinear emissions. To render the final expression finite and give it a physical meaning, these singularities can be absorbed in the renormalized PDFs. The good thing is that this kind of contributions completely decouple from the rest of the process and are unique to the type of parton flavor involved. Hence, one can calculate them once and reuse them for all the other processes

The functions which contain these singularities are called Altarelli-Parisi splitting functions [52] and formally they can be defined as:

$$|\mathcal{M}_{m+1}|^2 \; \mathrm{d}\Phi_{m+1} \to |\mathcal{M}_m|^2 \; \mathrm{d}\Phi_m \frac{\alpha_s}{2\pi}\frac{\mathrm{d}k_\perp^2}{k_\perp^2}\frac{\mathrm{d}\phi}{2\pi}\mathrm{d}z P_{ba}(z) \tag{2.36}$$

This can be visually seen in Fig. 2.4.

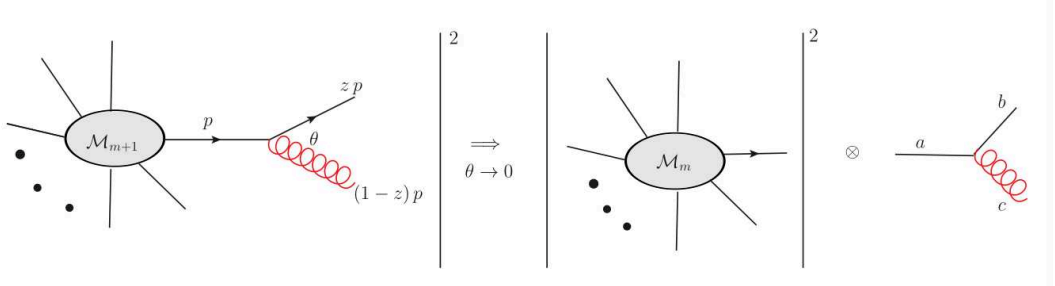


FIGURE 2.4: Factorization in the collinear limit. The Figure has been taken from [53].

The splitting functions have a perturbative expansion:

$$P_{ij}(x) = \frac{\alpha_s\left(\mu^2\right)}{2\pi} P_{ij}^{(0)}(x) + \left(\frac{\alpha_s\left(\mu^2\right)}{2\pi}\right)^2 P_{ij}^{(1)}(x) + \left(\frac{\alpha_s\left(\mu^2\right)}{2\pi}\right)^3 P_{ij}^{(2)}(x) + \dots \quad (2.37)$$

Meanwhile they are known up to the four-loop accuracy [54–56]. Below we give the expressions for the one-loop splitting functions:

$$P_{qq}^{(0)}(x) = C_F \left(\frac{1+x^2}{1-x}\right)_+, \quad (2.38)$$

$$P_{qg}^{(0)}(x) = T_R \left[(1-x)^2 + x^2\right], \quad (2.39)$$

$$P_{gq}^{(0)}(x) = C_F \frac{(1-x)^2+1}{x}, \quad (2.40)$$

$$P_{gg}^{(0)}(x) = 2C_A \left[\frac{x}{(1-x)_+} + \frac{1-x}{x} + x(1-x)\right] + \left(\frac{11}{6}C_A - \frac{2}{3}T_R N_f\right)\delta(1-x), \quad (2.41)$$

where the action of the plus distribution $[f(x)]_+$ on some smooth function $g(x)$ is defined as:

$$\int_0^1 \mathrm{d}x [f(x)]_+ g(x) = \int_0^1 \mathrm{d}x f(x) \left[g(x) - g(1)\right]. \quad (2.42)$$

To be able to renormalize PDFs we need a formal definition for them, which for example for quarks is given by [33, 34, 57]:

$$\phi_{q/P}(\xi) = \frac{1}{4\pi}\int_{-\infty}^{\infty} dy^- e^{-\mathrm{i}\xi p^+ y^-} \left\langle P \left|\bar{q}\left(0, y^-, 0_T\right)\gamma^+ q\left(0,0,0_T\right)\right| P\right\rangle_{A_+=0}. \quad (2.43)$$

Similar expressions can be written for antiquarks and gluons. Here we have introduced the light-cone coordinates $x^\pm = (x^0 \pm x^2)/\sqrt{2}$ and $\vec{x}_\perp = (x^1, x^2)$ (which implies that $g_{12} = g_{21} = -1, g_{33} = g_{44} = 1$). $A_+ = 0$ fixes the gauge. $q$ and $\bar{q}$ are quark and antiquark fields and $|P\rangle$ is a hadronic state, which contains the non-perturbative part and hence cannot be calculated analytically within our framework. However, we can replace the hadronic states with the partonic ones and define the quark in quark distribution, whose analytic calculation is possible:

$$\phi_{q/q}(\xi) = \frac{1}{4\pi}\int_{-\infty}^{\infty} \mathrm{d}y^- e^{-\mathrm{i}\xi p^+ y^-} \sum_\sigma \left\langle q(p,\sigma)\left|\bar{q}\left(0, y^-, 0_T\right)\gamma^+ q\left(0,0,0_T\right)\right| q(p,\sigma)\right\rangle_{A_+=0}, \quad (2.44)$$

where $\sigma$ denotes the spin of the incoming parton. The partonic states are defined in terms of the creation and annihilation operators:

$$\langle q(p,\sigma)| = \langle 0|a(p), \qquad |q(p,\sigma)\rangle = a^{\dagger}(p)|0\rangle\,. \tag{2.45}$$

Then, it is possible to plug in the quantized expression of the field operators in Eq. (2.44) and carry out the calculation at the fixed order.

With the formal expression of the PDFs on hand we can write the renormalized expression for them:

$$\phi_{j/H}(\xi) = \sum_{j'} \int_{\xi-}^{1+} \frac{\mathrm{d}z}{z} Z_{jj'}(z,g,\epsilon,\mu)\phi_{(0)j'/H}(\xi/z,\mu), \tag{2.46}$$

where $\phi_{(0)}$ is the bare PDF, $Z_{jj'}$ are renormalization coefficients which absorb the collinear poles of bare PDFs and $\mu$ is a factorization scale, which we had to introduce in accordance with the dimensional regularization procedure described above.

Since the physical quantity - the renormalized PDF, should not be dependent on the arbitrary scale $\mu$, we can apply the $\mathrm{d}/\mathrm{d}\ln\mu$ operation on the last equation and derive the RGE for the PDFs:

$$\frac{\mathrm{d}}{\mathrm{d}\ln\mu}\phi_{j/H}(\xi;\mu) = 2\sum_{j'}\int \frac{dz}{z} P_{jj'}(z,g)\phi_{j'/H}(\xi/z;\mu), \tag{2.47}$$

where $P$ is connected with $Z$ in the following way:

$$P = \frac{1}{2}\frac{\mathrm{d}}{\mathrm{d}\ln\mu}\ln Z\,. \tag{2.48}$$

The one-loop expressions of $P_{ij}$ for various partonic processes have been already given above - Eqs. (2.38)- (2.41).

The integro-differential equation (2.47) is known as the *Dokshizer-Gribov-Lipatov-Altarelli-Parisi (DGLAP)* [52, 58, 59] relation and it has a fundamental importance in QCD. One can calculate PDFs for a simple process at some scale and reuse it for more complicated processes at any scale, where the scale evolution is given by the DGLAP equations.

It is often more useful to work in the Mellin space, where convolutions like those in Eq. (2.46) reduce to simple products and factorization is fully manifest. We introduce Mellin moments of the PDFs and of the renormalization coefficients in the following way:

$$\overline{\phi}_{j/H}(N) = \int_0^{1+} \mathrm{d}\xi \xi^{N-1} \phi_{j/H}(\xi) \tag{2.49}$$

$$\overline{Z}_{jj'}(N) = \int_0^{1+} \mathrm{d}z z^{N-1} Z_{jj'}(z) \tag{2.50}$$

In terms of these moments, Eq. (2.46) becomes:

$$\overline{\phi}_{j/H}(J) = \sum_{j'} \overline{Z}_{jj'}(J) \overline{\phi}_{(0)j'/H}(J) \tag{2.51}$$

After applying the $\mathrm{d}/\mathrm{d}\ln\mu$ operation, we obtain:

$$\frac{\mathrm{d}}{\mathrm{d}\ln\mu} \overline{\phi}_{j/H}(N;\mu) = -2 \sum_{j'} \gamma_{jj'}(N,g) \overline{\phi}_{j'/H}(N;\mu), \tag{2.52}$$

where $\gamma_{ij}$ are called *anomalous dimensions* and they are defined as:

$$\gamma_{ij}(N) = -\int_0^1 \mathrm{d}z z^{N-1} P_{ij}(z) \tag{2.53}$$

Using Mellin moments Eq. (2.34) can be factorized into perturbative and non-perturbative parts:

$$\mathrm{d}\sigma = \sum_i \overline{\phi}_{i/P}(N,\mu_f) \mathrm{d}\hat{\sigma}(N,\mu_f,\mu_r) + \mathcal{O}\left(\frac{1}{N}\right), \tag{2.54}$$

where $\mu_r$ stands for the renormalization scale, coming from the dimensional regularization of the partonic cross-section, in order to get rid of UV poles and $\mu_f$ is the factorization scale, as discussed above.

The parton model, combined with the QCD factorization theorem and the DGLAP equations, provides a powerful framework for understanding the structure of hadrons and making predictions for a wide range of hadronic processes. It allows us to calculate cross sections and other observables in terms of perturbatively

calculable partonic cross sections convolved with non-perturbative, but universal, PDFs. This approach has been highly successful describing experimental data of hadronic collisions and has become an essential tool in modern particle physics.

## 2.2 Drell-Yan process

To demonstrate the nature of the IR singularities in this section we are going to review the Drell-Yan (DY) production process:

$$H_A + H_B \to l^+ + l^- \,, \tag{2.55}$$

which was first suggested and theoretically formulated by Sidney Drell and Tung-Mow Yan [60] in 1970. In the same year muon production from hadron pairs was discovered at the AGS experiment at the Brookhaven National Laboratory [61]. Meanwhile the theoretical calculations are available up to $N^3LO$ accuracy [62].

Studying this process is important because it illustrates the main concepts involved in more complicated calculations. In the following, we will analyze the NLO correction for the Drell-Yan process and observe in detail how the renormalization and cancellation of different singularities work. A very detailed derivation is available e.g. in Ref. [63].

The tree level diagram of DY process is shown in Fig. 2.5. Applying the Feynman

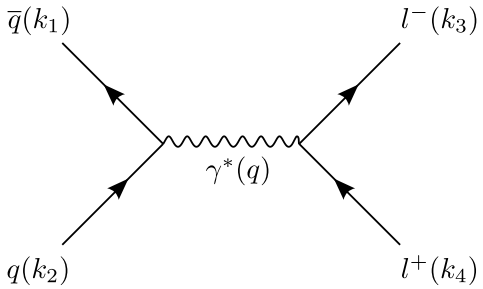


FIGURE 2.5: Tree level partonic DY process. The momenta of particles are indicated by the symbols in brackets.

rules to it we get:

$$i\mathcal{M}_0 = \delta_{ij} \left[\overline{v}\left(k_1\right)\left(Q_f e\right)\gamma_\mu u\left(k_2\right)\right] \frac{-i}{q^2} \left[\overline{u}\left(k_3\right)(-e)\gamma^\mu v\left(k_4\right)\right] \tag{2.56}$$

After squaring the equation above and performing the averaging over the initial state spin and color we get:

$$|\overline{\mathcal{M}_0}|^2 = \frac{1}{N_c}\frac{1}{4}\sum_{\text{spins}}|\mathcal{M}|^2 = \frac{Q_f^2 e^4}{N_c q^4} H_{\mu\nu}L^{\mu\nu}, \tag{2.57}$$

where the hadronic tensor $H_{\mu\nu}$ has been defined as,

$$\begin{aligned} H^{\mu\nu} &= \frac{1}{2}\,\mathrm{Tr}\left[\not{k}_1\gamma^\mu\not{k}_2\gamma^\nu\right] \\ &= 2\left[k_1^\mu k_2^\nu + k_1^\nu k_2^\mu - g^{\mu\nu}k_1\cdot k_2\right] \end{aligned} \tag{2.58}$$

and the leptonic tensor $L^{\mu\nu}$ as:

$$\begin{aligned} L^{\mu\nu} &= \frac{1}{2}\,\mathrm{Tr}\left[\not{k}_3\gamma^\mu\not{k}_4\gamma^\nu\right] \\ &= 2\left[k_3^\mu k_4^\nu + k_3^\nu k_4^\mu - g^{\mu\nu}k_3\cdot k_4\right] \end{aligned} \tag{2.59}$$

We introduce Mandelstam variables $s, t$ and $u$ in the standard way and express momentum scalar products using them:

$$k_1\cdot k_2 = k_3\cdot k_4 = \frac{s}{2}, \tag{2.60}$$

$$k_1\cdot k_3 = k_2\cdot k_4 = -\frac{t}{2}, \tag{2.61}$$

$$k_1\cdot k_4 = k_2\cdot k_3 = -\frac{u}{2}. \tag{2.62}$$

In the partonic center-of-mass system (cms) frame we have:

$$t = -\frac{s}{2}\left(1+\cos\theta^*\right), \quad u = -\frac{s}{2}\left(1-\cos\theta^*\right), \tag{2.63}$$

where $\theta^*$ is a scattering angle in the cms frame. Using these definitions we get:

$$H_{\mu\nu}L^{\mu\nu} = s^2\left(\cos^2\theta^* + D - 3\right) \tag{2.64}$$

The differential cross-section is given as:

$$\mathrm{d}\sigma_{\mathrm{DY}}^{(0)} = \frac{1}{2s}\frac{Q_f^2 e^4}{N_c q^4} H_{\mu\nu}L^{\mu\nu}\mathrm{dPS}^{(2)}, \tag{2.65}$$

where the expression of the two-particle phase space in D-dimensions can be found in Appendix A. After integration over the scattering angle we obtain the Born level total cross-section in $D$ dimensions:

$$\begin{aligned}\sigma_{\mathrm{DY}}^{(0)} &= \frac{4\pi Q_f^2 \alpha_s^2}{N_c s}\left(\frac{4\pi\mu^2}{s}\right)^{\epsilon}\frac{\sqrt{\pi}(1-\epsilon)^2}{2^{2-2\epsilon}\Gamma\left(\frac{5-2\epsilon}{2}\right)} \\ &= 3\sigma_{\mathrm{B}}\left(\frac{4\pi\mu^2}{s}\right)^{\epsilon}\frac{(1-\epsilon)^2}{(3-2\epsilon)(1-2\epsilon)}\frac{\Gamma(1-\epsilon)}{\Gamma(1-2\epsilon)},\end{aligned} \tag{2.66}$$

where we recognize the common tree level result of DY cross section in $D = 4$ dimensions:

$$\sigma_{\mathrm{B}} = \frac{4\pi Q_f^2 \alpha_s^2}{3N_c s} \tag{2.67}$$

To increase the accuracy at the NLO level, one has to consider the virtual and real emission corrections. Because we are interested in QCD corrections, we only focus on the hadronic tensor (left side of diagram shown in Fig. 2.5). For our purposes it is sufficient to assume that all the involved particle are massless. In this case it enough to consider only the graph depicted in Fig 2.6.

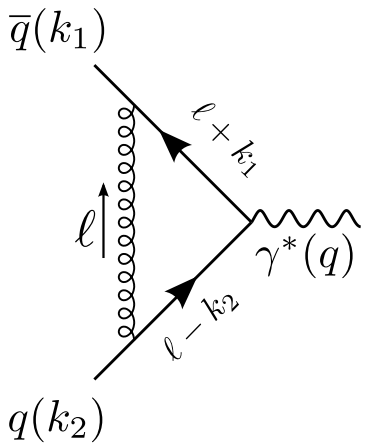


FIGURE 2.6: One-loop virtual correction to DY process.

The real corrections are shown in Fig. 2.7.

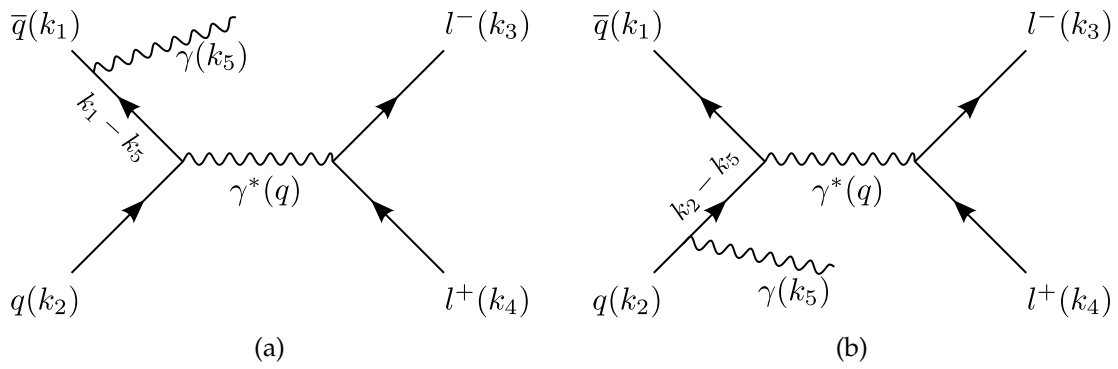


FIGURE 2.7: Real NLO corrections to DY process.

**Vertex correction**

After applying the Feynman rules on graph 2.6, we obtain:

$$\begin{aligned} i\mathcal{M}_V &= g_s^2 C_F \mu^{4-D} \int \frac{\mathrm{d}^D \ell}{(2\pi)^D} \frac{\overline{v}(k_1)\,\gamma^\alpha\,(\not{\ell}+\not{k}_1)\,\gamma^\mu\,(\not{\ell}-\not{k}_2)\,\gamma_\alpha u(k_2)}{\ell^2\,(\ell+k_1)^2\,(\ell-k_2)^2} \\ &= \overline{v}(k_1)\, i\Gamma^\mu u(k_2)\,. \end{aligned} \tag{2.68}$$

The NLO contribution to the cross-section comes from the interference term of the tree–level diagram and the vertex-corrected graph ($\langle|\mathcal{M}_V|^2\rangle$ would have one $\alpha_s$ too much for NLO). So the corresponding cross-section is given as:

$$\sigma_V^{(1)} = \int \mathrm{dPS}^{(2)} \frac{1}{2s} 2\mathrm{Re}\Big(\langle|\mathcal{M}_0 \mathcal{M}_V^*|\rangle\Big)\,. \tag{2.69}$$

Since we already did the phase space integration for the tree diagram and the virtual correction does not affect the final state kinematics we can reduce the above expression to the following form:

$$\sigma_V^{(1)} = 2\sigma^{(0)}\mathrm{Re}\Big(\frac{1}{D}\Gamma^\mu\gamma_\mu\Big), \tag{2.70}$$

where we use the fact that, the vertex correction is just a tree graph with replacement of vertex factor $\gamma^\mu \to \Gamma^\mu$. Since the $\gamma^\mu$ factor was already included in the Born level calculation we have to get rid of it from $\Gamma^\mu$ in the expression above. This is achieved by using the identity $\gamma^\mu\gamma_\mu = D$.

After performing the loop integration, renormalization and substitution of the result in Eq. (2.70) we get:

$$\sigma_V^{(1)} = C_F \frac{\alpha_s}{2\pi} \sigma^{(0)} \left(\frac{4\pi\mu^2}{s}\right)^{\epsilon} \frac{\Gamma(1-\epsilon)}{\Gamma(1-2\epsilon)} \left[-\frac{2}{\epsilon_{IR}^2} - \frac{3}{\epsilon_{IR}} - 8 + \frac{2\pi^2}{3} + \mathcal{O}(\epsilon)\right], \quad (2.71)$$

where the expression for the Born cross-section can be found in Eq. (2.66), and the notation $\epsilon_{IR}$ indicates that these poles have an infrared origin.

### Real correction

For the real correction we have to consider the graphs 2.7(a) and 2.7(b). The corresponding amplitude is given as:

$$i\mathcal{M}_R = Q_f e^2 g_s \mu^{(4-D)/2} \left[\overline{v}(k_2) S^{\mu\alpha} u(k_1)\right] T_{ij}^a \varepsilon_\nu^*(k_5) \frac{-i}{q^2} \left[\overline{u}(k_3) \gamma_\mu v(k_4)\right], \quad (2.72)$$

where $S^{\mu\nu}$ is vertex factor associated with a gluon emission:

$$S^{\mu\nu} = S_a^{\mu\nu} - S_b^{\mu\nu} = \gamma^\mu \frac{\not{k}_1 - \not{k}_5}{(k_1 - k_5)^2} \gamma^\nu - \gamma^\nu \frac{\not{k}_2 - k_5}{(k_2 - k_5)^2} \gamma^\mu \quad (2.73)$$

After squaring the amplitude and taking the color and spin average, we get:

$$\left|\overline{\mathcal{M}_R}\right|^2 = \frac{C_F}{N_c} \frac{g_s^2 \mu^{(4-D)} Q_f^4 e^4}{q^4} H^{\mu\nu} L_{\mu\nu}, \quad (2.74)$$

where the hadronic tensor has been defined as:

$$H^{\mu\nu} = \frac{1}{2} \mathrm{Tr}\left[\not{p}_b S^{\mu\alpha} \not{p}_a S_\alpha^\nu\right] \quad (2.75)$$

and the definition of the leptonic tensor is the same as for the Born process (2.59).

The integrated cross-section is given as:

$$\begin{aligned}\sigma_R^{(1)} &= \frac{1}{F} \int |\overline{\mathcal{M}}|^2 \mathrm{dPS}^{(3)} \\ &= \frac{C_F}{N_c} Q_f^2 e^4 g_s^2 \mu^{(4-D)} \frac{1}{2s} \int H_{\mu\nu} \frac{L^{\mu\nu}}{q^4} \mathrm{dPS}^{(3)}\end{aligned}$$

$$= \frac{C_F}{N_c} Q_f^2 e^4 g_s^2 \mu^{(4-D)} \frac{1}{2s} \int H_{\mu\nu} \mathrm{dPS}_H^{(2)} \iint \frac{\mathrm{d}q^2}{2\pi} \frac{L^{\mu\nu}}{q^4} \mathrm{dPS}_L^{(2)} \,. \tag{2.76}$$

The phase space integral over the final state leptons can be easily evaluated, by realizing, that, because of gauge invariance (Ward identity) it should vanish upon contracting with the photon momentum. That way we can easily extract the value of $L(q^2)$:

$$L(q^2) = -\left(\frac{4\pi\mu^2}{q^2}\right)^{\epsilon} \frac{1}{4\pi q^4} \frac{1-\epsilon}{(3-2\epsilon)(1-2\epsilon)} \frac{\Gamma(1-\epsilon)}{\Gamma(1-2\epsilon)} \,. \tag{2.77}$$

Following the analysis done in [64] we introduce the following new variables:

$$z = \frac{q^2}{s} \,, \tag{2.78}$$

$$y = \frac{1+\cos\theta}{2} \,. \tag{2.79}$$

Using these variables, we can rewrite kinematic invariants for our $2 \to 3$ process in the following way:

$$s = (k_1 + k_2)^2 = \frac{q^2}{z} \tag{2.80}$$

$$t = (k_1 - k_5)^2 = -2k_1 \cdot k_5 = -\sqrt{s}\left|\vec{k}_5\right|(1-\cos\theta) = \frac{-q^2}{z}(1-z)(1-y) \tag{2.81}$$

$$u = (k_2 - k_5)^2 = -2k_2 \cdot k_5 = \frac{-q^2}{z}(1-z)y \,. \tag{2.82}$$

The remaining integral in Eq. (2.76) looks like this:

$$\sigma_{\mathrm{R}}^{(1)} = \frac{C_F}{N_c} Q_f^2 e^4 g_s^2 \mu^{(4-D)} \frac{L(q^2)}{2s} \iint \frac{\mathrm{d}q^2}{2\pi} H_{\mu\nu}(q^2 g^{\mu\nu} + q^\mu q^\nu) \mathrm{dPS}_H^{(2)} \,. \tag{2.83}$$

The next step is to evaluate the hadronic integral. The explicit calculation of the trace in Eq. (2.75) by hand is involved because of the lengthy expressions and this task is better left to some symbolic manipulation program, in this case `FORM` [65] has been used. We get the following result:

$$H_{\mu\nu}(q^2 g^{\mu\nu} + q^\mu q^\nu) = -8(1-\epsilon)q^2 \left[\frac{(1-\epsilon)}{2}\left(\frac{1-y}{y} + \frac{y}{1-y}\right) - \epsilon + \frac{z}{(1-z)^2}\frac{1}{y(1-y)}\right] \,. \tag{2.84}$$

After integration over the hadronic phase-space and combination of the hadronic and leptonic results we obtain following expansion for the different cross-section:

$$\frac{d\sigma_R^{(1)}}{dq^2} = -\frac{C_F Q_f^2 e^4 g_s^2}{2\pi q^2 s N_c}\left(\frac{4\pi\mu^2}{q^2}\right)^{2\epsilon}\frac{\Gamma(1-\epsilon)}{\Gamma(1-2\epsilon)}\frac{(1-\epsilon)^2}{(3-2\epsilon)(1-2\epsilon)}\frac{z^\epsilon}{\epsilon}\frac{1+z^2}{(1-z)^{1+2\epsilon}} + \mathcal{O}(\epsilon)\,. \quad (2.85)$$

The last denominator in the expression above has some nontrivial poles when $z \to 1$ and $\epsilon \to 0$. Physically, these correspond to the soft-collinear emissions. We can make these singularities manifest as $\epsilon$-poles by means of the plus-distributions:

$$\frac{1}{(1-z)^{1+2\varepsilon}} = -\frac{1}{2\varepsilon}\delta(1-z) + \frac{1}{[1-z]_+} - 2\varepsilon\left[\frac{\ln(1-z)}{1-z}\right]_+ + \sum_{n=2}^{\infty}\frac{(-2\varepsilon)^n}{n!}\left[\frac{\ln^n(1-z)}{1-z}\right]_+ . \quad (2.86)$$

Upon plugging of Eq. (2.86) in Eq. (2.85) and expanding the result in $\epsilon$ powers we get our final result for the real correction:

$$\frac{d\sigma_R^{(1)}}{dq^2} = C_F\frac{\alpha_s}{2\pi}\frac{1}{s}\sigma^{(0)}\frac{\Gamma(1-\epsilon)}{\Gamma(1-2\epsilon)}\left(\frac{4\pi\mu^2}{q^2}\right)^\epsilon \times \left(\frac{2}{\epsilon_{\rm IR}^2}\delta(1-z) - \frac{2}{\epsilon_{\rm IR}}\frac{1+z^2}{(1-z)_+} + 4\left(1+z^2\right)\left[\frac{\ln(1-z)}{1-z}\right]_+ - 2\frac{1+z^2}{1-z}\ln z + \mathcal{O}(\epsilon)\right), \quad (2.87)$$

where again, the notation $\epsilon_{\rm IR}$ indicates that these poles have an infrared origin.

### Total NLO correction

Now we are almost ready to combine the virtual and the real contributions and obtain a final expression for the NLO correction of the DY process. Before doing so, we have to rewrite Eq. (2.71) in the differential form. This can be easily achieved by using the following identity:

$$1 = \int \mathrm{d}q^2\delta(q^2-s) = \int \mathrm{d}q^2\frac{1}{s}\delta\Big(z-1\Big), \quad (2.88)$$

which is basically a statement about the energy-momentum conservation. After inserting this identity in Eq. (2.71), the calculation of the differential virtual cross-section becomes straightforward:

$$\frac{\mathrm{d}\sigma_V^{(1)}}{\mathrm{d}q^2} = C_{\rm F}\frac{\alpha_s}{2\pi}\frac{1}{s}\sigma^{(0)}\left(\frac{4\pi\mu^2}{q^2}\right)^\epsilon\frac{\Gamma(1-\epsilon)}{\Gamma(1-2\epsilon)}\times$$

$$\left[-\frac{2}{\epsilon_{\mathrm{IR}}^2}-\frac{3}{\epsilon_{\mathrm{IR}}}-8+\frac{2\pi^2}{3}+\mathcal{O}(\epsilon)\right]\delta(1-z) \tag{2.89}$$

Now we are able to finalize the calculation and reproduce the well-known result [64]:

$$\begin{aligned}\frac{\mathrm{d}\sigma_{\mathrm{DY}}^{\mathrm{NLO}}}{\mathrm{d}q^2} &= \frac{\mathrm{d}\sigma_V^{(1)}}{\mathrm{d}q^2}+\frac{\mathrm{d}\sigma_R^{(1)}}{\mathrm{d}q^2}\\ &= \frac{\alpha_s}{2\pi}\frac{1}{s}\sigma^{(0)}\left(\frac{4\pi\mu^2}{q^2}\right)^{\epsilon}\frac{\Gamma(1-\epsilon)}{\Gamma(1-2\epsilon)}\left[\omega_{qq}(z)+\frac{2}{\epsilon}P_{qq}^{(1)}(z)\right]\\ &= \frac{\alpha_s}{2\pi}\frac{1}{s}\sigma^{(0)}\omega_{qq}(z)-\frac{2}{\epsilon}\frac{\alpha_s}{2\pi}\frac{1}{s}\sigma^{(0)}P_{qq}^{(0)}(z)\left(\frac{4\pi\mu^2}{q^2}\right)^{\epsilon}\frac{\Gamma(1-\epsilon)}{\Gamma(1-2\epsilon)}+\mathcal{O}(\epsilon)\,,\end{aligned} \tag{2.90}$$

where $\omega_{qq}(z)$ is defined as:

$$\omega_{qq}(z)=C_{\mathrm{F}}\left\{\left[\frac{2}{3}\pi^2-8\right]\delta(1-z)-2\frac{1+z^2}{1-z}\ln z+4(1+z^2)\left[\frac{\ln(1-z)}{1-z}\right]_+\right\} \tag{2.91}$$

and $P_{qq}^{(1)}$ is the well-known 1-Loop Altarelli-Parisi splitting function, discussed in Sec. 2.1.2.

At this point, we can make the following observations:

- The double poles, corresponding to soft and collinear emission from the partons, have been canceled perfectly.
- In our final result there is still a single - $\frac{1}{\epsilon}$ pole present (in the last term of Eq. (2.90)). The appearance of the splitting function is an indication that we might be able to absorb them in the renormalized PDFs, as it was discussed in Sec. 2.1.2.
- The result contains a plus distribution of the form $\left[\frac{\ln(1-z)}{1-z}\right]_+$, which we got after the improper cancellation of the IR-poles upon addition of the virtual and the real contributions.

At the first glance this result might seem surprising, as the well-known KLN (Kinoshita-Lee-Nauenberg) theorem states, the cross-section should be free of infrared divergences in every order of QCD perturbation theory [66, 67]. However,

one should remember that the KLN theorem holds, only if the sum is taken over all degenerate states, that means the process should be fully inclusive in both - final and initial states. In our case, the final state is degenerate, as we have not imposed any restriction on the leptons. On the contrary, because we require a gluon emission from the initial state, it restricts the degrees of freedom and as a result we ended up with a collinear singularity still present in our result.

These singularities can be easily dealt using the freedom of the PDF renormalization. In fact, if we redefine the PDFs in the following way [68]:

$$\phi_{a/b}(x,\mu,\epsilon)_{\overline{\text{MS}}} = \delta_{ab}\delta(1-x) + \frac{\alpha_s(\mu)}{2\pi} P_{ab}^{(0)}(x)\left(-\frac{1}{\epsilon} + \gamma_E - \ln 4\pi\right) \tag{2.92}$$

and expand the $\epsilon$-dependent prefactor of the splitting function from Eq. (2.90):

$$\frac{1}{\epsilon}\left(\frac{4\pi\mu^2}{M^2}\right)^{\epsilon} \frac{\Gamma(1-\epsilon)}{\Gamma(1-2\epsilon)} = \left(\frac{1}{\epsilon} + \ln 4\pi - \gamma_E + \ln\frac{\mu^2}{M^2}\right) \tag{2.93}$$

we see that at the scale $\mu^2 = M^2$ the $\epsilon$ dependence in Eq. (2.90) exactly cancels against the $\epsilon$ dependence of the PDFs.

## 2.3 Parametrizing Singular Limits: $z$ and $\lambda$ Variables

Perturbative calculations in quantum field theories involve the evaluation of matrix elements that can develop infrared (IR) divergences associated with the emission of massless particles. These divergences arise when virtual or real particles become soft (low energy) or collinear (parallel) to external particles. While such singularities cancel for suitably defined physical observables, their systematic treatment is crucial for obtaining finite and meaningful predictions. To achieve this, it is necessary to introduce a parametrization that exposes the singular limits in a controlled manner, allowing for their systematic subtraction and cancellation with virtual corrections. In this section, we discuss the light-cone decomposition and the parametrization of the soft and collinear limits using the variables $z$ and $\lambda$.

The light-cone decomposition provides a useful framework for analyzing the kinematics of massless particles and parametrizing the collinear limit. Given two distinct light-like vectors $p_i$ and $p_j$ satisfying $p_i^2 = p_j^2 = 0$ and $p_i \cdot p_j \neq 0$, any other Lorentz vector $p$ can be decomposed as:

$$p^\mu = p_{\parallel i} p_i^\mu + p_{\parallel j} p_j^\mu + p_\perp^\mu \,, \tag{2.94}$$

where the light-cone components are defined as:

$$p_{\parallel i} = \frac{p \cdot p_j}{p_i \cdot p_j}, \quad p_{\parallel j} = \frac{p \cdot p_i}{p_j \cdot p_i}, \quad p_\perp^\mu = p^\mu - p_{\parallel i} p_i^\mu - p_{\parallel j} p_j^\mu \,. \tag{2.95}$$

In this way, the vector $p_\perp$ is orthogonal to both $p_i$ and $p_j$.

In order to systematically handle infrared singularities arising from soft and collinear emissions, it is advantageous to introduce a parametrization that exposes these singular limits. The dimensionless variable $z$, defined as $z = p_F^2/s$, where $p_F$ is the momentum of the final state and $s$ is the partonic center-of-mass energy, naturally controls the proximity to the soft threshold. The range of $z$ is given by $0 < \tau \leq z \leq 1$, where $\tau = p_F^2/S$ and $S$ is the hadronic center-of-mass energy squared. The soft limit corresponds to $z \to 1$, or equivalently, $\bar{z} \equiv 1 - z \to 0$.

To parametrize the collinear singularities, we introduce the light-cone components $p_{X\parallel i}$ and $p_{X\parallel j}$, which measure the momentum fraction of the radiation $X$ along the directions of the initial-state partons $i$ and $j$, respectively. The variables $\lambda$ and $\tilde{\lambda}$ are then defined as:

$$\lambda = \frac{1}{\bar{z}} \frac{2 p_i \cdot p_X}{\bar{z} s}, \quad \tilde{\lambda} = \frac{1}{\bar{z}} \frac{2 p_j \cdot p_X}{\bar{z} s}. \tag{2.96}$$

The physical region is constrained by $0 \leq \lambda \leq 1$, $0 \leq \tilde{\lambda} \leq 1$, and $0 \leq \lambda + \tilde{\lambda} - 1 \leq \lambda\tilde{\lambda}$. When either $\lambda$ or $\tilde{\lambda}$ vanishes, the corresponding light-cone component $p_{X\parallel i}$ or $p_{X\parallel j}$ vanishes, indicating that all radiation is collinear to the other beam direction.

# Chapter 3

# Local Analytic Sector Subtraction

In the calculation of higher-order corrections in perturbative QCD, we need to consider not only virtual loop corrections but also real emission processes. To compute QCD predictions beyond the leading order, we need to consider processes with different final states that contribute to the same order in $\alpha_s$. Schematically, for the observable $X$ we have:

$$\sigma^{(X)}_{\mathrm{LO}} = \int_{\Phi_n} \mathrm{d}\sigma^{(X)}_{B}, \tag{3.1}$$

$$\sigma^{(X)}_{\mathrm{NLO}} - \sigma^{(X)}_{\mathrm{LO}} = \int_{\Phi_n} \mathrm{d}\sigma^{(X)}_{V} + \int_{\Phi_{n+1}} \mathrm{d}\sigma^{(X)}_{R}, \tag{3.2}$$

$$\sigma^{(X)}_{\mathrm{NNLO}} - \sigma^{(X)}_{\mathrm{NLO}} = \int_{\Phi_n} \mathrm{d}\sigma^{(X)}_{\mathrm{VV}} + \int_{\Phi_{n+1}} \mathrm{d}\sigma^{(X)}_{\mathrm{RV}} + \int_{\Phi_{n+2}} \mathrm{d}\sigma^{(X)}_{\mathrm{RR}}, \tag{3.3}$$

where $B$, $V$, $R$, $VV$, $RV$, and $RR$ denote the Born, virtual, real, double-virtual, real-virtual, and double-real contributions, respectively and the index of $\Phi$ indicates how many particles there are in the final state. Each of these contributions can be calculated using the perturbative expansion of the Feynman amplitude $\mathcal{A}$. At NLO we have:

$$R = \left|\mathcal{A}^{(0)}_{n+1}\right|^2, \qquad V = 2\,\mathbf{Re}\left[\mathcal{A}^{(0)\dagger}_{n}\,\mathcal{A}^{(1)}_{n}\right], \tag{3.4}$$

whereas at NNLO one has to calculate the following contributions:

$$\begin{aligned} RR &= \left|\mathcal{A}^{(0)}_{n+2}\right|^2, \quad RV = 2\,\mathbf{Re}\left[\mathcal{A}^{(0)\dagger}_{n+1}\,\mathcal{A}^{(1)}_{n+1}\right] \quad \text{and} \\ VV &= \left|\mathcal{A}^{(1)}_{n}\right|^2 + 2\,\mathbf{Re}\left[\mathcal{A}^{(0)\dagger}_{n+1}\,\mathcal{A}^{(2)}_{n+1}\right], \end{aligned} \tag{3.5}$$

where

$$\mathcal{A}_n(k_i) = \mathcal{A}_n^{(0)}(k_i) + \mathcal{A}_n^{(1)}(k_i) + \mathcal{A}_n^{(2)}(k_i) + \dots , \tag{3.6}$$

is a perturbative expansion of a Feynman amplitude for the given process.

The formulae in Eqs. (3.1) - (3.3) generalize to the arbitrary order expression as follows:

$$\sigma^{(X)}_{\mathrm{N^kLO}} - \sigma^{(X)}_{\mathrm{N^{k\text{-}1}LO}} = \sum_{i=0}^{k} \int_{\Phi_{n+i}} \mathrm{d}\sigma^{(X)}_{R^i V^{k-i}}. \tag{3.7}$$

As it was discussed in the previous chapter $V$ and $R$ contain IR singularities. In case of $V$ they are explicitly manifested in the dimensional regularization as $\epsilon$ poles and in case of the real radiation, these are phase-space singularities, which affect the integration procedure. Because for the involved processes with multiple particles in the final state it is difficult to carry out this integration analytically, one is often restricted to use the numeric integration techniques. Hence, for the numeric stability it is mandatory to treat these singularities before one starts the evaluation of the integral.

In subtraction schemes, one subtracts from every real-emission matrix element a quantity that approximates it in all singular limits, such that the difference is integrable in four dimensions. This subtraction term is then added back to the virtual contribution after integration in $D$ dimensions over the unresolved degrees of freedom and due to the virtue of KLN theorem this makes the calculation free of IR singularities. Schematically, for a cross section at NLO, we can write:

$$\sigma^{(X)}_{\mathrm{NLO}} - \sigma^{(X)}_{\mathrm{LO}} = \int_{\Phi_{n+1}} \left( \mathrm{d}\sigma^{(X)}_{R} - \mathrm{d}\sigma^{(X)}_{R,S} \right) + \int_{\Phi_n} \left( \mathrm{d}\sigma^{(X)}_{V} + \int_1 \mathrm{d}\sigma^{(X)}_{R,S} \right), \tag{3.8}$$

where $\mathrm{d}\sigma^{(X)}_{R,S}$ is an approximation to $\mathrm{d}\sigma^{(X)}_{R}$ in all unresolved singular limits, and the integral sign with subscript 1 stands for the integration over the one-particle unresolved phase space. At NNLO, we need to regulate both the $RR$ and $RV$ contributions, which can be achieved by setting

$$\begin{aligned} \sigma^{(X)}_{\mathrm{NNLO}} - \sigma^{(X)}_{\mathrm{NLO}} = & \int_{\Phi_{n+2}} \left( \mathrm{d}\sigma^{(X)}_{\mathrm{RR}} - \mathrm{d}\sigma^{(X)}_{\mathrm{RR,S}} \right) + \int_{\Phi_{n+1}} \left( \mathrm{d}\sigma^{(X)}_{\mathrm{RV}} - \mathrm{d}\sigma^{(X)}_{\mathrm{RV,S}} \right) \\ & + \int_{\Phi_n} \left( \mathrm{d}\sigma^{(X)}_{\mathrm{VV}} + \int_1 \mathrm{d}\sigma^{(X)}_{\mathrm{RV,S}} + \int_2 \mathrm{d}\sigma^{(X)}_{\mathrm{RR,S}} \right), \end{aligned} \tag{3.9}$$

where $\mathrm{d}\sigma^{(X)}_{\mathrm{RR,S}}$ approximates $\mathrm{d}\sigma^{(X)}_{\mathrm{RR}}$ in all limits where one or two partons become unresolved, and $\mathrm{d}\sigma^{(X)}_{\mathrm{RV,S}}$ approximates $\mathrm{d}\sigma^{(X)}_{\mathrm{RV}}$ in all kinematic configurations where one parton is either soft or collinear to another. We observe that taking the approximations to be exactly equal to their original expressions (e.g., $\mathrm{d}\sigma^{(X)}_{R,S} = \mathrm{d}\sigma^{(X)}_{R}$) sets the integrals over real-emission phase spaces to zero and formally gives back the original formulae in terms of $V$, $R$, $VV$, $RV$, and $RR$ contributions.

The freedom in defining the subtraction terms $\mathrm{d}\sigma^{(X)}_{R,S}$, $\mathrm{d}\sigma^{(X)}_{\mathrm{RV,S}}$ and $\mathrm{d}\sigma^{(X)}_{\mathrm{RR,S}}$ determines different subtraction schemes. The goal is to choose these approximations such that their integrals over the unresolved phase space can be carried out analytically or their expansion in $\epsilon$ can be easily performed before resorting to numerical methods. In order to use numerical techniques, it is necessary for every term in round brackets within the above equations to be integrable in four dimensions. However, in principle, one can afford for each of these terms to have a Laurent series in $\epsilon$, as long as the coefficients of the series can be integrated numerically.

In general, there is a lot of freedom in how the subtraction terms can be precisely defined. The key challenges involve correctly parametrizing the singular regions and avoiding any double counting. It is also important to note that each contribution differs with its phase-space configuration; hence, when the integrated subtraction terms are added back, care is needed to account for this correctly. Subtraction schemes primarily differ in their handling of these challenges.

The LASS scheme offers an elegant definition of the subtraction terms for the final state radiation for massless processes, which makes it possible to carry out the integration over the unresolved phase space analytically. The scheme was first introduced in Ref. [27], Ref. [29] describes the analytical integration procedure of various subtraction terms. In Ref. [28] the method was optimized by taking advantage of the fact that certain subtraction terms can be combined together and expressed using hard-collinear splitting kernels and the phase-space mappings were refined.

In this chapter, we review the main aspects of the LASS scheme and quote the core formulas which we will need to refer to while discussing the details of our implementation. To fully understand the motivation behind certain definitions, the reader is advised to check Refs. [27, 28].

## 3.1 Local Analytic Sector Subtraction at NLO

The general structure of NLO differential cross section for a process with $n$ final-state partons at Born level can be written as

$$\frac{d\sigma_{\text{NLO}}}{dX} = \int d\Phi_n \, V \, \delta_n(X) + \int d\Phi_{n+1} \, R \, \delta_{n+1}(X), \tag{3.10}$$

where $V$ and $R$ are the virtual and real contributions, respectively, and $\delta_n(X)$ and $\delta_{n+1}(X)$ fix the value of an infrared-safe observable $X$ to its prescribed value in $n$-body and $(n+1)$-body kinematics.

The subtraction is achieved by adding and subtracting a counterterm $\overline{K}$ that reproduces all singularities of the real contribution:

$$\frac{d\sigma_{\text{NLO}}}{dX} = \int d\Phi_n \, (V + I) \, \delta_n(X) + \int \left( d\Phi_{n+1} \, R \, \delta_{n+1}(X) - d\widehat{\Phi}_{n+1} \, \overline{K} \, \delta_n(X) \right), \tag{3.11}$$

where $I = \int d\widehat{\Phi}_{\text{rad}} \, \overline{K}$ is the integrated counterterm.

### 3.1.1 Sector Functions

A partition of the real-radiation phase space is introduced using sector functions $\mathcal{W}_{ij}$ inspired by the FKS method [4]:

$$\sum_{i,\, j \neq i} \mathcal{W}_{ij} \;=\; 1\,, \tag{3.12}$$

$$\mathbf{S}_i \, \mathcal{W}_{ab} \;=\; 0\,, \qquad \forall \, i \neq a\,, \tag{3.13}$$

$$\mathbf{C}_{ij} \, \mathcal{W}_{ab} \;=\; 0\,, \qquad \forall \, ab \notin \pi(ij)\,, \tag{3.14}$$

$$\mathbf{S}_i \sum_{k \neq i} \mathcal{W}_{ik} \;=\; 1\,, \qquad \mathbf{C}_{ij} \sum_{ab \, \in \, \pi(ij)} \mathcal{W}_{ab} \;=\; 1\,, \tag{3.15}$$

where $\mathbf{S}_i$ is the soft projection operator. It acts on the sector functions $\mathcal{W}_{ij}$ and selects only the soft singular configuration where parton $i$ becomes soft (its momentum approaches zero). Specifically, the property in Eq. (3.13) means that $\mathbf{S}_i$ acting on $\mathcal{W}_{ab}$ gives zero unless $a = i$, i.e., it selects only the soft singularity associated with

parton $i$. $\mathbf{C}_{ij}$ is the collinear projection operator. It acts on the sector functions $\mathcal{W}_{ij}$ and selects only the collinear singular configuration where partons $i$ and $j$ become collinear (their relative transverse momentum approaches zero). The property in Eq. (3.15) means that $\mathbf{C}_{ij}$ acting on $\mathcal{W}_{ab}$ gives zero unless $ab = ij$ or $ab = ji$, i.e., it selects only the collinear singularity associated with the $ij$ pair of partons. In the LASS formalism sectors at NLO level are parametrized as follows:

$$\mathcal{W}_{ij} \equiv \frac{\sigma_{ij}}{\sum_{k\neq l}\sigma_{kl}}, \tag{3.16}$$

where

$$\sigma_{ij} \equiv \frac{1}{e_i w_{ij}}, \qquad e_i \equiv \frac{s_{qi}}{s}, \qquad w_{ij} \equiv \frac{s s_{ij}}{s_{qi}s_{qj}}. \tag{3.17}$$

Upon substitution of Eq. (3.17) into Eq. (3.16) and accounting for the standard definition of $s_{ij} = 2k_i \cdot k_j$ one can easily check that conditions (3.12), (3.13), (3.14) and (3.15) are satisfied.

### 3.1.2 Definition of Local Counterterms and phase-space mapping

It is well understood that the phase-space singularities in the real radiation stem from the single soft and collinear limits. Thus, the candidate subtraction term at NLO level is formulated as follows:

$$K = \sum_i \sum_{i\neq j} K_{ij} = \sum_i \sum_{j\neq i} \mathbf{L}_{ij}^{(1)} R\,\mathcal{W}_{ij} \equiv \sum_i \sum_{j\neq i} \Big[\mathbf{S}_i + \mathbf{C}_{ij}(1-\mathbf{S}_i)\Big] R\,\mathcal{W}_{ij}. \tag{3.18}$$

The factorized structure of the real matrix element in unresolved limits enables expressing each contribution in Eq. (3.18) as a universal singular kernel and an appropriate Born-like matrix element. The Born-level matrix elements depend on kinematics that are not on-shell or momentum-conserving outside of the corresponding exact singular limit. A key ingredient of the local analytic sector subtraction is the momentum mapping, which factorizes the $n+1$ phase space into a single radiative phase space $d\Phi_{\text{rad}}$ and an $n$-body resolved phase space. This allows integrating the counterterm over the radiative phase space only, while forcing the Born kinematics to be on-shell and momentum-conserving throughout the phase space.

The mapping procedure has flexibility, exploited by introducing a Catani-Seymour final-state mapping [5]. This defines a set of $n$ on-shell momenta $\{\bar{k}\}^{(abc)}$ by combining three final-state momenta $k_a, k_b, k_c$ as shown in Eq. (3.19):

$$\{\bar{k}\}^{(abc)} \equiv \left\{ \{k\}_{\not a \not b \not c}, \bar{k}_b^{(abc)}, \bar{k}_c^{(abc)} \right\}, \qquad \text{where} \tag{3.19}$$

$$\bar{k}_b^{(abc)} = k_a + k_b - \frac{s_{ab}}{s_{ac}+s_{bc}} k_c \,, \bar{k}_c^{(abc)} = \frac{s_{abc}}{s_{ac}+s_{bc}} k_c \,, \bar{k}_i^{(abc)} = k_i \,, \quad \forall i \neq a,b,c \,. \tag{3.20}$$

The notation $\{k\}_{\not a \not b \not c}$ states that we are eliminating the momenta $k_i$, with $i = a, b, c$, from the initial set of $n+1$ momenta. Choosing $a, b, c$ according to the specific counterterm contribution allows for an analytical integration using standard techniques. The phase space factorizes in terms of the Catani-Seymour parameters $y$ and $z$:

$$y = s_{ab}/s_{abc} \,, \quad z = s_{ac}/(s_{ac}+s_{bc}) \,, \tag{3.21}$$

where $0 \leq y \leq 1$ and $0 \leq z \leq 1$.

The factorized phase-space can be expressed as:

$$d\Phi_{n+1} = d\Phi_n^{(abc)} \, d\Phi_{\text{rad}}^{(abc)} \,, \quad d\Phi_{\text{rad}}^{(abc)} \equiv d\Phi_{\text{rad}}\left(\bar{s}_{bc}^{(abc)}; y, z, \phi\right) . \tag{3.22}$$

The explicit expression of the radiative phase-space $\mathrm{d}\Phi_{\text{rad}}$ can be found in [27].

As for the specific mapping, for the soft limit, $a = i$ and $b = l, c = m$ are chosen, where $i$ identifies the soft parton, and $l, m$ the emitters. For the hard-collinear component, $a = i, b = j$, and $c = r$, with $i, j$ being the collinear partons, and $r$ an on-shell spectator. In the remapped kinematics, the contributions to Eq. (3.18) are given by Eqs. (3.23), (3.24) and (3.25):

$$\overline{\mathbf{S}}_i \, R = -\mathcal{N}_1 \sum_{\substack{l \neq i \\ m \neq i}} \mathcal{I}_{lm}^{(i)} \, B_{lm}(\{\bar{k}\}^{(ilm)}) \,, \tag{3.23}$$

$$\overline{\mathbf{C}}_{ij} \, R = \frac{\mathcal{N}_1}{s_{ij}} \, P_{ij}^{\mu\nu} \, B_{\mu\nu}(\{\bar{k}\}^{(ijr)}) \,, \tag{3.24}$$

$$\overline{\mathbf{S}}_i \, \overline{\mathbf{C}}_{ij} \, R = 2\mathcal{N}_1 \, C_{f_j} \, \mathcal{I}_{jr}^{(i)} \, B(\{\bar{k}\}^{(ijr)}) \,. \tag{3.25}$$

Here $\mathcal{I}_{lm}^{(i)} = \delta_{f_i g} \, s_{lm}/(s_{il} \, s_{im})$ is the eikonal kernel relative to parton $i$, $B_{lm}$ is the color-correlated Born matrix element, $P_{ij}^{\mu\nu}$ is the spin-dependent Altarelli-Parisi splitting

function, $B_{\mu\nu}$ is the spin-correlated Born matrix element (obtained by removing the polarization vector of emitted gluon with index $i$), $C_{f_j}$ is the quadratic Casimir relevant for the color representation of parton $j$ and $\mathcal{N}_1 = 8\pi\alpha_s(\mu^2 e^{\gamma_E}/(4\pi))^\epsilon$ is a normalization factor.

In terms of these improved limits the local counterterm $\overline{K}_{ij}$ for sector $ij$ is defined as:

$$\overline{K}_{ij} = (\overline{\mathbf{S}}_i + \overline{\mathbf{C}}_{ij} - \overline{\mathbf{S}}_i\,\overline{\mathbf{C}}_{ij})R\,\mathcal{W}_{ij}\,. \tag{3.26}$$

This expression is ready to be substituted in Eq. (3.11) and thanks to the mapping choices discussed above it is also straightforward to integrate.

### 3.1.3 Counterterm Integration

The integrated counterterm $I$ is obtained by summing over all sectors and integrating the counterterm in the radiation phase space:

$$I = \int d\hat{\Phi}_{\text{rad}}\,\overline{K} = I^{\,\text{s}} + I^{\,\text{hc}}\,, \tag{3.27}$$

where $I^{\,\text{s}}$ and $I^{\,\text{hc}}$ are the integrated soft and hard-collinear counterterms, respectively. The integration procedure is straightforward, and in Chapter 4, we will demonstrate more complex integration procedures. Therefore, we will avoid further discussion here and quote the results from Ref. [27].

The integrated counterterms are given by

$$\begin{aligned} I^{\,\text{s}} = -\frac{\alpha_s}{2\pi}\left(\frac{\mu^2}{s}\right)^\epsilon \Bigg[ &\sum_l C_{f_l}\, B(\{\bar{k}\}) \left(\frac{1}{\epsilon^2} + \frac{2}{\epsilon} + 6 - \frac{7}{2}\zeta_2\right) \\ &+ \sum_{l,\,m\neq l} B_{lm}(\{\bar{k}\})\,\ln\overline{\eta}_{lm}\left(\frac{1}{\epsilon} + 2 - \frac{1}{2}\ln\overline{\eta}_{lm}\right)\Bigg] + \mathcal{O}(\epsilon), \end{aligned} \tag{3.28}$$

$$\begin{aligned} I^{\,\text{hc}} = -\frac{\alpha_s}{2\pi}\left(\frac{\mu^2}{s}\right)^\epsilon \sum_p B(\{\bar{k}\}) \Bigg[ &\delta_{f_p g}\,\frac{C_A + 4\,T_R N_f}{6}\left(\frac{1}{\epsilon} + \frac{8}{3} - \ln\overline{\eta}_{pr}\right) \\ &+ \delta_{f_p\{q,\bar{q}\}}\,\frac{C_F}{2}\left(\frac{1}{\epsilon} + 2 - \ln\overline{\eta}_{pr}\right)\Bigg] + \mathcal{O}(\epsilon), \end{aligned} \tag{3.29}$$

where $\overline{\eta}_{ij} = s_{ijk}/s$ and $C_A$, $C_F$, and $T_R$ are the Casimir eigenvalues of the SU($N_c$) gauge group.

It was checked that the pole part of Eq. (3.27) correctly reproduces the poles of one-loop virtual correction, which are well known e.g. from [69], namely:

$$V_{\text{poles}} = \langle \mathcal{M}_0 | I^{(1)}_{\text{Catani}} | \mathcal{M}_0 \rangle, \tag{3.30}$$

where $\mathcal{M}_0$ is a Born amplitue and $I^{(1)}_{\text{Catani}}$ is defined as:

$$I^{(1)}_{\text{Catani}}(\epsilon, \mu^2; \{p\}) = \frac{1}{2}\frac{e^{-\epsilon\psi(1)}}{\Gamma(1-\epsilon)} \sum_i \frac{1}{\boldsymbol{T}_i^2}\, \mathcal{V}_i^{\text{sing}}(\epsilon) \sum_{j\neq i} \boldsymbol{T}_i \cdot \boldsymbol{T}_j \left(\frac{\mu^2 e^{-i\lambda_{ij}\pi}}{2p_i \cdot p_j}\right)^{\epsilon} , \tag{3.31}$$

where $e^{-i\lambda_{ij}\pi}$ is the unitarity phase ($\lambda_{ij} = +1$ if $i$ and $j$ are both incoming or outgoing partons and $\lambda_{ij} = 0$ otherwise) and the singular (for $\epsilon \to 0$) function $\mathcal{V}_i^{\text{sing}}(\epsilon)$ depends only on the parton flavor and is given by

$$\mathcal{V}_i^{\text{sing}}(\epsilon) = \boldsymbol{T}_i^2 \frac{1}{\epsilon^2} + \gamma_i \frac{1}{\epsilon} \ . \tag{3.32}$$

The flavor coefficients $\boldsymbol{T}_i^2$ and $\gamma_i$ are

$$\begin{aligned} \boldsymbol{T}_q^2 = \boldsymbol{T}_{\bar{q}}^2 = C_F \ , \qquad & \boldsymbol{T}_g^2 = C_A \ , \\ \gamma_q = \gamma_{\bar{q}} = \frac{3}{2} C_F \ , \qquad & \gamma_g = \frac{11}{6} C_A - \frac{2}{3} T_R N_f \ . \end{aligned} \tag{3.33}$$

## 3.2 Local Analytic Sector Subtraction at NNLO

The same general principles described in the previous section apply in case of the NNLO subtraction procedure as well. However, at NNLO the singularity content of individual contributions is more involved and this makes the whole analysis more cumbersome. One starts again by examining of the general structure of the differential cross section at NNLO, which is given as:

$$\frac{d\sigma_{\text{NNLO}}}{dX} = \int d\Phi_n \, VV \, \delta_n(X) + \int d\Phi_{n+1} \, RV \, \delta_{n+1}(X) + \int d\Phi_{n+2} \, RR \, \delta_{n+2}(X) \,, \tag{3.34}$$

where $VV$, $RV$ and $RR$ are defined according to Eq (3.5). Similar to the NLO case, the goal is to modify each contribution such that they are finite and integrable. To

achieve this goal, one has to correctly account for the singularity structure of each contribution:

- Real-real radiation features no explicit $\epsilon$ poles; however, it is plagued by phase-space singularities arising from unresolved radiation, which might be either single or double.
- Real-virtual radiation contains explicit $\epsilon$ poles starting from the order $\frac{1}{\epsilon^2}$, which originate from the virtual correction. It also features phase-space singularities due to single unresolved radiation.
- The virtual-virtual correction is free from phase-space singularities, but it exhibits explicit poles beginning at the order $\frac{1}{\epsilon^4}$.

Thus, the differential cross-section can be rewritten in terms of the subtracted contributions:

$$\frac{d\sigma_{\text{NNLO}}}{dX} = \int d\Phi_n \, VV_{\text{sub}}(X) + \int d\Phi_{n+1} \, RV_{\text{sub}}(X) + \int d\Phi_{n+2} \, RR_{\text{sub}}(X) \,, \quad (3.35)$$

where

$$RR_{\text{sub}}(X) \equiv RR\,\delta_{n+2}(X) - K^{(\mathbf{1})}\,\delta_{n+1}(X) - \left(K^{(\mathbf{2})} - K^{(\mathbf{12})}\right)\delta_n(X) \,, \quad (3.36)$$

$$RV_{\text{sub}}(X) \equiv \left(RV + I^{(\mathbf{1})}\right)\delta_{n+1}(X) - \left(K^{(\mathbf{RV})} + I^{(\mathbf{12})}\right)\delta_n(X) \,, \quad (3.37)$$

$$VV_{\text{sub}}(X) \equiv \left(VV + I^{(\mathbf{2})} + I^{(\mathbf{RV})}\right)\delta_n(X) \,. \quad (3.38)$$

$K^{(\mathbf{1})}$ is a counterterm that accounts for the single unresolved singularities, $K^{(\mathbf{2})}$ accounts for the double unresolved singularities, and $K^{(\mathbf{12})}$ is introduced to avoid double counting by removing the overlap between $K^{(\mathbf{1})}$ and $K^{(\mathbf{2})}$. At RV level there is still a possibility to introduce an additional subtraction term $K^{(\mathbf{RV})}$ which deals with the phase-space singularities of RV contribution. So in total one needs 4 kind of subtraction terms. The integrated versions of those subtraction terms are then added back. They are defined as:

$$I^{(\mathbf{1})} \equiv \int d\Phi_{\text{rad}} \, K^{(\mathbf{1})} \,, \qquad I^{(\mathbf{2})} \equiv \int d\Phi_{\text{rad},2} \, K^{(\mathbf{2})} \,,$$
$$I^{(\mathbf{12})} \equiv \int d\Phi_{\text{rad}} \, K^{(\mathbf{12})} \,, \qquad I^{(\mathbf{RV})} \equiv \int d\Phi_{\text{rad}} \, K^{(\mathbf{RV})} \,, \quad (3.39)$$

where $\Phi_{\text{rad}}$ parametrizes the phase-space of the single unresolved radiation and $\Phi_{\text{rad},2}$ - the phase-space of the double unresolved radiation.

In this way, if all the subtraction terms are parametrized correctly by the virtue of KLN theorem Eq. (3.35) will be indeed finite and integrable.

### 3.2.1 Construction of the subtraction terms

The parametrization of the subtraction terms begins with the construction of the sector functions. To correctly account for every possible singular configuration at the NNLO level, one must consider sector functions with four indices. The sectors are parametrized as follows:

$$\mathcal{W}_{abcd} \;=\; \frac{\sigma_{abcd}}{\sigma}\,, \qquad \sigma \;=\; \sum_{a,b\neq a}\;\sum_{\substack{c\neq a\\ d\neq a,c}} \sigma_{abcd}\,, \tag{3.40}$$

with the summation rule:

$$\sum_{a,b\neq a}\;\sum_{\substack{c\neq a\\ d\neq a,c}} \mathcal{W}_{abcd} \;=\; 1\,. \tag{3.41}$$

After introducing such partitioning one can rewrite $RR$ matrix element as:

$$\begin{aligned} RR \;&=\; \sum_{i,\,j\neq i}\;\sum_{k\neq i}\;\sum_{l\neq i,k} RR\;\mathcal{W}_{ijkl} \\ &=\; \sum_{i,\,j\neq i}\;\sum_{k\neq i,j}\left[RR\;\mathcal{W}_{ijjk} + RR\;\mathcal{W}_{ijkj} + \sum_{l\neq i,j,k} RR\;\mathcal{W}_{ijkl}\right]. \end{aligned} \tag{3.42}$$

Our choice for the functions $\sigma_{abcd}$ is given by

$$\sigma_{abcd} \;=\; \frac{1}{(e_a\,w_{ab})^{\alpha}}\,\frac{1}{(e_c+\delta_{bc}\,e_a)\,w_{cd}}\,, \qquad \alpha > 1\,. \tag{3.43}$$

Once these definitions are fixed one can identify the fundamental limits discussed previously that will impact each topological configuration. To fully describe the singularity structure of $RR$ the following limits should be considered:

$$RR\;\mathcal{W}_{ijjk}\;:\quad \mathbf{S}_i\,,\quad \mathbf{C}_{ij}\,,\quad \mathbf{S}_{ij}\,,\quad \mathbf{C}_{ijk}\,,\quad \mathbf{SC}_{ijk}\,;$$

$$\begin{aligned} RR\ \mathcal{W}_{ijkj}\ :&\quad \mathbf{S}_i\,,\quad \mathbf{C}_{ij}\,,\quad \mathbf{S}_{ik}\,,\quad \mathbf{C}_{ijk}\,,\quad \mathbf{SC}_{ijk}\,,\quad \mathbf{SC}_{kij}\,; \\ RR\ \mathcal{W}_{ijkl}\ :&\quad \mathbf{S}_i\,,\quad \mathbf{C}_{ij}\,,\quad \mathbf{S}_{ik}\,,\quad \mathbf{C}_{ijkl}\,,\quad \mathbf{SC}_{ikl}\,,\quad \mathbf{SC}_{kij}\,. \end{aligned} \tag{3.44}$$

In the expression above, $\mathbf{S}_{ij}$ parametrizes the situation when both partons $i$ and $j$ become soft, $\mathbf{C}_{ijk}$ parametrizes the scenario where all three partons $i$, $j$, and $k$ become collinear. Moreover, $\mathbf{SC}_{ijk}$ describes the configuration involving parton $i$ being soft and collinear to the combined system $(jk)$, which acts as the emitter of $j$ and $k$. Lastly, $\mathbf{C}_{ijkl}$ represents the limit when the parton pairs $(ij)$ and $(kl)$ become collinear to each other. The other limits $\mathbf{S}_i$ and $\mathbf{C}_{ij}$ were already introduced previously.

To explicitly parametrize these limits and enable analytic integration, one must perform a momentum mapping, factorizing the two-body phase-space such that the resulting $n$ momenta conserve energy and momentum. The particular momentum mapping employed here utilizes the Catani-Seymour mapping, similar to the approach used previously at NLO. At the NNLO level, however, multiple possibilities must be considered, depending on the number of particles involved in calculating a given limit. Three distinct cases have to be considered:

- To map six final-state particles, one fixes the momenta $k_a$, $k_b$, $k_c$, $k_d$, $k_e$, $k_f$ (all different) and constructs the $n$-tuple (without $k_a$ and $k_b$)

$$\{\bar{k}\}^{(acd,bef)} \;=\; \left\{\{k\}_{\not a\not b\not c\not d\not e\not f},\, \bar{k}_c^{(acd,bef)}, \bar{k}_d^{(acd,bef)}, \bar{k}_e^{(acd,bef)}, \bar{k}_f^{(acd,bef)}\right\}, \tag{3.45}$$

  with

$$\begin{aligned} \bar{k}_c^{(acd,bef)} &= k_a + k_c - \frac{s_{ac}}{s_{[ac]d}}\, k_d\,, & \bar{k}_d^{(acd,bef)} &= \frac{s_{acd}}{s_{[ac]d}}\, k_d\,, \\ \bar{k}_e^{(acd,bef)} &= k_b + k_e - \frac{s_{be}}{s_{[be]f}}\, k_f\,, & \bar{k}_f^{(acd,bef)} &= \frac{s_{bef}}{s_{[be]f}}\, k_f\,, \end{aligned} \tag{3.46}$$

  while all other momenta are left unchanged ($\bar{k}_n^{(acd,bef)} = k_n\,,\ n{\neq}a,b,c,d,e,f$), where following definition was introduced: $s_{[ab]c} = s_{ac} + s_{bc}$.

- For five particles the following labeling is used: $k_a$, $k_b$, $k_c$, $k_d$, $k_e$ (all different). The $n$-tuple (without $k_a$ and $k_b$) is constructed as follows:

$$\{\bar{k}\}^{(acd,bed)} \;=\; \left\{\{k\}_{\not a\not b\not c\not d\not e},\, \bar{k}_c^{(acd,bed)}, \bar{k}_d^{(acd,bed)}, \bar{k}_e^{(acd,bed)}\right\}, \tag{3.47}$$

with

$$\begin{aligned}
\bar{k}_c^{(acd,bed)} &= k_a + k_c - \frac{s_{ac}}{s_{[ac]d}}\, k_d\,, \qquad & \bar{k}_d^{(acd,bed)} &= \left(1 + \frac{s_{ac}}{s_{[ac]d}} + \frac{s_{be}}{s_{[be]d}}\right) k_d\,, \\
\bar{k}_e^{(acd,bed)} &= k_b + k_e - \frac{s_{be}}{s_{[be]d}}\, k_d\,, & &
\end{aligned} \tag{3.48}$$

while all other momenta are left unchanged ($\bar{k}_n^{(acd,bed)} = k_n\,,\ n{\neq}a,b,c,d,e$).

- And lastly, for 4 particles: $k_a$, $k_b$, $k_c$, $k_d$ are fixed (all different) and the $n$-tuple (without $k_a$ and $k_b$) is constructed as

$$\{\bar{k}\}^{(acd,bcd)} = \{\bar{k}\}^{(abc,bcd)} = \{\bar{k}\}^{(abcd)} = \left\{ \{k\}_{\not a \not b \not c \not d},\, \bar{k}_c^{(abcd)}, \bar{k}_d^{(abcd)} \right\}, \tag{3.49}$$

with

$$\bar{k}_c^{(abcd)} = k_a + k_b + k_c - \frac{s_{abc}}{s_{ad} + s_{bd} + s_{cd}}\, k_d\,, \qquad \bar{k}_d^{(abcd)} = \frac{s_{abcd}}{s_{ad} + s_{bd} + s_{cd}}\, k_d\,, \tag{3.50}$$

while all other momenta are left unchanged ($\bar{k}_n^{(abcd)} = k_n\,,\ n{\neq}a,b,c,d$).

Once all the momenta mappings are correctly defined it is possible to express the counterterms in terms of the remapped momenta and sector functions as follows:

$$K^{(\mathbf{1})} = \sum_{i,j\neq i} \sum_{\substack{k\neq i \\ k>j}} \overline{\mathbf{S}}_i\, RR\, \overline{\mathcal{Z}}_{jk} + \sum_{i,j>i} \sum_{k\neq i} \sum_{\substack{l\neq i \\ l>k}} \overline{\mathbf{HC}}_{ij}\, RR\, \overline{\mathcal{Z}}_{kl}\,. \tag{3.51}$$

$$\begin{aligned}
K^{(\mathbf{2})} = {} & \sum_{i,j>i} \overline{\mathbf{S}}_{ij}\, RR + \sum_{i,j\neq i} \sum_{\substack{k\neq i \\ k>j}} \overline{\mathbf{SHC}}_{ijk} \left(1 - \overline{\mathbf{C}}_{ijk}\right) RR \\
& + \sum_{i,j>i} \sum_{k>j} \overline{\mathbf{HC}}_{ijk} RR + \sum_{i,j>i} \sum_{\substack{k\neq j \\ k>i}} \sum_{\substack{l\neq j \\ l>k}} \overline{\mathbf{HC}}_{ijkl}\, RR\,.
\end{aligned} \tag{3.52}$$

$$\begin{aligned}
K^{(\mathbf{12})} = {} & \sum_{i,j\neq i} \overline{\mathbf{S}}_i \left[ \sum_{k\neq i,j} \overline{\mathbf{S}}_{ij}\, RR\, \overline{\mathcal{Z}}_{\mathrm{s},jk} + \sum_{\substack{k\neq i \\ k>j}} \left( \overline{\mathbf{SHC}}_{ijk} + \overline{\mathbf{HC}}_{ijk}^{(\mathbf{s})} \right) RR \right] \\
& + \sum_{i,j>i} \sum_{k\neq i,j} \overline{\mathbf{HC}}_{ij} \left[ \overline{\mathbf{S}}_{ij}\, RR\, \overline{\mathcal{Z}}_{\mathrm{s},jk} + \sum_{l\neq i,k} \overline{\mathbf{SC}}_{kij}\, RR\, \overline{\mathcal{Z}}_{\mathrm{s},kl} \right.
\end{aligned}$$

$$+ \overline{\mathbf{HC}}^{(\mathbf{c})}_{ijk}\, RR + \sum_{\substack{l\neq i,j \\ l>k}} \overline{\mathbf{HC}}^{(\mathbf{c})}_{ijkl}\, RR \Big] . \tag{3.53}$$

It is important to note that the counterterms above are all expressed in terms of $\mathcal{Z}$ sector functions instead of $\mathcal{W}$. These are the symmetrized versions of the previously defined $\mathcal{W}$-type sectors. The three particle sectors are symmetrized in the following way:

$$\begin{aligned} \mathcal{Z}_{ijk} &= \mathcal{W}_{ijjk} + \mathcal{W}_{ikkj} + \mathcal{W}_{jiik} + \mathcal{W}_{jkki} + \mathcal{W}_{kiij} + \mathcal{W}_{kjji} \\ &+ \mathcal{W}_{ijkj} + \mathcal{W}_{ikjk} + \mathcal{W}_{jiki} + \mathcal{W}_{jkik} + \mathcal{W}_{kiji} + \mathcal{W}_{kjij} . \end{aligned} \tag{3.54}$$

Similarly, in the four-particle sectors $\mathcal{W}_{ijkl}$, the symmetries of the improved limit $\overline{\mathbf{C}}_{ijkl}$ are utilized :

$$\mathcal{Z}_{ijkl} = \mathcal{W}_{ijkl} + \mathcal{W}_{ijlk} + \mathcal{W}_{jikl} + \mathcal{W}_{jilk} + \mathcal{W}_{klij} + \mathcal{W}_{klji} + \mathcal{W}_{lkij} + \mathcal{W}_{lkji} . \tag{3.55}$$

The two index symmetrized sectors are defined as:

$$\mathcal{Z}^{(\alpha)}_{ij} \equiv \mathcal{W}^{(\alpha)}_{ij} + \mathcal{W}^{(\alpha)}_{ji} , \qquad \mathcal{Z}_{ij} \equiv \mathcal{Z}^{(1)}_{ij} , \tag{3.56}$$

and

$$\mathcal{Z}^{(\alpha)}_{\mathrm{s},ij} \equiv \mathbf{S}_i\, \mathcal{Z}^{(\alpha)}_{ij} = \mathbf{S}_i\, \mathcal{W}^{(\alpha)}_{ij} = \frac{\frac{1}{w^{\alpha}_{ij}}}{\sum\limits_{l\neq i} \frac{1}{w^{\alpha}_{il}}} , \qquad \mathcal{Z}_{\mathrm{s},ij} \equiv \mathcal{Z}^{(1)}_{\mathrm{s},ij} . \tag{3.57}$$

The symmetrization of the sector functions allows us to avoid the proliferation of the terms in Eqs. (3.51) - (3.53) and combine certain limits under the newly defined hard-collinear limits:

$$\overline{\mathbf{HC}}_{ij} \equiv \overline{\mathbf{C}}_{ij} \left(1 - \overline{\mathbf{S}}_i - \overline{\mathbf{S}}_j\right) , \tag{3.58}$$

$$\overline{\mathbf{HC}}_{abc} \equiv \overline{\mathbf{C}}_{abc} \left(1 - \overline{\mathbf{S}}_{ab} - \overline{\mathbf{S}}_{bc} - \overline{\mathbf{S}}_{ac}\right) , \tag{3.59}$$

$$\overline{\mathbf{HC}}^{(\mathbf{s})}_{abc} \equiv \overline{\mathbf{C}}_{abc} \left(1 - \overline{\mathbf{S}}_{ab} - \overline{\mathbf{S}}_{ac}\right) \left(1 - \overline{\mathbf{SC}}_{abc}\right) , \tag{3.60}$$

$$\overline{\mathbf{HC}}^{(\mathbf{c})}_{abc} \equiv \overline{\mathbf{C}}_{abc} \left(1 - \overline{\mathbf{S}}_{ab} - \overline{\mathbf{SC}}_{cab}\right) , \tag{3.61}$$

$$\overline{\mathbf{HC}}_{abcd} \equiv \overline{\mathbf{C}}_{abcd} \left(1 + \overline{\mathbf{S}}_{ac} + \overline{\mathbf{S}}_{bc} + \overline{\mathbf{S}}_{ad} + \overline{\mathbf{S}}_{bd} - \overline{\mathbf{SC}}_{acd}\right.$$

$$-\overline{\mathbf{SC}}_{bcd} - \overline{\mathbf{SC}}_{cab} - \overline{\mathbf{SC}}_{dab}\big) \,, \tag{3.62}$$

$$\overline{\mathbf{HC}}^{(\mathbf{c})}_{abcd} \equiv \overline{\mathbf{C}}_{abcd}\left(1 - \overline{\mathbf{SC}}_{cab} - \overline{\mathbf{SC}}_{dab}\right) , \tag{3.63}$$

$$\overline{\mathbf{SHC}}_{abc} \equiv \overline{\mathbf{SC}}_{abc}\left(1 - \overline{\mathbf{S}}_{ab} - \overline{\mathbf{S}}_{ac}\right) . \tag{3.64}$$

The explicit parametrizations of how each limit in Eqs. (3.51) - (3.53) affects an $RR$ matrix element are given in Ref. [28].

The analysis of the $RV$ contribution is straightforward: the $RV$ matrix element features explicit $\epsilon$-poles, which by construction will get canceled against $I^{(\mathbf{1})}$. However, both of them also feature phase-space singularities, and these need to be addressed as well. The phase-space singularities of $I^{(\mathbf{1})}$ will be handled by construction with $I^{(\mathbf{12})}$, and the addition-subtraction term $K^{(\mathbf{RV})}$ should be constructed such that it correctly accounts for the phase-space singularities of $RV$. This can be achieved by using the following definition of $K^{(\mathbf{RV})}$:

$$K^{(\mathbf{RV})}_{ij} = \Big[\overline{\mathbf{S}}_i + \overline{\mathbf{C}}_{ij}\left(1 - \overline{\mathbf{S}}_i\right)\Big] RV\, \mathcal{W}_{ij} + \Delta_{ij} \,, \tag{3.65}$$

where the additional $\Delta_{ij}$ terms are being introduced. They are absolutely necessary, because without it $K^{(\mathbf{RV})}$ would fail to satisfy the condition of canceling the poles of $I^{(\mathbf{12})}_{ij}$, which arises from integrating the strongly-ordered counterterm over the phase space of the most unresolved radiation. This mismatch stems from subtleties associated with the specific phase-space mappings employed to define the improved limits in the real-virtual counterterm, as well as the kinematics of the collinear sector. To address this issue, the authors of Refs. [27, 28] introduce additional delta terms, $\Delta_{ij}$, in the refined definition of $K^{(\mathbf{RV})}_{ij}$. These terms are carefully constructed to capture the mismatched contributions, thereby ensuring the desired cancellation of poles without introducing new phase-space singularities, while preserving the correct singular behavior dictated by the factorization properties of the theory. Because the whole expression should be free of poles, one gets following conditions for the $\Delta_{ij}$ terms:

$$\begin{aligned}
\Big[\overline{\mathbf{S}}_i\, RV\, \mathcal{W}_{ij} + \Big(\Delta_{\mathrm{S},i} + I^{(\mathbf{12})}_{\mathrm{S},ij}\Big)\, \mathcal{W}_{\mathrm{s},ij}\Big]_{\text{poles}} &= 0 \,, \\
\Big[\overline{\mathbf{C}}_{ij}\, RV\, \mathcal{W}_{ij} + \Big(\Delta_{\mathrm{C},ij} + I^{(\mathbf{12})}_{\mathrm{C},ij}\Big)\Big]_{\text{poles}} &= 0 \,, \\
\Big[\overline{\mathbf{S}}_i\, \overline{\mathbf{C}}_{ij}\, RV\, \mathcal{W}_{ij} + \Big(\Delta_{\mathrm{SC},ij} + I^{(\mathbf{12})}_{\mathrm{SC},ij}\Big)\Big]_{\text{poles}} &= 0 \,,
\end{aligned} \tag{3.66}$$

where $\Delta_{ij}$ was decomposed as:

$$\Delta_{ij} \equiv \Delta_{\mathrm{S},i}\,\mathcal{W}_{\mathrm{s},ij} + \Delta_{\mathrm{C},ij} - \Delta_{\mathrm{SC},ij}\,. \tag{3.67}$$

The conditions given in Eq. (3.66) can be used to determine the explicit expressions for $\Delta_{ij}$. We will come back to this topic in Chapter 4 once we describe how the integration of the subtraction terms works.

# Chapter 4

# Integration of NNLO counterterms

Once the subtraction terms have been explicitly defined, the integration over the unresolved phase-space is, in most cases, a fairly straightforward procedure. Every necessary ingredient for the integration is provided in Ref. [29]. In the majority of cases, the arising integrals reduce to the Euler integral of the first kind, and it is quite trivial to obtain their $\epsilon$ expansions. The most complicated integrals arise from the terms which contain the triple-colinear limits $\mathcal{C}_{ijk}$. For example Eq. (3.52) features a term $\mathbf{C}_{ijk}\,RR$ which is defined as:

$$\mathbf{C}_{ijk}\,RR \;=\; \frac{\mathcal{N}_1^2}{s_{ijk}^2}\left[P_{ijk}\,B(\{k\}_{[ijk]}) + Q_{ijk}^{\mu\nu}\,B_{\mu\nu}(\{k\}_{[ijk]})\right], \tag{4.1}$$

where $P_{ijk}$ and $Q_{ijk}$ are the collinear and azimuthal splitting kernels respectively and their expressions can be found in [70]. Most of these splitting kernels have an intricate structure, often resulting in integrands with a complex form. Although it is possible to integrate them analytically using conventional methods, the procedure can be somewhat involved. While Ref. [29] already contains a strategy to perform such integrations, we believe it is worthwhile to elucidate this procedure more clearly and provide the explicit expressions of all the master integrals that appear in this calculation. Moreover, this approach provides a valuable cross-check of the lengthy expressions against potential mistakes and typographical errors listed in Ref. [29]. Thus, in the next section, we will discuss how this integration process works.

## 4.1 Integration of the triple-collinear splitting kernels

According to Eq. (3.39) to obtain $I^{(2)}$ the terms appearing in $K^{(2)}$ should be integrated over the phase-space of the two unresolved particles. The integrals of the azimuthal tensor kernel $Q^{\mu\nu}_{ijk}$ vanish because of their Lorentz structure. Therefore, we only have to consider the integrals of this type:

$$J^{ijkr}_{\rm cc} \equiv \mathcal{N}_1^2 \int d\Phi^{(ijkr)}_{\rm rad,2} \frac{P_{ijk}}{s^2_{ijk}} \tag{4.2}$$

The radiative phase-space is expressed in terms of the Catani-Seymour mapping variables discussed in Chapter 3 as follows [29]:

$$\begin{aligned}\int d\Phi^{(abcd)}_{\rm rad,2} &= 2^{-2\epsilon}\, N^2(\epsilon) \left(\bar{s}^{(abcd)}_{cd}\right)^{2-2\epsilon} \int_0^1 dw' \int_0^1 dy' \int_0^1 dz' \int_0^\pi d\phi\, (\sin\phi)^{-2\epsilon} \int_0^1 dy \int_0^1 dz \\ &\times \Big[w'(1-w')\Big]^{-1/2-\epsilon} \Big[y'(1-y')^2 z'(1-z')\, y^2(1-y)^2 z(1-z)\Big]^{-\epsilon} \\ &\times (1-y')\, y(1-y)\,, \end{aligned} \tag{4.3}$$

where $w' = (1-\cos\phi')/2$ parametrizes the azimuth $\phi'$ of $k_a$ in the reference frame where $k_a + k_b + k_c$ is at rest, while $\phi$ is the azimuth of $\bar{k}^{(abc)}_b$.

The triple-collinear splitting kernels are expressed in terms of the kinematic invariants ($s_{ij}$, $s_{jk}$ and so on). To match the splitting kernels listed in [70] with the notation used in [29] one has to remap the indices ($1 \to i$, $j \to 2$, $k \to 3$) and perform the following substitution:

$$t_{ij,k} \equiv 2\frac{z_i s_{jk} - z_j s_{ik}}{z_i + z_j} + \frac{z_i - z_j}{z_i + z_j} s_{ij}. \tag{4.4}$$

In this way, we reproduce all the expressions of the splitting kernels listed in Ref. [29], except for the following:

$$\begin{aligned} P^{(2g)}_{ijk} &= C_F^2 \left\{ \frac{s^2_{ijk}\, z_k}{2 s_{ik} s_{jk}} \left[\frac{1 + z_k^2 - \epsilon z_{ij}^2}{z_i z_j} + \epsilon(1-\epsilon)\right] - (1-\epsilon)^2 \frac{s_{jk}}{s_{ik}} + \epsilon(1-\epsilon) \right. \\ &\qquad \left. + \frac{s_{ijk}}{s_{ik}} \left[\frac{z_k z_{jk} + z_{ik}^3 - \epsilon z_{ik} z_{ij}^2}{z_i z_j} + \epsilon\, z_{ik} + \epsilon^2 (1 + z_k)\right] \right\} \\ &\quad + C_F C_A \left\{ (1-\epsilon) \frac{s^2_{ijk}}{4 s^2_{ij}} \left(\frac{s_{jk}}{s_{ijk}} - \frac{s_{ik}}{s_{ijk}} + \frac{z_i - z_j}{z_{ij}}\right)^2 - \frac{s^2_{ijk}\, z_k}{4 s_{ik} s_{jk}} \left[\frac{z_{ij}^2 (1-\epsilon) + 2 z_k}{z_i z_j} + \epsilon(1-\epsilon)\right] \right. \end{aligned}$$

$$
\begin{aligned}
&+\frac{s_{ijk}^2}{2s_{ij}s_{ik}}\left[\frac{z_{ij}^2(1-\epsilon)+2z_k}{z_j}+\frac{z_j^2(1-\epsilon)+2z_{ik}}{z_{ij}}\right]+\frac{1}{4}(1-\epsilon)(1-2\epsilon)\\
&+\frac{s_{ijk}}{2s_{ik}}\left[(1-\epsilon)\frac{z_{ik}^3+z_k^2-z_j}{z_jz_{ij}}-2\epsilon\,\frac{z_{ik}(z_j-z_k)}{z_jz_{ij}}\right.\\
&\qquad\left.-\frac{z_kz_{jk}+z_{ik}^3}{z_iz_j}+\epsilon\,z_{ik}\frac{z_{ij}^2}{z_iz_j}-\epsilon(1+z_k)-\epsilon^2z_{ik}\right]\\
&+\frac{s_{ijk}}{2s_{ij}}\left[(1-\epsilon)\frac{z_i(2z_{jk}+z_i^2)-z_j(6z_{ik}+z_j^2)}{z_jz_{ij}}+2\epsilon\,\frac{z_k(z_i-2z_j)-z_j}{z_jz_{ij}}\right]\Bigg\}\\
&+(i\leftrightarrow j)\,.
\end{aligned}
\tag{4.5}
$$

The difference occurs in the second line of this expression in the highlighted term [1]. For the integration purposes one has to express the variables $z_i$, $z_j$, $z_{ij}$ in terms of the invariants as well. This is achieved by this substitutions:

$$
z_{i,j}=z_i+z_j\,,\quad z_i=1-z_j-z_k\,,\quad z_j=\frac{s_{jr}}{s_{jr}+s_{jr}+s_{kr}}\,. \tag{4.6}
$$

To be able to perform the integral (4.2), it is necessary to express the phase-space element (4.3) in terms of the invariants as well. To this end, it is necessary to solve the following system of equations and make an appropriate substitution in Eq. (4.3).

$$
\begin{cases}
y'=\frac{s_{ab}}{s_{abc}}\,,\quad z'=\frac{s_{ac}}{s_{ac}+s_{bc}}\,,\quad y=\frac{\bar{s}_{bc}^{(abc)}}{\bar{s}_{bcd}^{(abc)}}\,,\quad z=\frac{\bar{s}_{bd}^{(abc)}}{\bar{s}_{bd}^{(abc)}+\bar{s}_{cd}^{(abc)}}\,,\\
1-2w'=\frac{y'(1-z')\bar{s}_{cd}^{(abc)}+z'\bar{s}_{bd}^{(abc)}-s_{ad}}{2\sqrt{y'z'(1-z')\bar{s}_{bd}^{(abc)}\bar{s}_{cd}^{(abc)}}}\,,\\
4w'(1-w')=-\frac{\Lambda(y'(1-z')\bar{s}_{cd}^{(abc)},z'\bar{s}_{bd}^{(abc)},s_{ad})}{4y'z'(1-z')\bar{s}_{bd}^{(abc)}\bar{s}_{cd}^{(abc)}}\,,\\
s_{ab}+s_{ac}+s_{bc}=s_{abc}\,,\quad \bar{s}_{bc}^{(abc)}+\bar{s}_{bd}^{(abc)}+\bar{s}_{cd}^{(abc)}=\bar{s}_{bcd}^{(abc)}\,,\\
s_{abc}+s_{ad}+s_{bd}+s_{cd}=s_{abcd}\,,\quad s_{abcd}=\bar{s}_{bcd}^{(abc)}\,,\\
s_{abc}=\bar{s}_{bc}^{(abc)}\,,\quad \bar{s}_{cd}^{(abc)}=\frac{s_{abc}}{s_{ac}+s_{bc}}s_{cd}\\
\bar{s}_{bcd}^{(abc)}=\bar{s}_{cd}^{(abcd)}\,,
\end{cases}
\tag{4.7}
$$

[1] The presence of this typo was communicated with the authors of Refs. [27, 28].

where $\Lambda(a,b,c) = a^2 + b^2 + c^2 - 2ab - 2bc - 2ca$ is the Källén function. To synchronize the indices used for the parametrization of the phase-space element and the splitting kernels one has to perform following relabelings:

$$a \to i\,, \quad b \to j\,, \quad c \to k\,, \quad d \to r\,. \tag{4.8}$$

Now we are ready for the integration. Below we outline the recipe to perform the integration:

1. In order to reduce the arising integrals to the simplest form, simplifications described in Sec. 3.2 of Ref. [29] have been applied. The goal of this procedure is to only allow the appearance of the predetermined combinations of invariants $s_{ab}, s_{ac}, s_{ad}, s_{bc}, s_{bd}, s_{cd}$ in the denominator. Notice, that to achieve this, it is not sufficient to implement the simplifications in the strict order as they are listed in the paper. Different order of simplification rules will lead to different master integrals. The precise ordering should be determined case-by-case, keeping in mind the desired combinations of the invariants in the final result. In practice it means, exchanging the order of rule 2 and 3 in Ref. [29] for certain terms.

2. The splitting kernels are symmetric under the permutation of $i$, $j$, $k$ indices, hence it is sufficient to focus only on one permutation and multiply the result by the number of permutations.

3. In all splitting kernels considered, the integration over the azimuthal variable $\phi$ is trivial since the double-collinear splitting kernels have no explicit dependence on the latter.

4. The resulting function in the integrand is expanded. In all terms the dependence over the variable $y$ is factorized as it is characterized by the following master integral:

$$I_{A,B} = \int_0^1 dy y^A (1-y)^B = \frac{\Gamma(A+1)\Gamma(B+1)}{\Gamma(A+B+2)}\,. \tag{4.9}$$

   Therefore the integration over $y$ is straightforward.

5. At this point each term takes the following general form:

$$I_{a,A,B,C,D,E,F,G} = \int_0^1 dy' \int_0^1 dz \int_0^1 dz' \int_0^1 dw' \times$$

$$\times \frac{\left(w'\left(1-w'\right)\right)^{-1/2+\epsilon}\left(1-y'\right)^{A}\left(y'\right)^{B}\left(1-z\right)^{C}z^{D}\left(1-z'\right)^{E}\left(z'\right)^{F}}{\left[1-\left(1-y'\right)z'\right]^{G-1}\mathcal{D}^{a}}, \tag{4.10}$$

where

$$\mathcal{D} \equiv \left[z\left(1-z'\right)+y'(1-z)z'+2\left(1-2w'\right)\sqrt{y'}\sqrt{(1-z)z}\sqrt{\left(1-z'\right)z'}\right]. \tag{4.11}$$

We note that, for the splitting kernels under consideration only certain values of the parameters $(a, A, B, C, D, E, F, G)$ are relevant.

6. To greatly reduce the number of master integrals needed to calculate, we repeatedly make use of the following partial fractioning relations for the variables $y', z, z'$:

$$(1-x)^{m}x^{n} = (1-x)^{m-1}x^{n} - (1-x)^{m-1}x^{n+1} \tag{4.12}$$

and

$$1 = \frac{1}{1-(1-y')z'} - \frac{\left(1-y'\right)z'}{1-(1-y')z'}. \tag{4.13}$$

The resulting master integrals are listed below (see the explicit derivations in Appendix B):

$$\begin{aligned} I_{A,B,C,D,E} &= \int_0^1 dz \int_0^1 dy' \left(1-y'\right)^{A}\left(y'\right)^{B}(1-z)^{C}z^{D}\frac{1}{\left(z+(1-z)y'\right)^{E}} \\ &= \frac{\Gamma(A+1)\Gamma(B+1)}{\Gamma(A+B+2)}\frac{\Gamma(C+1)\Gamma(B+D+2-E)}{\Gamma(B+C+D+3-E)}\times \\ &\times {}_3F_2(A+B+2-E, B+1, C+1, A+B+2, B+C+D+3-E, 1), \end{aligned} \tag{4.14}$$

$$\begin{aligned} I_{b,\beta,\gamma,A,B,C,D,E} &= \int_0^1 dy' \int_0^1 dz \int_0^1 dz' \int_0^1 dw' \times \\ &\times \frac{\left(w'\left(1-w'\right)\right)^{1/2-b}z^{\beta}(1-z)^{\gamma}\left(1-y'\right)^{A}\left(y'\right)^{B}\left(1-z'\right)^{C}\left(z'\right)^{D}}{\left[1-\left(1-y'\right)z'\right]^{E-1}\mathcal{D}} \\ &= 2^{4(b-1)}\pi\frac{\Gamma(3-2b)\Gamma(n+1)}{\Gamma(2-b)\Gamma(n+3-2b)}\sum_{k=0}^{n}\frac{\Gamma(n-k-b+1)}{\Gamma(n-k+1)}I_{A,B,D,C+k,E+k}, \end{aligned} \tag{4.15}$$

$$I_{a,b,A,B,C,D,E} = \int_0^1 dy' \int_0^1 dz \int_0^1 dz' \int_0^1 dw' \times$$
$$\times \frac{\left(w'\left(1-w'\right)\right)^{1/2-b} \left(z(1-z)\right)^{1-b} \left(1-y'\right)^A \left(y'\right)^B \left(1-z'\right)^C \left(z'\right)^D}{\left[1-\left(1-y'\right)z'\right]^{E-1} \mathcal{D}^a}$$
$$= 2^{4(b-1)} \pi \frac{\Gamma(2-b-a)\Gamma(3-2b)}{\Gamma(2-b)\Gamma(4-2b-a)} I_{A,B,D,C,E+a-1}\,. \tag{4.16}$$

Two more master integrals of the following type $I_{1,A,B,-1-\epsilon,-\epsilon,-\epsilon,F,2}$ and $I_{1,m-\epsilon,-\epsilon,-\epsilon,-1-\epsilon,-\epsilon,3-\epsilon}$ with $m \geq 0$ require intermediate expansion in $\epsilon$ power series before the complete integration and they have been calculated using the `FORM` [71, 72] routines [73, 74] up to the $\epsilon^2$ accuracy.

The steps 1 and 2 are implemented in `Mathematica`, while the computationally intensive task of the master integral recognition and substitution is performed in `FORM`. The hypergeometric functions which appear in Eqs. (4.14) - (4.16) are expanded using the `Mathematica` package `HypExp` [75].

Based on the method described above a dedicated package was created which fully automatizes the calculation steps described above. Among other things, this package also provides the routines for the seamless communication of `Mathematica` and `FORM` and by the utilization of the parallel computing makes it possible to successfully reproduce all the results listed in Ref. [29] within a couple minutes.

To derive the results from [28], which uses the hard-collinear formalism, an additional step is required. The hard-collinear limits contain the hard-collinear splitting functions, which are related to the regular splitting functions discussed above using the transformation:

$$P^{\rm hc}_{ijk(r)} \equiv P_{ijk(r)} - s^2_{ijk}\left[C_{f_k}\left(4\,C_{f_k}\mathcal{E}^{(i)}_{kr}\mathcal{E}^{(j)}_{kr} - \mathcal{E}^{(ij)}_{kr}\right) + (i \leftrightarrow k) + (j \leftrightarrow k)\right]. \tag{4.17}$$

Here, $\mathcal{E}^{(i)}_{kr}$ and $\mathcal{E}^{(ij)}_{kr}$ are particular combinations of the eikonal kernels, expressed in terms of the kinematic invariants, as discussed in Ref. [29]. Their denominator structure is no more complicated than that of the original triple-collinear splitting kernels. Thus, the master integrals provided above are completely sufficient to cover these cases as well. Therefore, to obtain the integrated subtraction terms from Ref. [28], one can take the results from Ref. [29] and subtract the integral over the second

square bracket of Eq. (4.17). In this way, we have rederived the integrated subtraction terms listed in Ref. [28] as well.

An alternative approach has also been developed [76] for the purpose of making independent cross-checks. The latter version relies on `Mathematica` for all the steps described above and differs from the first one in that a different approach for the reduction of master integrals based on Eqs. (4.12) - (4.13)) is adopted. As a consequence, the number and type of master integrals that are computed generally differs in the two implementations. This fact adds even more robustness to our cross-checks.

Once the integrated subtraction terms $I^{(\mathbf{1})}$, $I^{(\mathbf{2})}$ and $I^{(\mathbf{12})}$ have been determined one is ready to study the *RV* contribution.

## 4.2 Determination of the $\Delta_{ij}$ terms

In Chapter 3 we discussed the need of including $\Delta_{ij}$ in the subtracted *RV* contribution and outlined the strategy of the determination of these terms. Namely, once the $K^{(\mathbf{12})}$ contribution has been integrated and the expression of $I^{(\mathbf{12})}$ is available it is a straightforward procedure to fix the value of $\Delta_{ij}$ terms such, that conditions in Eq. (3.66) are fulfilled. Repeating this calculation demonstrated in [28] we arrive at the following observations: For the collinear term $\Delta_{C,ij}$ our result agrees with the result reported in [28]:

$$
\begin{aligned}
\Delta_{\mathrm{C},ij} \;=\; & \frac{\alpha_{\mathrm{S}}}{2\pi}\mathcal{N}_1\frac{P^{\mu\nu}_{ij(r)}}{s_{ij}}\frac{1}{\epsilon^2}\sum_{c\neq i,j}\Bigg\{\sum_{d\neq i,j,c}\left[\left(\frac{s_{cd}}{\bar{s}^{(ijr)}_{cd}}\right)^{-\epsilon}-1\right]\overline{B}^{(ijr)}_{\mu\nu,cd}+2\left[1-\left(\frac{\bar{s}^{(ijr)}_{jc}}{s_{[ij]r}}\right)^{-\epsilon}\right]\overline{B}^{(ijr)}_{\mu\nu,[ij]c} \\
& +\Bigg\{\rho^{(\mathrm{C})}_{ij}\left[\left(\frac{\bar{s}^{(jri)}_{ic}}{\bar{s}^{(jri)}_{ir}}\right)^{-\epsilon}-\left(\frac{s_{ir}\bar{s}^{(jri)}_{ic}}{\bar{s}^{(jri)}_{ir}s_{ic}}\right)^{-\epsilon}\right]\overline{B}^{(jri)}_{\mu\nu,[ij]c} \\
& +\tilde{f}^{q\bar{q}}_{ij}\left[\left(\frac{\bar{s}^{(jri)}_{ic}}{\mu^2}\right)^{-\epsilon}-\left(\frac{\bar{s}^{(jri)}_{ic}}{s_{ic}}\right)^{-\epsilon}\right]\overline{\mathcal{B}}^{(jri)}_{\mu\nu,[ij]c}+(i\leftrightarrow j)\Bigg\}\Bigg\}\mathcal{W}_{\mathrm{c},ij(r)} \\
+ \; & \frac{\alpha_{\mathrm{S}}}{2\pi}\mathcal{N}_1\sum_{k\neq i,j}\left(\frac{\gamma^{\mathrm{hc}}_k}{\epsilon}+\phi^{\mathrm{hc}}_k\right)\left[\frac{P^{\mu\nu}_{ij(r)}}{s_{ij}}\overline{B}^{(ijr)}_{\mu\nu}\mathcal{W}_{\mathrm{c},ij(r)}-\frac{P^{\mu\nu}_{ij(r')}}{s_{ij}}\overline{B}^{(ijr')}_{\mu\nu}\mathcal{W}_{\mathrm{c},ij(r')}\right].
\end{aligned}
\tag{4.18}
$$

The soft-collinear term also agrees with [28], but only if one considers the symmetrized sector functions $Z_{ij}$ instead of $W_{ij}$ used in Eq. (3.66). Because in the end the LASS scheme is implemented using the symmetrized sector function it is safe to

implement the following expression:

$$\begin{aligned}\Delta_{\mathrm{SC},ij} \;=\; & \frac{\alpha_s}{2\pi}\,2\,\mathcal{N}_1\,C_{f_j}\,\mathcal{E}^{(i)}_{jr}\,\frac{1}{\epsilon^2}\sum_{c\neq i,j}\Bigg\{\sum_{d\neq i,j,c}\left[\left(\frac{s_{cd}}{\bar{s}^{(ijr)}_{cd}}\right)^{-\epsilon}-1\right]\overline{B}^{(ijr)}_{cd}+2\left[\left(\frac{s_{jr}}{s_{[ij]r}}\right)^{-\epsilon}-\left(\frac{\bar{s}^{(ijr)}_{jc}}{s_{[ij]r}}\right)^{-\epsilon}\right]\overline{B}^{(ijr)}_{[ij]c}\\ & +\frac{C_A}{C_{f_j}}\left[\left(\frac{\bar{s}^{(jri)}_{ic}}{\bar{s}^{(jri)}_{ir}}\right)^{-\epsilon}-\left(\frac{s_{ir}\bar{s}^{(jri)}_{ic}}{\bar{s}^{(jri)}_{ir}s_{ic}}\right)^{-\epsilon}\right]\overline{B}^{(jri)}_{[ij]c}+\frac{2\,C_{f_j}-C_A}{C_{f_j}}\left[\left(\frac{\bar{s}^{(irj)}_{jc}}{\bar{s}^{(irj)}_{jr}}\right)^{-\epsilon}-\left(\frac{s_{jr}\bar{s}^{(irj)}_{jc}}{\bar{s}^{(irj)}_{jr}s_{jc}}\right)^{-\epsilon}\right]\overline{B}^{(irj)}_{[ij]c}\Bigg\}\\ & +\frac{\alpha_s}{2\pi}\,2\,\mathcal{N}_1\,C_{f_j}\Bigg[J^{j}_{\mathrm{hc}}(s_{jr})\,\mathcal{E}^{(i)}_{jr}\left(\overline{B}^{(ijr)}-\overline{B}^{(irj)}\right)\\ & \qquad +\sum_{k\neq i,j}\left(\frac{\gamma^{\mathrm{hc}}_k}{\epsilon}+\phi^{\mathrm{hc}}_k\right)\left(\mathcal{E}^{(i)}_{jr}\overline{B}^{(ijr)}-\mathcal{E}^{(i)}_{jr'}\overline{B}^{(ijr')}\right)\Bigg]. \end{aligned}\tag{4.19}$$

For the soft term $\Delta_{\mathrm{S},i}$ we find that in order to satisfy the condition given in Eq. (3.66) it should have the following form: The equation is:

$$\begin{aligned}\Delta_{\mathrm{S},i} \;=\; & -\frac{\alpha_s}{2\pi}\,\mathcal{N}_1\sum_{\substack{c\neq i\\ d\neq i,c}}\mathcal{E}^{(i)}_{cd}\Bigg\{\frac{1}{2\epsilon^2}\sum_{\substack{e\neq i,c\\ f\neq i,c,e}}\left[\left(\frac{s_{ef}}{\bar{s}^{(icd)}_{ef}}\right)^{-\epsilon}-1\right]\overline{B}^{(icd)}_{efcd}\\ & \qquad +\frac{1}{\epsilon^2}\sum_{e\neq i,d}\left[\left(\frac{s_{ed}}{\mu^2}\right)^{-\epsilon}-1\right]\left(\overline{B}^{(icd)}_{edcd}-\overline{B}^{(idc)}_{edcd}\right)\\ & \qquad +\left[\left(\frac{1}{\epsilon^2}+\frac{2}{\epsilon}\right)2\,C_{f_c}+\frac{\gamma^{\mathrm{hc}}_c}{\epsilon}\right]\left(\overline{B}^{(icd)}_{cd}-\overline{B}^{(idc)}_{cd}\right)\Bigg\}\\ & -\frac{\alpha_s}{2\pi}\,\mathcal{N}_1\sum_{\substack{k\neq i\\ c\neq i,k,r}}\mathcal{E}^{(i)}_{cr}\,\frac{\gamma^{\mathrm{hc}}_k}{\epsilon}\left(\overline{B}^{(irc)}_{cr}-\overline{B}^{(icr)}_{cr}\right), \qquad r=r_{ik}\,. \end{aligned}\tag{4.20}$$

The expression above the term on the second line differs from the $\Delta_{\mathrm{S},i}$ given in [29] by the highlighted term on the second line. In general, this is expected to have implications on the pole structure of $I^{(\mathbf{RV})}$, and this issue needs to be addressed. Additionally, the $\Delta_{ij}$ terms constructed in this way feature finite parts as well. Strictly speaking, this is not necessary, as the main purpose of these terms is to cancel the explicit poles in the $RV$ contribution, and if included, it makes the integration procedure more involved than necessary. In our approach, we neglect any finite contribution coming from the $\Delta_{ij}$ terms in the $RV$ contribution and shift them to $VV$. The issue of the pole structure of $I^{(\mathbf{RV})}$ will be addressed in the future. For the rest of this study, we stick with the original formulation of $I^{(\mathbf{RV})}$ given by Ref. [29].

## 4.3 $VV$ - Consistency check

As outlined in Chapter 3, in the LASS scheme, the subtraction procedure begins by defining the subtraction terms for the contribution with the most unresolved radiation. It then works its way through the contributions with fewer unresolved radiations until reaching the process with no unresolved radiation, which we conveniently call the $n$-parton line (where $n$ is the number of final-state particles at the Born level). Along the way, the integrated subtraction terms are added back. When arriving at the last contribution, there is no freedom left to introduce a new subtraction term. Thus, if the scheme is properly defined and the subtraction terms are correctly defined and integrated, the singularities of the $n$-parton line should automatically cancel. As seen in Eq. (3.38), $I^{(\mathbf{1})} + I^{(\mathbf{RV})}$ is responsible for the VV contribution. The singularity structure of the double-virtual correction is well-known [69]. Hence, after obtaining the results for $I^{(\mathbf{1})}$ and $I^{(\mathbf{RV})}$ using the integration technique described above, one can perform an analytical check for the explicit $\epsilon$-pole cancellation in the VV contribution. This check was already done in Ref. [29], where the authors used VV poles motivated by the ideas of Soft-Collinear Effective Field Theory [77–79]. We repeated the calculation using the formulation of [69], where the 2-loop pole structure is defined as:

$$
\begin{aligned}
VV_{\text{poles}} = \\
&2\Re\Bigg[ -\frac{1}{2}\left\langle \mathcal{M}^{(0)} \middle| \boldsymbol{I}^{(1)}_{\text{Catani}}(\epsilon)\boldsymbol{I}^{(1)}_{\text{Catani}}(\epsilon) \middle| \mathcal{M}^{(0)} \right\rangle - \frac{\beta_0}{\epsilon}\left\langle \mathcal{M}^{(0)} \middle| \boldsymbol{I}^{(1)}_{\text{Catani}}(\epsilon) \middle| \mathcal{M}^{(0)} \right\rangle \\
&\quad + \left\langle \mathcal{M}^{(0)} \middle| \boldsymbol{I}^{(1)}_{\text{Catani}}(\epsilon) \middle| \mathcal{M}^{(1)} \right\rangle \\
&\quad + e^{-\epsilon\gamma}\frac{\Gamma(1-2\epsilon)}{\Gamma(1-\epsilon)}\left(\frac{\beta_0}{\epsilon} + K\right)\left\langle \mathcal{M}^{(0)} \middle| \boldsymbol{I}^{(1)}_{\text{Catani}}(2\epsilon) \middle| \mathcal{M}^{(0)} \right\rangle \\
&\quad + \left\langle \mathcal{M}^{(0)} \middle| \boldsymbol{H}^{(2)}(\epsilon) \middle| \mathcal{M}^{(0)} \right\rangle \Bigg] \\
&+\Re\left[ 2\left\langle \mathcal{M}^{(1)} \middle| \boldsymbol{I}^{(1)}_{\text{Catani}}(\epsilon) \middle| \mathcal{M}^{(0)} \right\rangle - \left\langle \mathcal{M}^{(0)} \middle| \boldsymbol{I}^{(1)\dagger}_{\text{Catani}}(\epsilon)\boldsymbol{I}^{(1)}_{\text{Catani}}(\epsilon) \middle| \mathcal{M}^{(0)} \right\rangle \right],
\end{aligned}
\tag{4.21}
$$

where $\boldsymbol{I}^{(1)}_{\text{Catani}}$ is given in Eq. (3.31) and the K coefficient is defined as:

$$
K \equiv \left(\frac{67}{18} - \frac{\pi^2}{6}\right) C_A - \frac{10}{9} T_R N_f \,. \tag{4.22}
$$

The convenient definition of $\boldsymbol{H}^{(2)}$ can be found in Ref. [80]. To match with the notation employed in the LASS papers one has to relate $\boldsymbol{H}^{(2)}$ with the two-loop collinear anomalous dimension $\gamma_i^{(2)}$ used there. This relation is given by the following formula:

$$\boldsymbol{H}^{(2)} = \gamma_i^{(2)} + \frac{1}{4}\Sigma_\gamma \hat{\gamma}_K^{(2)} + C_F \frac{\beta_0 \pi^2}{16}\,, \tag{4.23}$$

where the definitions of $\Sigma_\gamma$ and $\hat{\gamma}_K^{(2)}$ are given in Ref. [29].

After making this transformation, substituting Eq. (3.31) into Eq. (4.21) and expanding everything in $\epsilon$-series one reproduces Eq. (7.21) from [29] which indeed matches with the $\epsilon$ expansion of $I^{(\mathbf{1})} + I^{(\mathbf{RV})}$. Moreover, it was also confirmed that the finite part of $I^{(\mathbf{1})} + I^{(\mathbf{RV})}$ is indeed given by Eq. (7.24) from [29], assuming the one-loop virtual amplitude $V$ is only expanded up to the finite term. If $V$ also contains the terms up to $\mathcal{O}(\epsilon^2)$ it is necessary to re-expand $I^{(\mathbf{RV})}$ accounting the extra $\epsilon$ dependence in $V$.

# Chapter 5

# Color correlators, color decomposition and generation of color bases

While implementing the LASS scheme one often has to evaluate the following objects:

$$B_{cd} \equiv \mathcal{A}_n^{(0)\dagger} \mathbf{T}_c \cdot \mathbf{T}_d \mathcal{A}_n^{(0)} , \qquad B_{cdef} \equiv \mathcal{A}_n^{(0)\dagger} \{\mathbf{T}_c \cdot \mathbf{T}_d, \mathbf{T}_e \cdot \mathbf{T}_f\} \mathcal{A}_n^{(0)} , \tag{5.1}$$

$$V_{cd} \equiv 2\,\mathbf{Re}\left[\mathcal{A}_n^{(1)\dagger} \mathbf{T}_c \cdot \mathbf{T}_d \mathcal{A}_n^{(0)}\right] , \tag{5.2}$$

where $\mathbf{T_i}$ is a color generator of the parton $i$ ($t^a_{ij}$ for quarks, $(-t^a_{ij})$ for antiquarks and $(if^{abc})$ for gluons, see Eqs. (2.5) and (2.6)). The objects defined above are called color correlated Born and 1-loop virtual contributions. For the simple processes the color and kinematics factorize, hence it is a quite straightforward procedure to calculate such objects (e.g. see Ref. [5]). However, in general this is not the case and one has to carry out the calculation explicitly. One of the ways to achieve this is to perform the color decomposition of the amplitude and introduce an additional gluon exchange between two partons. The method which automatizes this kind of calculations for a generic process is described in Ref. [81]. The main complication in this procedure is the construction of the color basis for an arbitrary process.

There are a number of ways the color basis can be generated. The most widely used one is a trace basis, which involves the generation of all possible color exchanges between incoming and outgoing partons using the quark lines [82, 83], see Figure 5.1. Later on a method better suited for Monte Carlo generators was developed based

on the color flow decomposition [84]. There are packages available which can generate such bases [85, 86] automatically for any process. The issue with these kind of bases is, that they overdescribe the color information of the process. Hence, they are not orthogonal and this makes all the subsequent analytical calculations very complicated.

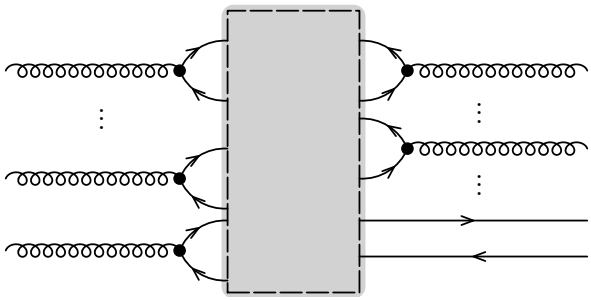

FIGURE 5.1: Demonstration of the construction of the trace basis. Each gluon is represented as a combination of quark- antiquark lines. The dashed box should be filled with the fermion lines connecting the incoming and outgoing partons in all possible nonvanishing ways.

The improved approach relies on the multiplet decomposition of the initial and the final states and matching them with each other. This requires the construction of appropriate projectors for each multiplet state. The first reference of such a calculation is [87], where for $N_c = 3$ the color structure of a two gluon ($gg$) state has been analyzed. The generalized method for arbitrary $N_c$ has been formulated in Ref. [88] and it requires solving characteristic equations of group invariant matrices. Combining the approaches of Refs. [88] and [89] a general algorithm has been formulated [90], which is well suited for automation and this is the method of our choice in this work. We also draw attention to a recently published method [91] which introduces a novel approach to performing color decomposition within a multiplet basis, circumventing the explicit construction of said basis through the utilization of Wigner 6j symbols.

In Section 5.1 we briefly review the method developed in Ref. [90]. In Section 5.2 we discuss the technical details of our implementation. Section 5.3 demonstrates the usage of the tools developed in this study and Section 5.4 discusses the possibilities to validate the obtained results. Section 5.5 describes how the projectors are combined into the basis vectors.

## 5.1 Method

In this Section we summarize the method formulated in [90]: Let us denote by $N_g$ the number of incoming and outgoing gluons and by $n_q$ the number of incoming quarks and outgoing antiquarks. In QCD $n_q$ will be also equal to the number of incoming antiquarks and outgoing quarks. The quarks transform under the fundamental representation of SU($N_c$) and hence, they are the elements of $V = C^{N_c}$, whereas antiquarks are the elements of dual space $\overline{V} \cong C^{N}_{c}$, which transform as complex conjugates of the fundamental representation. The gluons transform under the adjoint representation with the dimension of $N_c^2 - 1$ and they are the elements of $A \cong C^{N_c^2-1}$. In this notation the color information of every process in QCD can be characterized by a tensor $\mathbf{c} \in G \equiv (V \otimes \overline{V})^{\otimes n_q} \otimes A^{N_g}$.

The idea of the construction of the multiplet color basis is to decompose $G$ as a direct sum of irreducible representations, which we refer to as *multiplets states*. Such decomposition can be achieved using the rules of Young tableau multiplication, see, e.g., Chapter 48 in Ref. [92]. The next step is to match the initial state multiplets with the final state multiplets. Figure 5.2 demonstrates this procedure for the annihilation of a quark-antiquark pair and production of two gluons in SU(3), i.e., $q\bar{q} \to gg$ scattering.

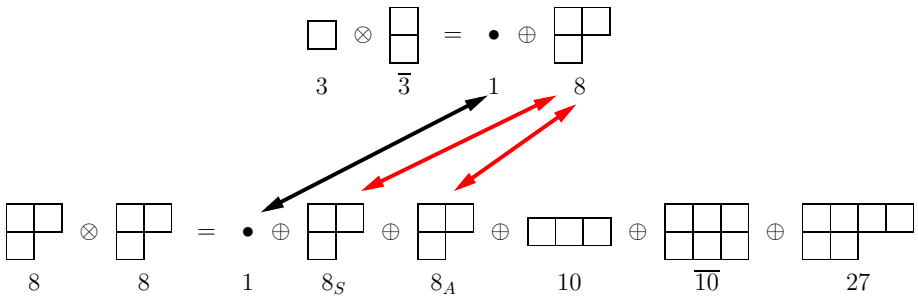


FIGURE 5.2: Multiplet decomposition and matching for $q\bar{q} \to gg$ in SU(3). There is one possibility to match the initial state singlet with the final state singlet and there are two possibilities to match the octets. Hence, the basis is three dimensional.

After performing the decomposition and the matching of corresponding multiplets, the next step is to construct projectors for each of these states.

In principle the (anti-)quark and gluon projectors require different treatments. However, one can use the fact that for every quark-antiquark pair $\overline{V} \otimes V = \bullet \oplus A$. The

singlet state does not add any extra color information to the system and the octet state acts as an additional gluon. Thus, the analysis of $(\overline{V} \otimes V)^{\otimes n_q} \otimes A^{\otimes N_g}$ color structure is equivalent to the analysis of the $A^{\otimes(N_g+n_q)}$ color structure. Hence, it is sufficient to focus on the generation of gluon projectors.

The construction of the projectors depends on the creation history of the associated multiplets. For each multiplet state the number $n_f(M) = 0, 1, 2, \ldots, N_g$ is defined as a first appearance of multiplet $M$ in the sequence:

$$A^{\otimes 0}\,,\; A^{\otimes 1} = A\,,\; A^{\otimes 2} = A \otimes A\,,\; A^{\otimes 3} = A \otimes A \otimes A\,,\; \ldots\,,\; A^{\otimes N_g}. \tag{5.3}$$

For example a SU(3) singlet has a first appearance $n_f = 0$, the octet has a first appearance $n_f = 1$, $n_f(10) = n_f(\overline{10}) = n_f(27) = 2$ and so on.

The gluon projectors are always constructed recursively depending on their creation history. This means, that, if the multiplet $M'$ appears in the decomposition of $M \otimes A$, the projector for $M$ will be used for the construction. The exact strategy depends whether the desired projector $M'$ has already appeared previously in the sequence $A^{\otimes N_g}$ (meaning that $n_f(M') \leq n_f(M) < N_g$) or whether it is an entirely new one, with $n_f = N_g$.

First we deal with the *new projectors*. This strategy can be used to generate projectors of 10-plet, $\overline{10}$-plet and 27-plet in the SU(3) expansion of $8 \otimes 8$. The strategy can be summarized as follows:

1. Contract the first $N_g - 1$ gluon lines in the projector of multiplet $M$.
2. The $N_g$-th gluon line remains uncontracted.
3. Each gluon line should be split into quark antiquark pairs.
4. All the quark lines should be contracted to some Young operator [88] $\mathbf{P}_q$ and all the antiquark lines should be contracted to another Young operator $\mathbf{P}_{\overline{q}}$.
5. The respective Young tableaux $\mathcal{Y}_q$ and $\mathcal{Y}_{\overline{q}}$ should consist of exactly $N_g$ cells and their product $\mathcal{Y}_{\overline{q}} \otimes \mathcal{Y}_q$ should contain the first occurrence of the multiplet $M'$.

This procedure is illustrated below using the *birdtrack* notation [85, 88]:

$\mathbf{T}^{\dots M,M'} =$ 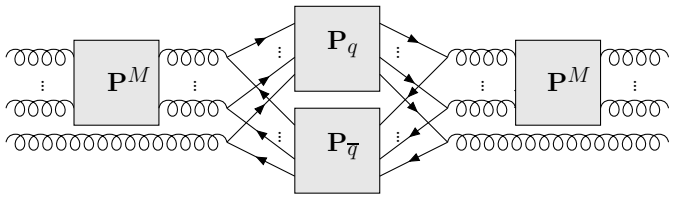

. (5.4)

Since the product $\mathcal{Y}_{\overline{q}} \otimes \mathcal{Y}_q$ will also contain known multiplets, i.e., those ones which were already previously encountered in the expansion of $A^{\otimes N_g - 1}$, such *old multiplets* have to be removed in a Gram-Schmidt step:

$$\widetilde{\mathbf{T}} = \mathbf{T} - \sum_{M\,\text{old}} \frac{\text{tr}(\mathbf{P}_M \mathbf{T})}{\dim M} \mathbf{P}_M \,. \tag{5.5}$$

After normalizing of $\widetilde{T}$ we obtain the desired projector:

$$\mathbf{P}_{M'_k} = \frac{\dim M'_k}{\text{tr}\widetilde{\mathbf{T}}} \widetilde{\mathbf{T}} \,. \tag{5.6}$$

The generation of the projectors on *old multiplet* states is more involved. This strategy is applicable for example for the projectors of singlet and octet states in $8 \otimes 8$ expansion. The general recipe is to construct the following operator:

$\mathbf{C}^{\dots M,M'} =$ 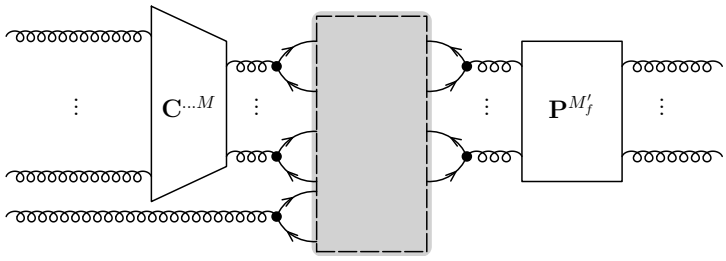

, (5.7)

where $\mathbf{C}^{\dots M}$ are Clebsch-Gordan coefficients defined as follows:

$\mathbf{P}^M =$ 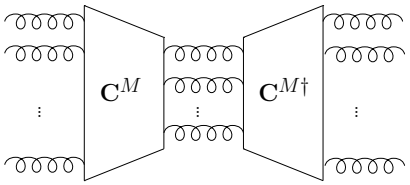

. (5.8)

To obtain $\mathbf{C}^{\dots M}$ appearing in the left box of Eq. (5.7) one should apply Eq. (5.7) recursively, until everything is expressed in terms of known Clebsch-Gordan coefficients.

In Eq. (5.7) the dashed gray rectangle connects the right quark and antiquark lines (coming from $n_f(M)+1$ gluons) with the left ones (recombining in $n_f(M')$ gluons) in such a way that the whole expression does not vanish. After the correct normalization $\mathbf{P}^{\dots M,M'} = \mathbf{C}^{\dots M,M'}\mathbf{C}^{\dots M,M'\dagger}$ defines the desired projector. In the general case, the determination of the appropriate connection inside the gray box case can be quite cumbersome. Hence in Ref. [90] the special cases were analyzed, for which the procedure simplifies and this was sufficient to analyze the $ggg \to ggg$ color structure, involving six gluons. Below we briefly summarize these special cases, however, we also note that starting from four gluons one will always need to turn back to general formula in Eq. (5.7). In the next section we will propose an efficient algorithm to realize this formula.

There are three cases which can be simplified further:

1. If $n_f(M) < N_g - 1$ the projector is given as:

$$\mathbf{P}^{\dots,M,M'} = $$

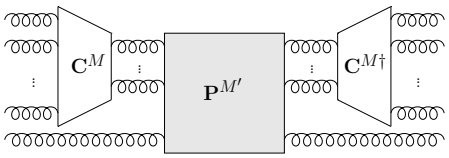


. (5.9)

2. If $n_f(M) = N_g - 1$ and $n_f(M') = N_g - 2$:

$$\mathbf{P}^{\dots,M,M'} = \frac{\dim M'}{\dim M}$$

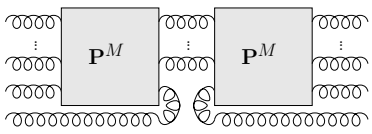


. (5.10)

3. If $n_f(M) = n_f(M') = N_g - 1$:

$$\mathbf{P}^{\dots,M,M'} = \frac{\dim(M')}{B(M,M')}$$

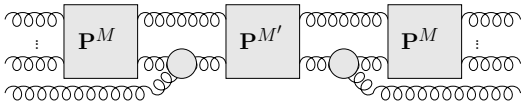


, (5.11)

where both gray circles are either $d$- or $f$-tensors or a linear combination of them and the normalization factor is determined as follows:

$$B(M, M') = \quad .$$

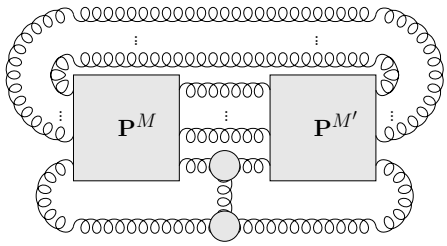


(5.12)

For more than three gluons the above method will sometimes yield 0 and one has to refer back to Eq. (5.7). This finishes the summary of the ideas outlined in Ref. [90]. Now we describe how this is implemented in practice.

## 5.2 Implementation

The first step is to perform the decomposition of $A^{\otimes N_g}$ in terms of the irreducible representations, like it is shown in Fig. 5.2. This can be achieved using the rules of the Young tableau manipulation as described in Ref. [92]. There are a number of `Mathematica` packages available implementing these rules [93, 94]. However, these tools only work if the number of colors $N_c$ is fixed in advance to some integer value, and they become very inefficient for large values of $N_g$. Out of the box they do not preserve the creation history of the multiplets and the symmetry information of the multiplets is also lost. For example, there is no distinction between $8_A$ and $8_S$ in the decomposition of $8 \otimes 8$ for $\mathrm{SU}(3)$.

We employ a novel approach to efficiently solve these issues. The core idea of our method is to use the `Z3 SMT-solver` [95] to find the solutions of the constrained combinatorial problems. `Z3` is a *satisfiability modulo theories* (SMT) solver developed by Microsoft Research with a purpose of solving logical formulas and constraints over various theories, such as arithmetic, arrays, uninterpreted functions, and bit-vectors. In the background it employs a combination of different algorithms and techniques to solve SMT problems efficiently. Below we list couple such algorithms which are relevant for our problem: `Z3` is based on the *Conflict Driven Clause Learning* (CDCL) [96], the *Davis–Putnam–Logemann–Loveland* (DPLL) algorithm [97, 98], the *Simplex algorithm* [99], the *Congruence Closure algorithm* [100], the *Fourier-Motzkin variable elimination* [101], the *E-matching* [102], and the *Nelson-Oppen method* [103].

Hence, Z3 is superior to brute force methods because it leverages these sophisticated algorithms and techniques that intelligently prune the search space, handle complex theories and quantifiers efficiently, support incremental solving, and utilize parallelization, making it highly scalable and efficient for solving complex logical formulas and constraints, as opposed to the computationally infeasible exhaustive exploration employed by brute force methods.

When multiplying two Young tableaux, this means that instead of iteratively adding the cells from the right tableau to the left one, we combine all the cells together imposing the rules of the multiplication on the final tableau and let Z3 find the solutions. Graphically this procedure is depicted in Figure 5.3. It is important to note that, thanks to the sophisticated algorithms listed above, the method illustrated in the bottom scheme of Fig. 5.3 is not equivalent to generating all possible fillings of the larger tableau and then examining which ones should be retained. Were this the case, we would have to consider 484 diagrams when multiplying two octets within SU(3) group.

To be able to provide the full SU($N_c$) description of the problem we account the fact that, when multiplying $N_g$ adjoint representations ($A^{\otimes N_g}$) the largest possible resulting diagram can have the dimension $N_c \times 2N_g$. Hence, we offer the user a possibility to carry out the calculation for SU($2N_g$) group, which is still very efficient because of the scalability feature of Z3 discussed above. The choice of SU($2N_g$) guarantees that every possible shape of Young diagrams will be generated. The resulting tableaux and consequently the respective projectors are parametrized using the $N_c$ notation, thus providing a possibility to take the $N_c \to 3$ limit in the end, should one be interested in applications to QCD phenomenology.

The next challenge is to construct the birdtrack diagrams described in the previous Section. The first difficulty is to find the $\mathcal{Y}_q$ and $\mathcal{Y}_{\bar{q}}$ Young diagrams which are necessary for the 5th step to construct Eq. (5.4) for an arbitrary multiplet. Since this is a combinatorial problem by its nature, we are using again Z3 to solve it efficiently.

Another difficulty is to find the nonzero connection inside the gray box of Eq. (5.7). Although this is also a combinatorial problem, Z3 cannot be used directly in this case, because the restrictions are imposed on symbolic tensorial expressions, which are not supported in Z3. To construct the tensorial expressions and apply the rules of the color algebra we use FORM [71], which we interfaced with Z3 and let the Z3

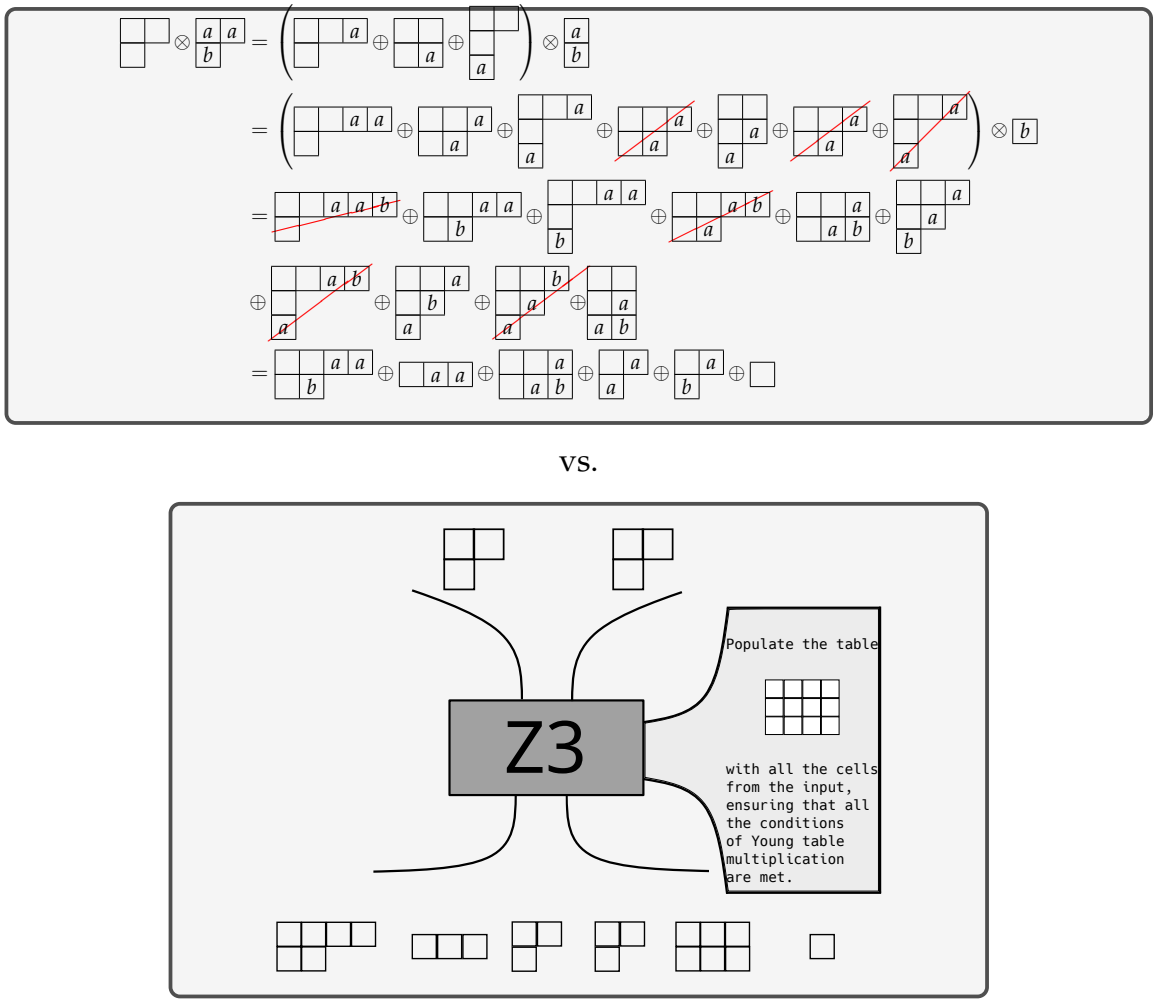


FIGURE 5.3: The schematic demonstration of the typical approach of multiplying two Young tableaux (top) vs. our approach using `Z3` `SMT-solver` (bottom).

`SMT-solver` guide the writing of the `FORM` code. `FORM` provides the result of evaluation back to `Z3`. In this way, we indirectly use the DPLL algorithm within `FORM`.

The aforementioned approach is realized in an extensible `Python` library `OrthoBase`. We use a `Python` *Application Programming Interface* (API) of `Z3` [104] to implement the constraints mentioned above. Due to the nature of the problem it is most effective if the multiplet decomposition is performed in a serial manner. On the other hand, the projector construction can massively benefit using parallelization. Therefore, we use the *Message Passing Interface* (MPI) protocol to not only allow parallelization across the different cores of the CPU, but also enable parallelization over multiple

computer nodes accessible over the network. To this end we use an open source MPI implementation `OpenMPI` [105], with a python API `mpi4py` [106, 107]. The tensorial expressions of the resulting projectors are written as a `FORM` program, which can be embedded in other programs for further calculations.

## 5.3 Manual of `OrthoBase`

### 5.3.1 Installation

Before installing of `OrthoBase`, the following dependencies need to be present on the system: `z3-solver` [108], `Open MPI` [109], `mpi4py` [110]. The prepackaged version of the `OrthoBase` library itself can be installed as follows:

```
python3 -m pip install --user --upgrade OrthoBase
```

It is also possible to build the latest version from the source of a `git` repository:

```
git clone https://github.com/rakab/OrthoBase.git
cd OrthoBase
pip install --user .
```

### 5.3.2 Demonstration

We demonstrate the functionality of `OrthoBase` using the illustrative example. The code below will construct expressions of all 13 026 164 projectors for the $\underbrace{ggggggggg}_{\text{10 gluons}} \to \underbrace{ggggggggg}_{\text{10 gluons}}$ transition for SU(3):

```
#!/usr/bin/env python3
from OrthoBase import YoungTools as YT
from OrthoBase import Projectors as P

#Define the number of colors
Nc = 3
#Define the SU(3) octet (gluon)
```

```
8  g = YT.YoungTableau([Nc-1,1],Nc)
9
10 #Perform the decomposition of gggggggggg state
11 multiplets = g*g*g*g*g*g*g*g*g*g
12 #Print the result of the decomposition
13 multiplets.print()
14
15 #Construct the projectors
16 projectors = P(multiplets, '/where/to/save/')
17 projectors.parallel_evaluation = True
18 projectors.nodes = [
19     "MySuperComputer1.edu",
20     "MySuperComputer2.edu",
21     "MySuperComputer3.edu",
22     ]
23 #Number of parallel processes for MPI
24 #For simple processes it is pointless to have more processes than
   ↪  the number of multiplets
25 projectors.mpi_np = 900
26 #Number of threads FORM is allowed to use
27 projectors.FORM_np = 12
28 projectors.run()
```

The results will be written in the directory indicated on the last line. This path should be accessible by every node configured on line 18. The nodes should be able to establish the SSH-connection with each other without entering of the password manually (for example using SSH keypairs) and each of them should have same version of OpenMPI installed along with other dependencies of OrthoBase. It is possible to manually configure the options for MPI see Section 5.3.3 for more details.

### 5.3.3 Reference manual

OrthoBase consists of two major components: YoungTools and Projectors. The relation of different classes within the library and their purposes are summarized in Figure 5.4.

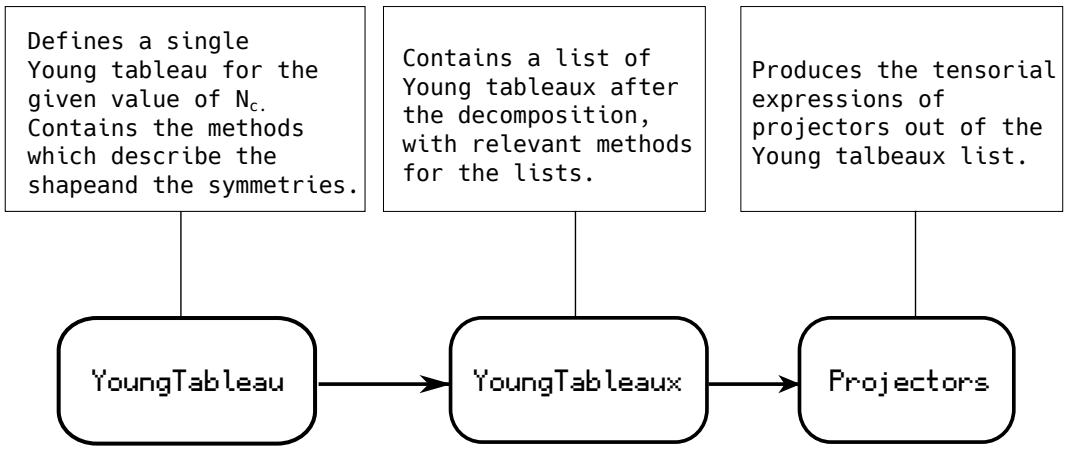


FIGURE 5.4: Flowchart showing the main building blocks of `OrthoBase`. The arrows in the flowchart represent the relationships between the classes: `YoungTableaux` is derived from `YoungTableau`, `Projectors` takes `YoungTableau` as an input.

Below we provide the short description of the most important functions in these classes. The user is advised to check the online documentation [1] which will be kept updated with the upcoming versions of the package.

`YoungTools`

The purpose of this module is to define the object Young tableau and provide the methods to manipulate them. This module contains two classes, `YoungTableau` and `YoungTableaux`. The following program defines a sextet and decouplet of SU(3):

```
»> from OrthoBase import YoungTools as YT
»> sextet = YT.YoungTableau([1,1],3)
»> decouplet = YT.YoungTableau([1,1,1],3)
```

To decompose their direct product it is sufficient to run:

```
»> multiplets = sextet*decouplet
»> multiplets.print(latex=True)
```

[1] https://orthobase.readthedocs.io/

As a result the following output will be produced:

$$6 \otimes 10 = 1 \cdot \overline{15} \oplus 1 \cdot 21 \oplus 1 \cdot 24 \tag{5.13}$$

We note that the dimension of the multiplet does not always distinctly identify the representation. For example the two Young tableaux below both have a dimension 405 in SU(3), but they clearly possess different symmetry properties:

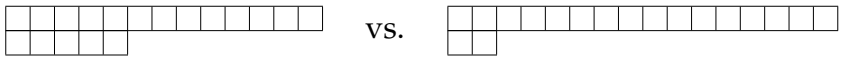 vs. 

In such cases the textual output of the decomposition will be marked accordingly:

$$405_{(13,5)} \qquad \text{vs.} \qquad 405_{(16,2)}$$

`Projectors`

The purpose of this module is to construct the symbolic expressions of the projectors for the multiplets contained in `OrthoBase.YoungTableau`. In addition to that, if the projectors of all previous generations are available, the `FORM`-code can be run automatically in parallel fashion to simplify the color algebra. If this is the case, the resulting projectors will be expressed in terms of simple delta functions, only containing the indices of incoming and outgoing gluons. The output will be saved in the directory provided by the user. This module utilizes `MPI` to parallelize the computation. Since the exact choice of the parameters for `MPI` depends on the particular architecture and installation, the user is expected to provide this input. Otherwise, the package will try to automatically determine the optimal values and in case of the failure the whole calculation will run in the single-threaded mode. The online documentation provides the user access to observe the implementation details of the configuration process.

## 5.4 Validation

There are number of ways the results can be validated. Using this package we were able to repeat the calculation of $ggg \to ggg$ projectors and correctly reproduce the

results reported in [90]. For any process it is straightforward to check the orthogonality of any pair of projectors. Moreover, one can check the completeness relation:

$$\sum_{M\in A^{\otimes N_g}} \mathbf{P}^{M}_{g_1\,g_2\,\cdots,g_{N_g},g_{N_g+1}\cdots g_{2N_g}} = \delta_{g_1\,g_{N_g+1}}\delta_{g_2\,g_{N_g+2}}\cdots\delta_{g_{N_g}\,g_{2N_g}} \tag{5.14}$$

`OrthoBase` automatically generates `FORM` routines for users to run and make sure that the calculation is correct.

## 5.5 Construction of the basis vectors

So far, we have only discussed the construction of the projectors. Ultimately, for the purposes of this study, we are interested in obtaining the color basis for $2 \to n$ processes. This can be achieved using the following strategy:

1. Count the number of gluons, denoted as $n_g$, in the process of interest.
2. If present, count each quark-antiquark pair as one additional gluon (motivated by the decomposition $3 \otimes \overline{3} = 8 \oplus 1$).
3. Calculate all the projectors for $\underbrace{gg\ldots g}_{n_g} \to \underbrace{gg\ldots g}_{n_g}$ according to the strategy described in the previous sections. Identify the multiplets that need to be matched between the initial and final states, similar to what was done in Fig. 5.2.
4. For every multiplet in this list, construct the basis vector using the following formula:

$$C^{M}_{\text{initial}} C^{M\dagger}_{\text{final}}\,, \tag{5.15}$$

   where $M$ denotes the particular multiplet matched in step 4. $C^{M}$initial is a Clebsch-Gordan coefficient constructed for $2 \to 2$ transitions, and $C^{M\dagger}$final is a coefficient for $n_g \to n_g$ transition.

   If a quark-antiquark pair was present in the input, account for the occurrence of the singlet correctly, as it does not produce any new multiplet states but increases the possibilities for pairing the particles.

In this way, one can efficiently construct the orthogonal color basis for any process, perform the color decomposition, and evaluate the color-correlated matrix elements.

We also emphasize that the combined use of an SMT-Solver and a symbolic manipulation program opens novel avenues for calculations within the domain of theoretical particle physics.

# Chapter 6

# Numeric implementation

The integration over physical phase space is managed using an in-house implementation of the VEGAS+ algorithm [111]. The integrator performs the Monte Carlo (MC) integration over a hypercube of unity and a given point in this hypercube gets mapped to the physical phase space by iteratively constructing it.

The phase space construction considers all possible s-channel particle branchings within QCD and uses the inverted FKS mapping to construct three partons out of two using three position coordinates from the hypercube of unity. The phase space is separately constructed for all available subprocesses by merging various final state particles, keeping track of these mergings and continuing the procedure until the program reaches a two-particle configuration with two particles being back-to-back. When the phase space is generated the program, hence, starts with a back-to-back configuration and as already mentioned by using the inverted FKS mapping a new configuration with three particles in the final state is created. Each and every step the code is aware of all possible branchings and the next one is determined in a completely random fashion. The procedure finishes when the number of final state particles reach the desired multiplicity. This method creates the physical phase space in a very economic and fast way such that it is aware of all s-channel singularities making it possible for the integrator to adapt over these singularities for a more efficient integration over phase space.

The package is currently in an active development phase. Therefore, we refrain from providing detailed technical specifications and instead focus our discussion on the key aspects of Monte Carlo integration and how we leverage the advanced features offered by the VEGAS+ algorithm.

## 6.1 Monte Carlo Integration

Monte Carlo integration is a powerful numerical technique for evaluating multi-dimensional integrals, particularly when the integrand is highly complex or exhibits intricate structures that make analytical solutions difficult or impossible [112, 113]. Unlike traditional deterministic integration methods, which rely on quadrature rules or series expansions, Monte Carlo integration is a stochastic approach that leverages random sampling to approximate the integral value [114].

### 6.1.1 Principles of Monte Carlo Integration

The fundamental principle of Monte Carlo integration is based on the law of large numbers and the concept of importance sampling [115, 116]. Consider an integral of the form:

$$I = \int_{D_n} f(x) dx \,, \tag{6.1}$$

where $f(x)$ is the integrand function, and $D_n$ is the integration domain in $n$-dimensional space.

The Monte Carlo approach estimates the integral $I$ by generating a large number of random points $x_i$ within the integration domain $D_n$, evaluating the integrand $f(x_i)$ at each point, and computing the average of the integrand values weighted by the volume element $dx$:

$$I \approx \frac{1}{N} \sum_{i=1}^{N} f(x_i)\, w(x_i) \,. \tag{6.2}$$

Here, $N$ is the number of random points sampled, and $w(x_i)$ is a weight function that accounts for the probability distribution used to generate the random points.

The key to efficient Monte Carlo integration lies in the choice of the sampling strategy and the weight function $w(x_i)$. Various techniques have been developed to improve the convergence rate and reduce the variance of the Monte Carlo estimate, including importance sampling, stratified sampling, and adaptive sampling methods [117–119].

## 6.2 The VEGAS+ Algorithm for Monte Carlo Integration

Monte Carlo integration is a powerful technique for evaluating multidimensional integrals numerically, particularly when the integrand is highly complex or exhibits pronounced structures. The VEGAS (Vector Evaluated Gaussian Sampling) algorithm, introduced by Peter Lepage in 1978 [120], has been widely used for this purpose. However, for integrands with sharp peaks or intricate features in high-dimensional spaces, the original VEGAS algorithm can struggle to achieve accurate and efficient results.

The VEGAS+ algorithm [111], is an enhanced version of the VEGAS algorithm that addresses these limitations. It introduces several improvements and modifications, making it more suitable for integrating highly peaked or structured functions in high-dimensional spaces. This chapter provides a comprehensive overview of the VEGAS+ algorithm, its working principles, and the advantages it offers over the original VEGAS algorithm.

## 6.3 The VEGAS+ Algorithm

### 6.3.1 Stratified Sampling with Hypercubes

One of the key innovations in VEGAS+ is the use of hypercubes for stratified sampling. Unlike the original VEGAS algorithm, which partitions the integration domain into a grid of rectangular boxes (strata), VEGAS+ employs a more flexible stratification scheme using hypercubes. The integration domain is divided into a collection of hypercubes, allowing for better adaptation to the integrand's behavior, especially in regions with pronounced structures or peaks.

The hypercube stratification in VEGAS+ is achieved through the following steps:

1. The integration domain is initially partitioned into a set of hypercubes, each with equal volume.
2. A predetermined number of sampling points are distributed among the hypercubes using a stratified sampling approach, ensuring that each hypercube receives an adequate number of points.

3. The integrand is evaluated at each sampling point, and the contribution of each hypercube to the overall integral is estimated.
4. Based on the estimated contributions, the algorithm adaptively refines the stratification by subdividing the hypercubes with significant contributions into smaller hypercubes for the next iteration.

This adaptive refinement of the stratification allows VEGAS+ to concentrate sampling efforts in regions that contribute the most to the integral value, leading to more accurate and efficient integration.

### 6.3.2 Importance Sampling with Recursive Stratification

Building upon the hypercube stratification, VEGAS+ employs a recursive stratification technique for importance sampling. Each hypercube can be further subdivided into smaller hypercubes if the integrand variation within that region is significant. This recursive stratification allows the algorithm to focus on regions that contribute the most to the integral value, leading to more efficient importance sampling.

The recursive stratification process in VEGAS+ works as follows:

1. After the initial stratification into hypercubes, the algorithm evaluates the integrand at the sampling points within each hypercube.
2. For each hypercube, the algorithm computes the variance of the integrand values within that region.
3. If the variance exceeds a predefined threshold, the hypercube is marked for subdivision into smaller hypercubes.
4. The subdivision process continues recursively until the variance within each hypercube falls below the threshold or a maximum subdivision level is reached.

By recursively subdividing regions with significant integrand variation, VEGAS+ can concentrate sampling efforts in the most important regions, leading to a more accurate and efficient Monte Carlo estimate.

### 6.3.3 Reweighting Technique

In the original VEGAS algorithm, the samples from previous iterations are discarded, and only the samples from the current iteration are used to estimate the integral. However, VEGAS+ employs a reweighting technique to combine the results from different iterations, potentially improving the convergence rate and reducing the overall variance of the Monte Carlo estimate.

The reweighting scheme in VEGAS+ works as follows:

1. After each iteration, the algorithm constructs an importance-sampled probability density function (PDF) based on the samples collected so far.
2. The samples from previous iterations are then reweighted using the updated PDF, ensuring that their contributions are appropriately accounted for in the final integral estimate.
3. The reweighted samples from all iterations are combined to compute the final Monte Carlo estimate of the integral.

This reweighting technique allows VEGAS+ to make efficient use of all the samples collected throughout the iterations, potentially leading to faster convergence and reduced variance compared to discarding samples from previous iterations.

### 6.3.4 Parallelization

One of the significant advantages of the VEGAS+ algorithm is its ability to be easily parallelized, allowing for efficient utilization of multiple processors or cores. This parallelization can significantly speed up the computation for high-dimensional integrals, where the computational cost can be prohibitive on a single processor.

The parallelization in VEGAS+ is achieved through the following steps:

1. The integration domain is partitioned into multiple subdomains, each assigned to a separate processor or core.
2. Each processor independently performs the VEGAS+ algorithm on its assigned subdomain, including stratification, importance sampling, and reweighting.

3. After completing the iterations, the partial integral estimates from all processors are combined to obtain the final Monte Carlo estimate of the integral.

The parallelization in VEGAS+ is facilitated by the stratified sampling approach and the independence of the subdomains. This allows for efficient load balancing and minimal communication overhead between processors, ensuring scalable performance as the number of processors increases.

Additionally, the recursive stratification and reweighting techniques employed in VEGAS+ can be parallelized independently, further enhancing the computational efficiency on modern parallel computing architectures.

## 6.4 Implementation

The primary objective is to develop a versatile computational tool capable of performing the Local Analytic Sector Subtraction for an arbitrary scattering process. In our implementation [121], we divide the calculation process into two main steps:

1. Generation of the subtraction terms and sector functions.
2. Integration over the phase-space.

Step 1 is implemented algebraically in `FORM`, while step 2 relies on `fortran90` for numerical integration.

After providing the process description as input, the `FORM` routines generate all the analytical expressions of the subtraction terms required for the calculation. The output is optimized using the Horner's scheme [122–124] and automatically rewritten in `fortran90` code for numerical integration.

The VEGAS+ algorithm, together with the phase-space generation procedure described above, is implemented in `fortran90`. By taking advantage of Horner's scheme for symbolic expression optimization, combined with compiler-level optimizations in `fortran90`, we can perform numeric evaluations very efficiently. Moreover, we exploit the ability to parallelize the `VEGAS+` algorithm wherever possible.

For random number generation, which is essential for every Monte Carlo (MC) generator, we rely on the "minimal standard" linear congruential generator [125]. We employ good practices used by MC generators: each parallel process is started with

a different seed, ensuring that the statistics genuinely increase, and the seeds are tracked, making every calculation reproducible.

As a development safety measure, we have hard-coded several well-known results in the package, which can be reproduced using this MC generator. This practice ensures that after introducing any changes, the MC generator continues to function correctly.

Although the package is still under active development, it is already fully functional. In the next chapter, we will showcase numerous results obtained using this package.

# Chapter 7

# A case of $e^+e^- \to 3$ jets

As a proof-concept-calculation we study the leptonic production of 3 hadronic jets. The $e^+e^- \to 3$ jets process, where an electron-positron pair annihilates into a final state with 3 jets of hadrons, is one of the important observables for testing Quantum Chromodynamics (QCD) at electron-positron colliders.

It is particularly interesting because it provides a direct probe of the triple gluon vertex, which is a distinctive feature of the non-abelian nature of QCD. Precise measurements of the $e^+e^- \to 3$ jets process can shed light on the detailed dynamics of gluon interactions and the strong coupling constant $\alpha_s$.

Experimentally, the $e^+e^- \to 3$ jets process, which was first observed at the PETRA collider [126], has been extensively studied at various colliders, such as LEP [127, 128] and HERA [129], over a wide range of center-of-mass energies, allowing for the collection of precise data on the 3-jet event rates and jet distributions.

On the theoretical side corrections up to NNLO are known and extensively studied [80, 130–133].

For us, this is an interesting process because even though at NNLO this process contains multiple subprocesses with involved kinematics, it is the simplest process to which the LASS scheme can be applied. The particular phase-space mappings employed in the current formulation of the LASS do not allow one to study the much simpler $e^+e^- \to 2$ jet process, as there are not enough partons in the final state to choose as a reference during the factorization. Having said that, advantageously, because the 3-jet process provides a rich singularity structure, it makes it possible to test all kinds of limits entering the subtraction terms, which would not be the

case for the 2-jet calculation. Consequently, studying the 3-jet process provides a stringent test for the LASS scheme.

At NNLO in QCD following subprocesses contribute to 3 jet production:

$$
\begin{aligned}
RR: \quad & e^+e^- \to q\bar{q}q\bar{q}g && (7.1)\\
& e^+e^- \to q\bar{q}r\bar{r}g && (7.2)\\
& e^+e^- \to q\bar{q}gg && (7.3)\\
RV: \quad & e^+e^- \to q\bar{q}q\bar{q} && (7.4)\\
& e^+e^- \to q\bar{q}r\bar{r} && (7.5)\\
& e^+e^- \to q\bar{q}gg && (7.6)\\
VV: \quad & e^+e^- \to q\bar{q}g, && (7.7)
\end{aligned}
$$

where the notation $q$ and $r$ is used to distinguish between quarks of different flavors. The processes in Eqs. (7.1) – (7.3) involve only tree-level kinematics and helicity amplitudes, from which the squared matrix elements can be constructed using the results in Refs. [134–136]. The processes in Eqs. (7.4) – (7.6) contain one-loop virtual corrections, and their matrix elements can be constructed using the method described in Ref. [137]. Finally, the process in Eq. (7.7) involves two-loop virtual corrections, and the corresponding matrix element can be found in Refs. [80, 131].

The primary objective of this segment of our study is to validate the well-established results for 3-jet event shape observables by employing Eq. (3.35). This serves as a rigorous test of the accuracy and reliability of the adopted scheme and its computational implementation. Furthermore, it presents an opportunity to gain valuable insights into the efficiency and performance of the calculation methodology. In the subsequent sections, we detail the comprehensive checks and cross-validations we have performed specifically for the 3-jet process, along with preliminary results for the distributions of event shape observables. While our efforts are ongoing, and the complete final results are yet to be obtained, the partial findings presented herein demonstrate the first NNLO calculation performed using the LASS scheme, laying the foundation for the ultimate goal to efficiently automatize the NNLO calculations.

## 7.1 VV contribution: pole cancellation and the finite part

Among all the components entering the NNLO calculation, the $VV$ contribution is the easiest to treat from an integration standpoint. Although we have formally confirmed in Chapter 6 that $I^{(\mathbf{1})} + I^{(\mathbf{12})}$ always cancels the poles of the $VV$ contribution based on the factorization properties of IR radiation in QCD, we can also explicitly demonstrate the same for this specific process. For future reference, we provide the result of the explicit calculation of the pole expansion of the $I^{(\mathbf{1})} + I^{(\mathbf{12})}$ operator specifically for 3-jet production.

$$
\begin{aligned}
&(I^{(\mathbf{1})} + I^{(\mathbf{12})})^{3\text{jets}}_{\text{poles}} = \\
&B\left(\frac{\alpha_S}{2\pi}\right)^2 \Bigg\{ \frac{1}{\epsilon^4}\left[\frac{C_A^2}{2} + \left(2C_F - \frac{17}{3}\right)C_A + 2C_F^2 - \frac{34C_F}{3}\right] \\
&\quad + \frac{1}{\epsilon^3}\Bigg[\left(L_{12} - L_{13} - L_{23} + \frac{11}{24}\right)C_A^2 + \left(-\frac{N_f T_R}{6} - 6L_{12} + \frac{26L_{13}}{3} + C_F\left(-2L_{13} - 2L_{23} + \frac{47}{12}\right) + \frac{26L_{23}}{3} - \frac{164}{9}\right)C_A \\
&\qquad + \frac{34N_f T_R}{9} + C_F^2(6 - 4L_{12}) + C_F\left(-\frac{N_f T_R}{3} + \frac{32L_{12}}{3} + 6L_{13} + 6L_{23} - \frac{98}{3}\right)\Bigg] \\
&\quad + \frac{1}{\epsilon^2}\Bigg[\left(-\frac{5\pi^2}{8} + L_{13}^2 + L_{23}^2 + \frac{35L_{12}}{12} - L_{12}L_{13} - \frac{11L_{13}}{4} - L_{12}L_{23} + L_{13}L_{23} - \frac{35L_{23}}{12} + \frac{467}{72}\right)C_A^2 \\
&\qquad + \Bigg(\frac{119\pi^2}{36} + \frac{5L_{12}^2}{2} - \frac{35L_{13}^2}{6} - \frac{35L_{23}^2}{6} - \frac{178L_{12}}{9} + \frac{10}{3}L_{12}L_{13} + \frac{427L_{13}}{18} + N_f T_R\left(-\frac{L_{12}}{3} + L_{13} + \frac{L_{23}}{3} - \frac{37}{18}\right) \\
&\qquad\quad + \frac{10}{3}L_{12}L_{23} - 6L_{13}L_{23} + \frac{74L_{23}}{3} \\
&\qquad\quad + C_F\left(-\frac{29\pi^2}{12} - 2L_{12}^2 + L_{13}^2 + L_{23}^2 + \frac{5L_{12}}{3} + 2L_{12}L_{13} - \frac{20L_{13}}{3} + 2L_{12}L_{23} - \frac{13L_{23}}{2} + \frac{463}{18}\right) - \frac{4951}{108}\Bigg)C_A \\
&\qquad + N_f T_R\left(\frac{2L_{12}}{9} - \frac{52L_{13}}{9} - 2L_{23} + \frac{413}{27}\right) + C_F^2\left(-\frac{7\pi^2}{3} + 4L_{12}^2 - 13L_{12} + L_{23} + \frac{49}{2}\right) \\
&\qquad + C_F\left(\frac{119\pi^2}{18} - 5L_{12}^2 + \frac{69L_{12}}{2} - 6L_{12}L_{13} + 9L_{13} + N_f T_R\left(\frac{2L_{12}}{3} + \frac{4L_{13}}{3} - \frac{46}{9}\right) - 6L_{12}L_{23} + \frac{37L_{23}}{6} - \frac{481}{6}\right)\Bigg] \\
&\quad + \frac{1}{\epsilon}\Bigg[C_A^2\left(-\frac{1}{3}L_{12}^3 + \frac{1}{2}L_{13}L_{12}^2 + \frac{1}{2}L_{23}L_{12}^2 + \frac{L_{12}^2}{12} - \frac{5}{4}\pi^2 L_{12} + \frac{1}{2}L_{13}^2 L_{12} + \frac{1}{2}L_{23}^2 L_{12} - \frac{23}{6}L_{13}L_{12} - 4L_{23}L_{12} + \frac{205L_{12}}{12}\right. \\
&\qquad - \frac{2L_{13}^3}{3} - \frac{2L_{23}^3}{3} - \frac{319\pi^2}{144} + \frac{11L_{13}^2}{3} - \frac{1}{2}L_{13}L_{23}^2 + \frac{47L_{23}^2}{12} - \frac{103\zeta_3}{12} + \frac{5}{4}\pi^2 L_{13} - \frac{49L_{13}}{3} + \frac{5}{4}\pi^2 L_{23} \\
&\qquad\qquad \left. - \frac{1}{2}L_{13}^2 L_{23} + \frac{23}{6}L_{13}L_{23} - \frac{205L_{23}}{12} + \frac{1625}{54}\right) \\
&\qquad + C_A\left(-\frac{7}{9}L_{12}^3 - \frac{3}{2}L_{13}L_{12}^2 - \frac{3}{2}L_{23}L_{12}^2 + \frac{107L_{12}^2}{12} + \frac{7}{2}\pi^2 L_{12} - \frac{1}{6}L_{13}^2 L_{12} - \frac{1}{6}L_{23}^2 L_{12} + \frac{119}{18}L_{13}L_{12} + \frac{20}{3}L_{23}L_{12}\right. \\
&\qquad - \frac{1391L_{12}}{27} + \frac{22L_{13}^3}{9} + \frac{22L_{23}^3}{9} + \frac{287\pi^2}{27} - \frac{263L_{13}^2}{18} + \frac{3}{2}L_{13}L_{23}^2 - \frac{187L_{23}^2}{12} + \frac{425\zeta_3}{9} - \frac{91}{18}\pi^2 L_{13} + \frac{6751L_{13}}{108} \\
&\qquad \left. - \frac{91}{18}\pi^2 L_{23} + \frac{3}{2}L_{13}^2 L_{23} - \frac{23}{2}L_{13}L_{23} + \frac{199L_{23}}{3} + N_f T_R\left(\frac{29\pi^2}{36} + \frac{L_{12}^2}{3} - \frac{4L_{13}^2}{3} - \frac{L_{23}^2}{3} - \frac{11L_{12}}{3} + \frac{2}{3}L_{12}L_{13}\right.\right.
\end{aligned}
$$

$$
\begin{aligned}
&+\frac{59L_{13}}{9}-\frac{2}{3}L_{13}L_{23}+\frac{11L_{23}}{3}-\frac{40}{3}\Bigg)+C_F\Bigg(2L_{12}^3-L_{13}L_{12}^2-L_{23}L_{12}^2-\frac{89L_{12}^2}{12}+\frac{1}{6}\pi^2L_{12}-L_{13}^2L_{12}-L_{23}^2L_{12}\\
&+\frac{43}{6}L_{13}L_{12}+8L_{23}L_{12}-\frac{17L_{12}}{4}-\frac{L_{13}^3}{3}-\frac{L_{23}^3}{3}-\frac{527\pi^2}{72}+\frac{10L_{13}^2}{3}+\frac{11L_{23}^2}{4}-\frac{239\zeta_3}{6}+\frac{7}{3}\pi^2L_{13}-\frac{479L_{13}}{18}\\
&+\frac{7}{3}\pi^2L_{23}-\frac{1}{2}L_{13}L_{23}-\frac{313L_{23}}{12}+\frac{22217}{216}\Bigg)-\frac{11192}{81}\Bigg)\\
&+N_f^2T_R^2\left(\frac{32}{27}-\frac{4L_{13}}{9}\right)+N_fT_R\Bigg(-\frac{119\pi^2}{54}+\frac{35L_{13}^2}{9}+\frac{16L_{12}}{27}-\frac{2}{9}L_{12}L_{13}-\frac{557L_{13}}{27}+2L_{13}L_{23}-\frac{16L_{23}}{3}+\frac{3508}{81}\Bigg)\\
&+C_F^2\left(-\frac{8}{3}L_{12}^3+\frac{27L_{12}^2}{2}+\frac{14}{3}\pi^2L_{12}-L_{23}L_{12}-\frac{105L_{12}}{2}-\frac{15\pi^2}{2}-\frac{L_{23}^2}{2}-\frac{82\zeta_3}{3}+\frac{7L_{23}}{2}+\frac{723}{8}\right)\\
&+C_F\Bigg(\frac{14L_{12}^3}{9}+3L_{13}L_{12}^2+3L_{23}L_{12}^2-\frac{199L_{12}^2}{12}-\frac{56}{9}\pi^2L_{12}-\frac{21}{2}L_{13}L_{12}-\frac{32}{3}L_{23}L_{12}+\frac{1037L_{12}}{12}+\frac{343\pi^2}{18}+\frac{35L_{23}^2}{12}\\
&+\frac{850\zeta_3}{9}-\frac{7}{2}\pi^2L_{13}+30L_{13}+N_fT_R\Bigg(\frac{25\pi^2}{18}-\frac{2L_{12}^2}{3}-\frac{2L_{13}^2}{3}+7L_{12}-\frac{4}{3}L_{12}L_{13}+\frac{50L_{13}}{9}-\frac{L_{23}}{3}-\frac{650}{27}\Bigg)\\
&-\frac{7}{2}\pi^2L_{23}+\frac{3}{2}L_{13}L_{23}+\frac{245L_{23}}{12}-\frac{745}{3}\Bigg)\Bigg]\Bigg\}\\
&+V_{\text{fin}}\left(\frac{\alpha_S}{2\pi}\right)\left\{\frac{1}{\epsilon^2}\Big[C_A+2C_F\Big]+\frac{1}{\epsilon}\left[-\frac{2}{3}N_fT_R+C_F\left(3-2L_{12}\right)+C_A\left(L_{12}-L_{13}-L_{23}+\frac{11}{6}\right)\right]\right\}. \qquad (7.8)
\end{aligned}
$$

The expansion assumes that $V$ is only expanded up to $\mathcal{O}(1)$. Under the same assumption, the same expansion with the opposite sign can be extracted from Ref. [80], which confirms the $VV$ pole cancellation once again.

Regarding the finite remainder, we note that the finite contributions given in both Refs. [80, 131] were derived with the 1-loop virtual contribution, which includes terms up to $\mathcal{O}(\epsilon^2)$ with no straightforward way to turn off these contributions. Thus, if one uses these references for a calculation involving the LASS scheme, Eq.(7.24) from [29] is not directly applicable, and it is necessary to re-derive the finite part. Given that the expressions for $I^{(\mathbf{1})}$ and $I^{(\mathbf{RV})}$ are quite generic, this does not pose a serious challenge.

Concerning the numeric integration itself, since $VV$ does not feature phase-space singularities, the MC generator can easily handle the finite integrand.

## 7.2 Limiting behavior of the subtraction terms

The $RV$ and $RR$ contributions involve phase-space singularities, making the integration procedure more intricate. Before attempting to integrate the assembled integrand over the entire phase-space, it is advisable to examine the limiting behavior of all the subsection terms entering the calculation. While this part of the calculation

is unnecessary for end-users interested solely in applying the LASS scheme, it is an essential step in the development process, as it can expose any shortcomings of the phase-space mapping or sector function definition employed.

To this end, we construct every possible subtraction term entering the calculation and check the consistency of those definitions by approaching various singular limits. This is achieved by introducing the scaling parameter $\lambda$, similar to the approach described in Sec. 2.3. We iteratively decrease the value of $\lambda$ and observe the ratios of the various terms, which should cancel out. To precisely observe this cancellation effect, high numerical accuracy is crucial. Therefore, we employ the `MPFUN20` library [138], a powerful arbitrary-precision arithmetic tool, enabling us to perform all subsequent calculations in this section with a precision of 100 decimal digits. This meticulous level of precision is essential in rigorously validating the consistency of our definitions across singular limits, ensuring the robustness of our approach.

### 7.2.1 *RR*

The real-real radiation process exhibits a rich structure of singularities. Although the subsequent calculation was performed for every subprocess listed in Eqs. (7.1) – (7.3), in this thesis, we limit our discussion to the subprocess in Eq. (7.3). This subprocess features every type of subtraction term and diverges in all possible singular limits, making it an ideal candidate for our analysis. There are several ways to test the limiting behavior of the *RR* subtraction. For instance, if the definition of the projection operators is correct, the following relation should hold:

$$\lim_{i,j\to 0} \frac{S_{ij}C_{ijk}}{C_{ijk}} \to 1 \tag{7.9}$$

One can construct similar relations for all kinds of projectors appearing in Eq. (3.44). Additionally, it is possible to monitor the ratio of the squared matrix element and a subterm or the full contribution:

$$\lim_{P} \frac{|\mathcal{M}|^2}{P} \to 1\,, \qquad \lim_{P} \frac{|\mathcal{M}|^2}{K^{(\mathbf{1})} + K^{(\mathbf{2})} + K^{(\mathbf{12})}} \to 1\,, \tag{7.10}$$

where $P$ can be any singular limit affecting the given subprocess, and the notation

"$\lim_{P}$" means that we are approaching that particular limit. For example, "$\lim_{C_{ijk}}$" corresponds to the case when partons $i$, $j$, and $k$ become collinear.

The $e^+e^- \to q\bar{q}ggg$ subprocess features 49 different singular limits, and there can be a total of 187 different ratios to check. We examine all of them, and in Figs. 7.1 – 7.4, we present the limiting behavior of the last ratio from Eq. (7.10). On the horizontal axis, we plot the different values of the $\lambda$ variable, which parametrizes the distance from the particular singular limit. On the vertical axis, we plot $\log_{10}(1 - R)$, where $R$ is defined in the plots, indicating the number of digits of accuracy with which $R$ matches unity.

In all cases, we observe that as the values of $\lambda$ decrease, the plotted ratio approaches unity more closely. This strongly confirms the correct definition and implementation of the subtraction terms.

### 7.2.2 *RV*

The same principles apply to the *RV* contribution. However, in this case, the singular structure is much simpler. As described in Chapter 3, at this level, the only subtraction term featuring the singular projectors is $K^{(\mathbf{RV})}$. The remaining terms are the integrated subtraction terms $I^{(\mathbf{1})}$ and $I^{(\mathbf{12})}$. Since $K^{(\mathbf{RV})}$ is designed to cancel the phase-space singularities of *RV*, and $I^{(\mathbf{12})}$ cancels the singularities of $I^{(\mathbf{1})}$, it is sufficient to examine their respective ratios in the singular limits appearing in the $K^{(\mathbf{RV})}$ term. This has been done for each individual subprocess listed in Eqs. (7.4) – (7.6).

Due to the simpler singular kinematics for these subprocesses compared to the *RR* subprocesses, there are fewer limits to examine. The $e^+e^- \to q\bar{q}q\bar{q}$ process features a total of 4 singular limits, $e^+e^- \to q\bar{q}r\bar{r}$ features two, and $e^+e^- \to q\bar{q}gg$ features 7 singular limits.

The results for the ratios of $I^{(\mathbf{1})}$ and $I^{(\mathbf{12})}$ are plotted in Figs. 7.5 – 7.7, while the ratios of *RV* and $K^{(\mathbf{RV})}$ are plotted in Figs. 7.8 – 7.10. On these plots, the absolute value of the numbers read from the vertical axis indicates the number of digits of accuracy with which the ratio matches unity.

Similar to the *RR* case, we observe that for *RV*, the subtraction terms behave correctly in all cases.

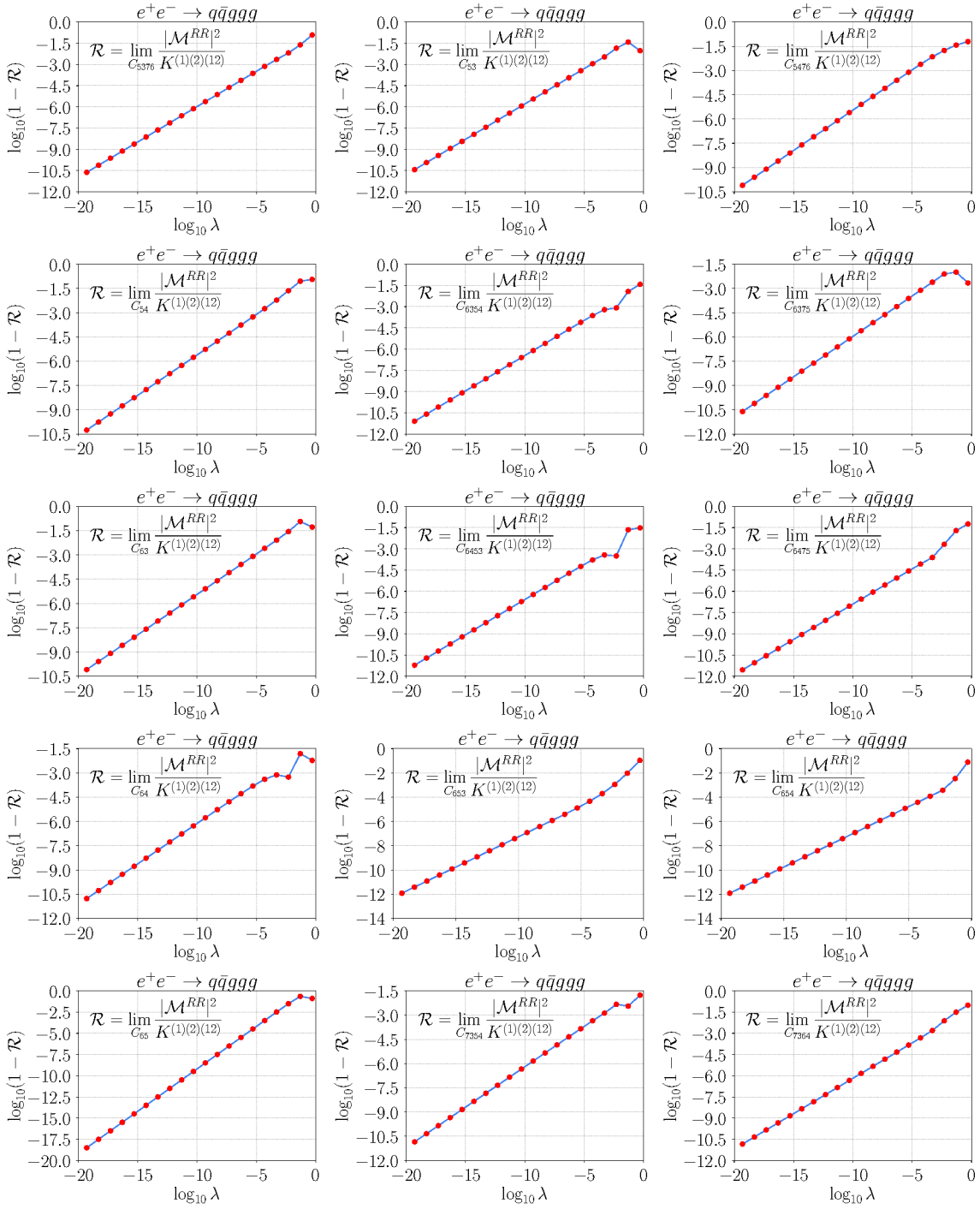


FIGURE 7.1: Limiting behavior of the ratio between the double-real squared matrix element and the $RR$ subtraction terms in various singular limits for the $e^+e^- \to q\bar{q}ggg$ contribution. Each plot corresponds to a different singular limit, as indicated on the respective plot. The shorthand notation $K^{(\mathbf{1})(\mathbf{2})(\mathbf{12})} = K^{(\mathbf{1})} + K^{(\mathbf{2})} + K^{(\mathbf{12})}$ is used.

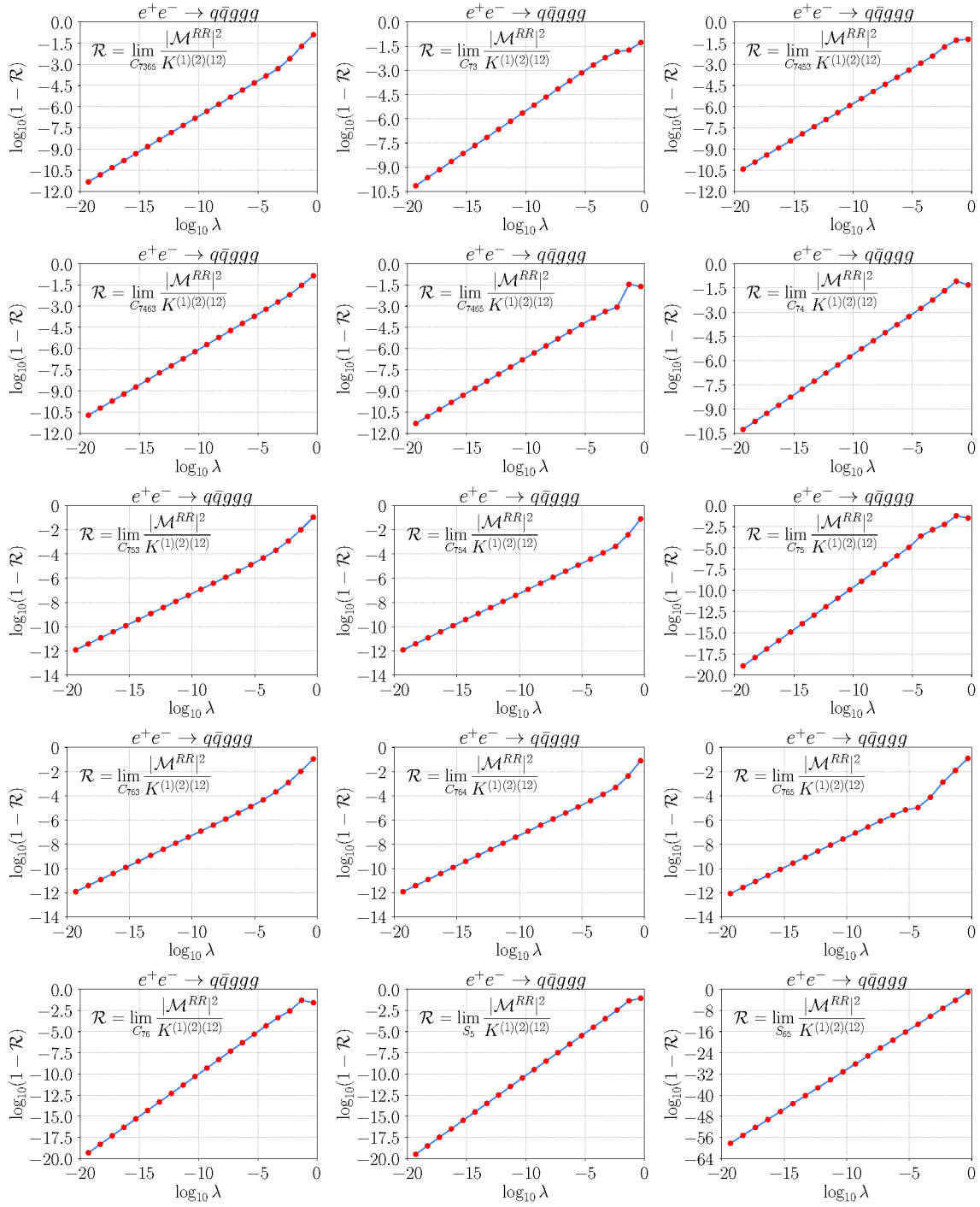


FIGURE 7.2: Limiting behavior of the ratio between the double-real squared matrix element and the $RR$ subtraction terms in various singular limits for the $e^+e^- \to q\bar{q}ggg$ contribution. Each plot corresponds to a different singular limit, as indicated on the respective plot. The shorthand notation $K^{(\mathbf{1})(\mathbf{2})(\mathbf{12})} = K^{(\mathbf{1})} + K^{(\mathbf{2})} + K^{(\mathbf{12})}$ is used.

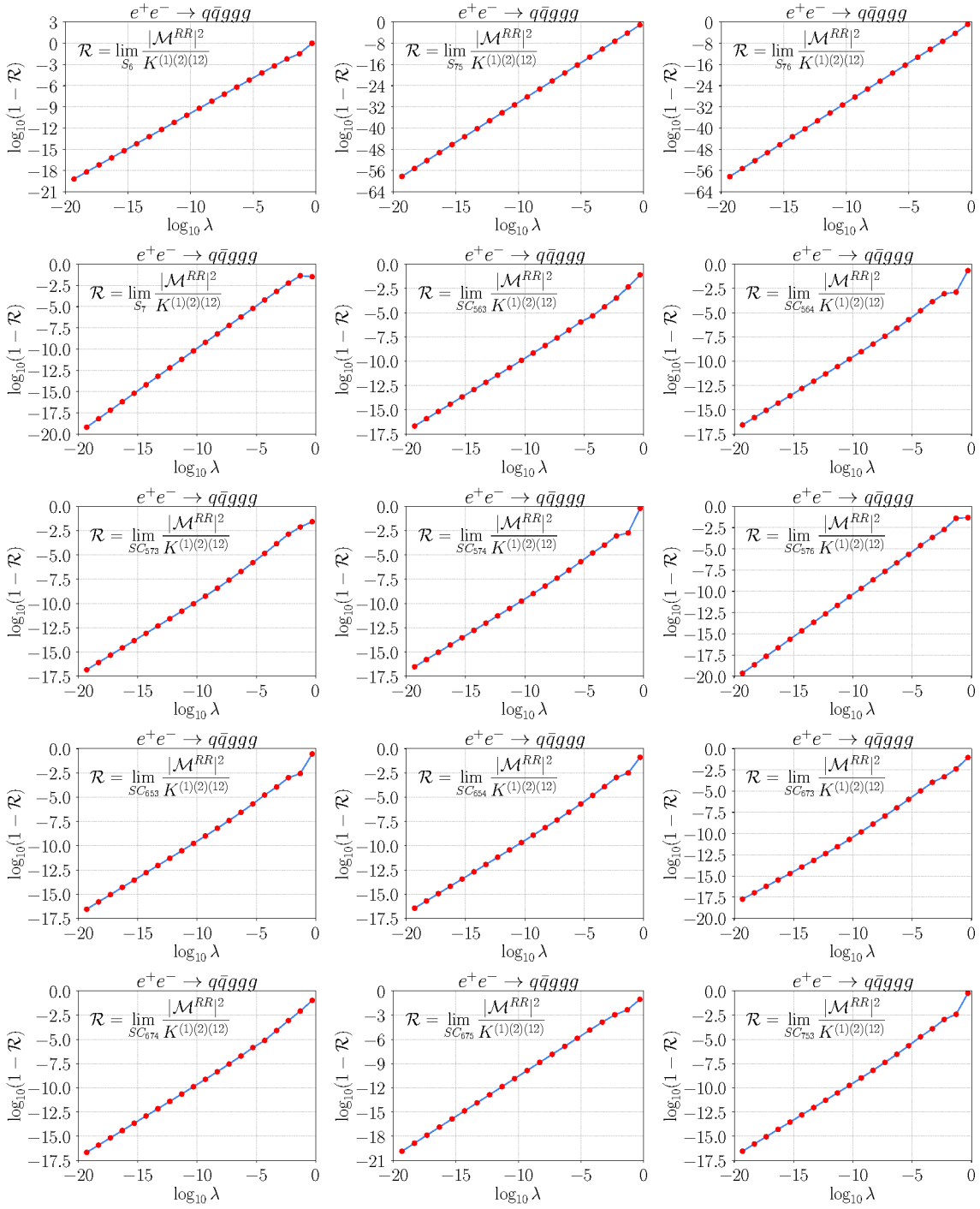


FIGURE 7.3: Limiting behavior of the ratio between the double-real squared matrix element and the $RR$ subtraction terms in various singular limits for the $e^+e^- \to q\bar{q}ggg$ contribution. Each plot corresponds to a different singular limit, as indicated on the respective plot. The shorthand notation $K^{(\mathbf{1})(\mathbf{2})(\mathbf{12})} = K^{(\mathbf{1})} + K^{(\mathbf{2})} + K^{(\mathbf{12})}$ is used.

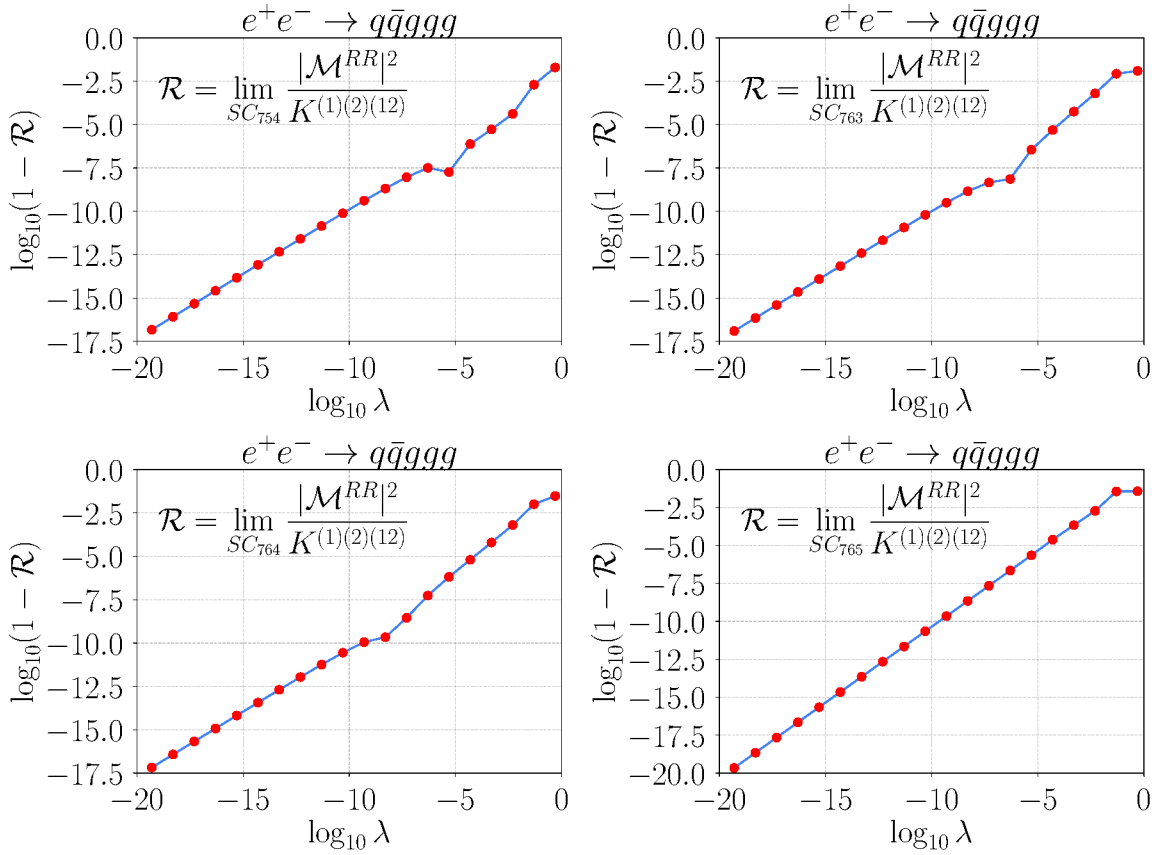


FIGURE 7.4: Limiting behavior of the ratio between the double-real squared matrix element and the $RR$ subtraction terms in various singular limits for the $e^+e^- \to q\bar{q}ggg$ contribution. Each plot corresponds to a different singular limit, as indicated on the respective plot. The shorthand notation $K^{(1)(2)(12)} = K^{(1)} + K^{(2)} + K^{(12)}$ is used.

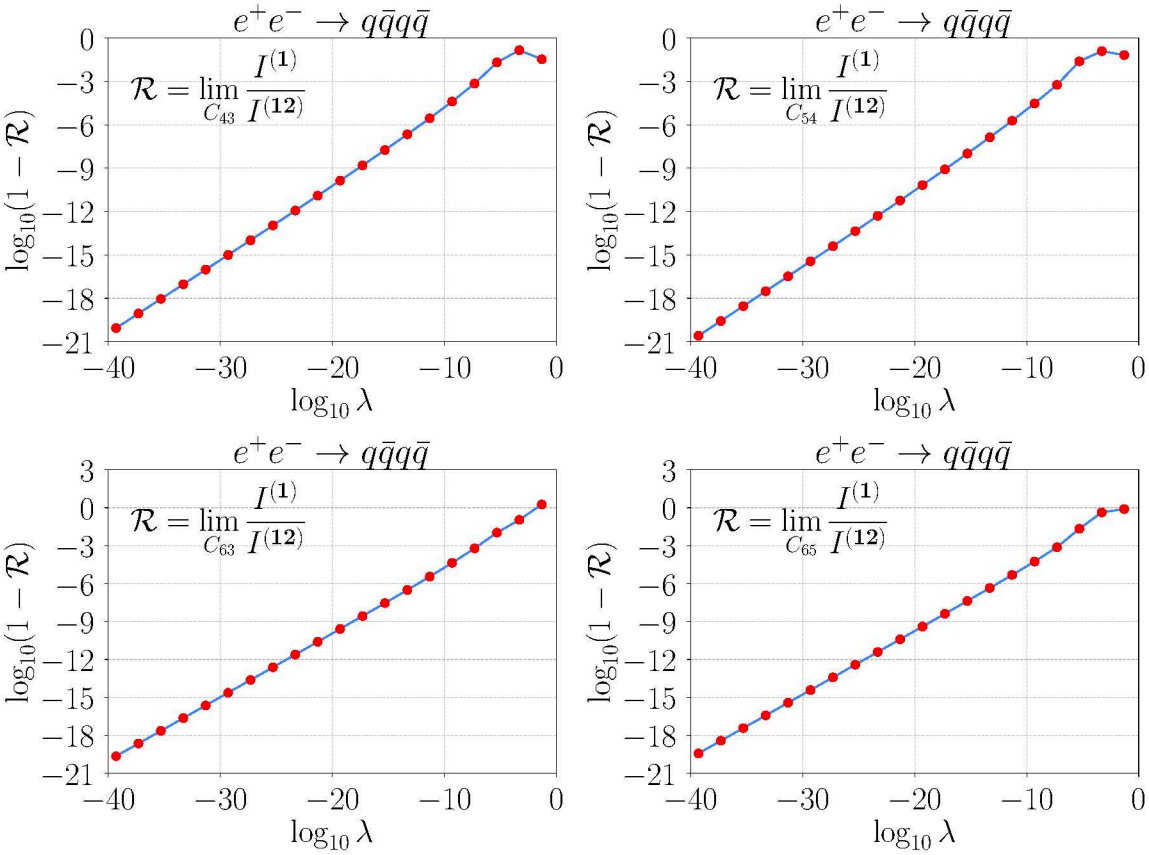


FIGURE 7.5: Limiting behavior of the ratio between $I^{(1)}$ and $I^{(12)}$ terms in various singular limits for the one-loop correction to $e^+e^- \to q\bar{q}q\bar{q}$ contribution. Each plot corresponds to a different singular limit, as indicated on the respective plot.

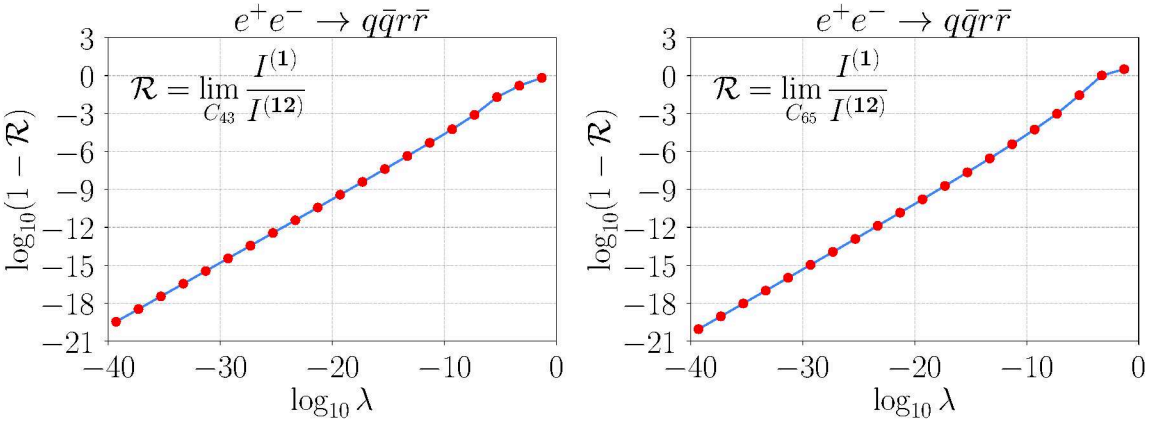


FIGURE 7.6: Limiting behavior of the ratio between $I^{(1)}$ and $I^{(12)}$ term in various singular limits for the one-loop correction to $e^+e^- \to q\bar{q}r\bar{r}$ contribution. Each plot corresponds to a different singular limit, as indicated on the respective plot.

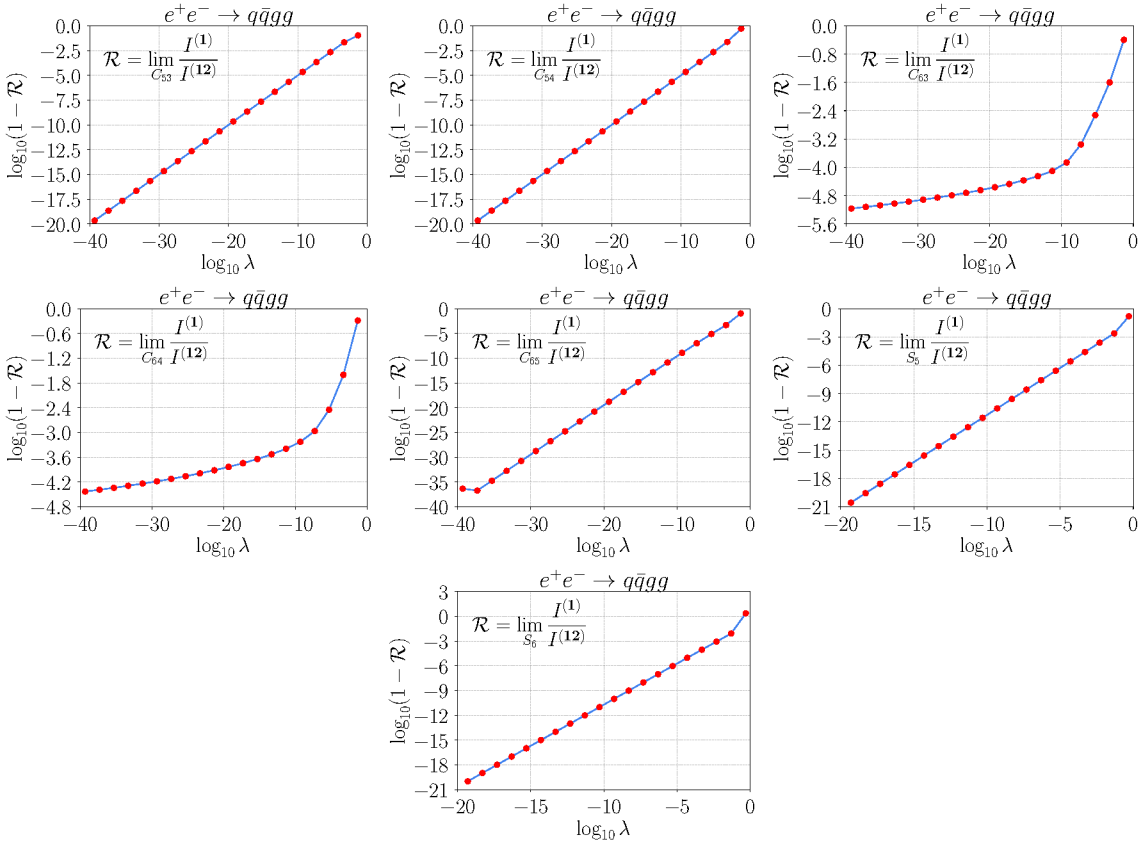


FIGURE 7.7: Limiting behavior of the ratio between $I^{(1)}$ and $I^{(12)}$ term in various singular limits for the one-loop correction to $e^+e^- \to q\bar{q}gg$ contribution. Each plot corresponds to a different singular limit, as indicated on the respective plot.

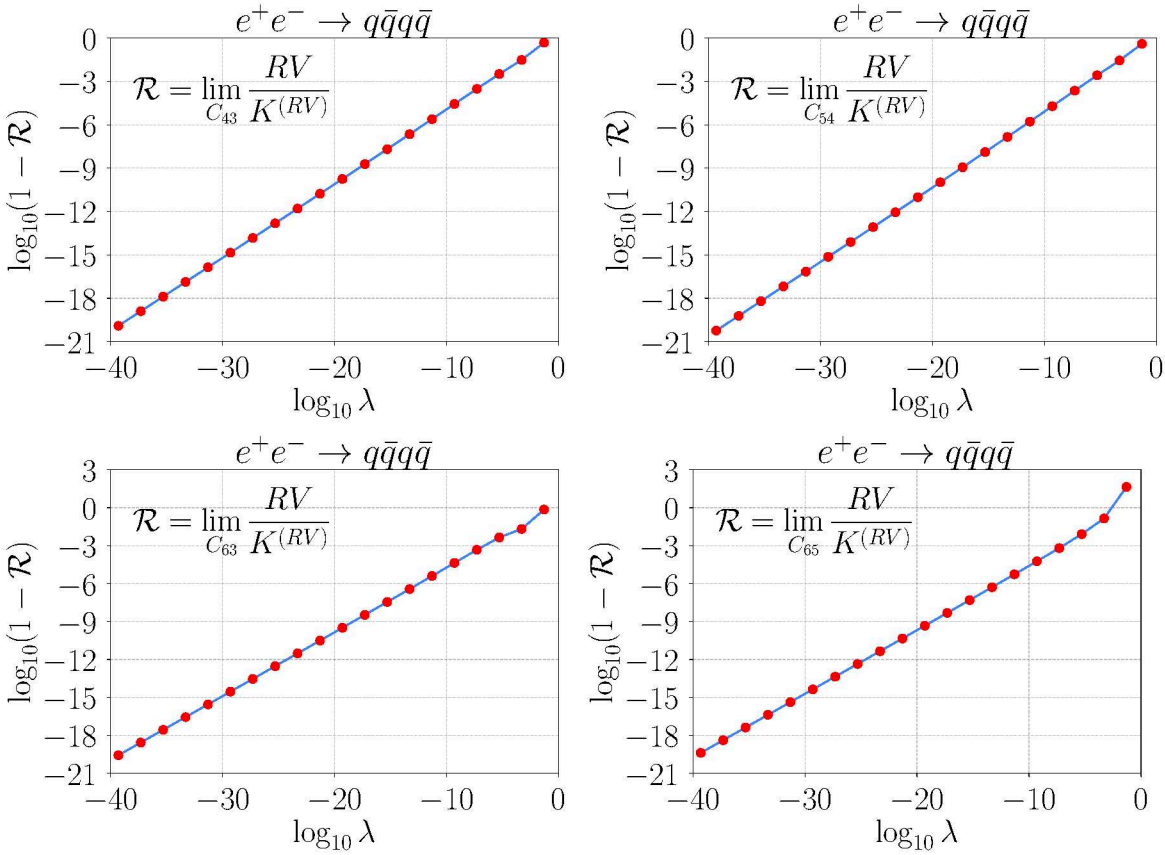


FIGURE 7.8: Limiting behavior of the ratio between $RV$ and $K^{(\mathbf{RV})}$ terms in various singular limits for the one-loop correction to $e^+e^- \to q\bar{q}q\bar{q}$ contribution. Each plot corresponds to a different singular limit, as indicated on the respective plot.

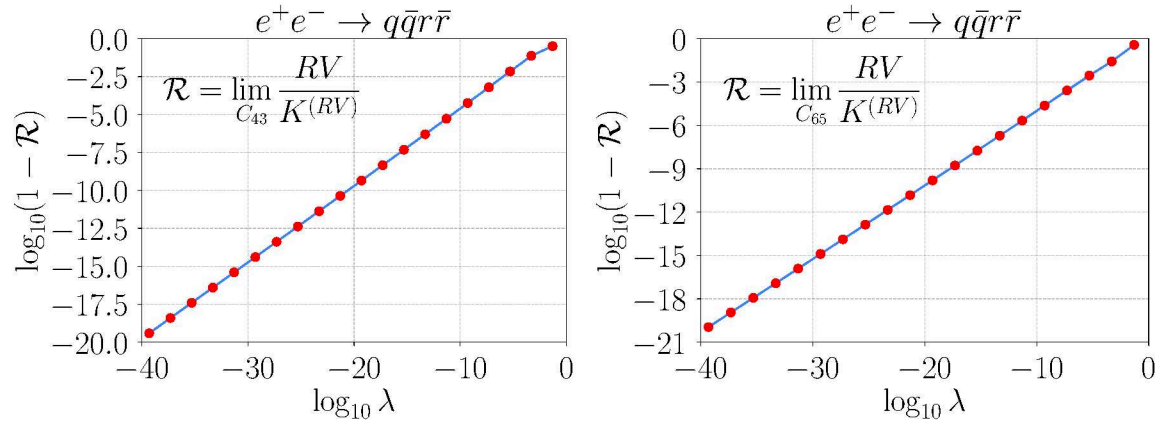


FIGURE 7.9: Limiting behavior of the ratio between $RV$ and $K^{(\mathbf{RV})}$ terms in various singular limits for the one-loop correction to $e^+e^- \to q\bar{q}r\bar{r}$ contribution. Each plot corresponds to a different singular limit, as indicated on the respective plot.

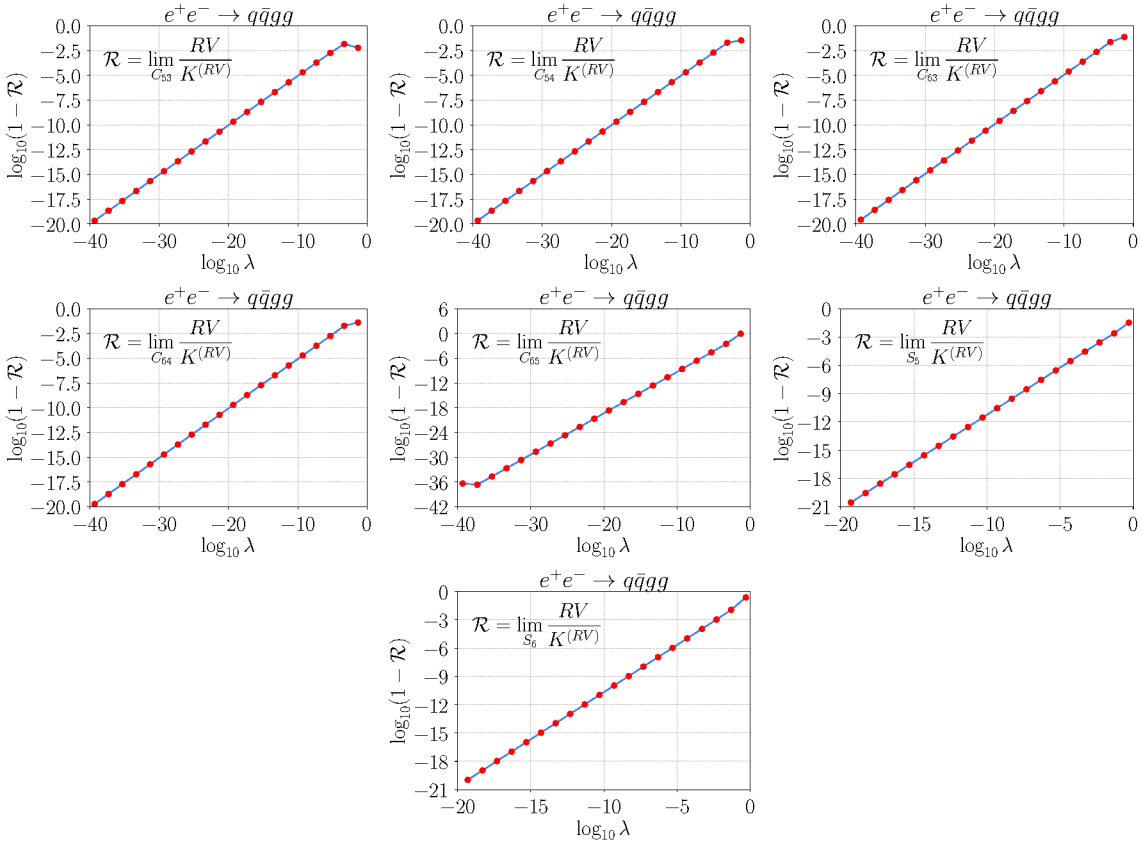


FIGURE 7.10: Limiting behavior of the ratio between $RV$ and $K^{(\mathbf{RV})}$ terms in various singular limits for the one-loop correction to $e^+e^- \to q\bar{q}gg$ contribution. Each plot corresponds to a different singular limit, as indicated on the respective plot.

## 7.3 Technical cut

As it was outlined in Chapter 6 the integration should be carried out numerically using a Monte Carlo program. Due to the internal representation of real numbers in computers, adhering to the IEEE 754 floating-point standard, real numbers can only be stored with a finite number of digits. This finite representation allocates a fixed number of bits to store the significand (mantissa) and exponent of a number.

While this representation is generally sufficient for end results, providing about 14 to 16 significant digits, when higher-order computations are carried out, the limitation in precision can pose challenges at intermediate steps. As the phase-space points are generated closer to the kinematic singularities of unresolved emissions, the cross-section becomes larger. Consequently, the analytically correct subtraction terms may involve operands with vastly different magnitudes.

In such cases, the finite precision of the IEEE 754 representation can lead to a phenomenon known as "loss of significance" or "catastrophic cancellation" [139, 140]. When adding or subtracting numbers with significantly different exponents, the alignment of the mantissas requires shifting the smaller number's mantissa to match the exponent of the larger number. During this process, leading digits from the smaller number may be lost, resulting in a loss of precision or accuracy.

Thus, we end up with pervasive erroneous large numbers hindering the convergence of our Monte Carlo integration due to the finite number of stored digits and the loss of significance when dealing with operands of vastly different magnitudes.

This behavior was observed early on when the first NLO QCD computations were performed, and as a solution, a small (technical) cut was imposed on the physical phase space. Later on the similar phase-space cut was used at NNLO level as well [141].

In the following work we examined the three choices of $y_{\min}$:

$$\begin{aligned} y_{\min}^{(1)} &= \min_{i,j} \frac{s_{ij}}{s}\,, \qquad y_{\min}^{(2)} = \min_{i,j\neq i,k\neq j,i} (e_i^2,\, w_{ij},\, e_i^2 w_{jk})\,, \\ & y_{\min}^{(3)} = \min_{i,j\neq i,k\neq j,i} (e_i^2,\, w_{ij})\,, \end{aligned} \tag{7.11}$$

where $e_i$ and $w_{ij}$ were defined in Eq. (3.17). The choice of $y_{\min}^{(1)}$ is motivated by

Ref. [141], while the choices of $y_{\text{min}}^{(2)}$ and $y_{\text{min}}^{(3)}$ are motivated by the construction of sector functions in the LASS scheme. In the notation above, the indices $i$, $j$, and $k$ iterate through all possible parton configurations, and the values are fixed to the configuration that generates the minimal value for the listed arguments.

The distinction between $y_{\text{min}}^{(3)}$ and $y_{\text{min}}^{(2)}$ lies in the fact that the former excludes the overlap terms of $e_i^2$ and $w_{ij}$. The construction of overlap terms is manageable for $RV$ radiation. However, $RR$ processes exhibit a much richer overlap structure, and by conducting this study, we can gain insights into whether accounting for the overlap is necessary or not.

The study is conducted as follows: For every choice of $y_{\text{min}}$ from Eq. (7.11), we fix the actual value of $y_{\text{min}}$ to $10^{-4}$ and gradually decrease it in small intervals until it reaches $10^{-10}$. For each value of $y_{\text{min}}$, we perform the Monte Carlo integration as described in the previous chapter by generating $10,000,000$ phase-space points and optimizing the grid 40 times. After every iteration, we calculate a new estimate of the cross-section. Once all 40 iterations are completed, we plot the resulting differential cross-section as a function of the particular choice of $y_{\text{min}}$.

To gain further insights, we combine the results of these 40 independent estimates in each bin using two methods. First, we calculate the average of the estimates. Second, we calculate the weighted average, where the inverse values of the mean squared errors are used as weights. This latter method effectively gives preference to more stable integration iterations with smaller errors.

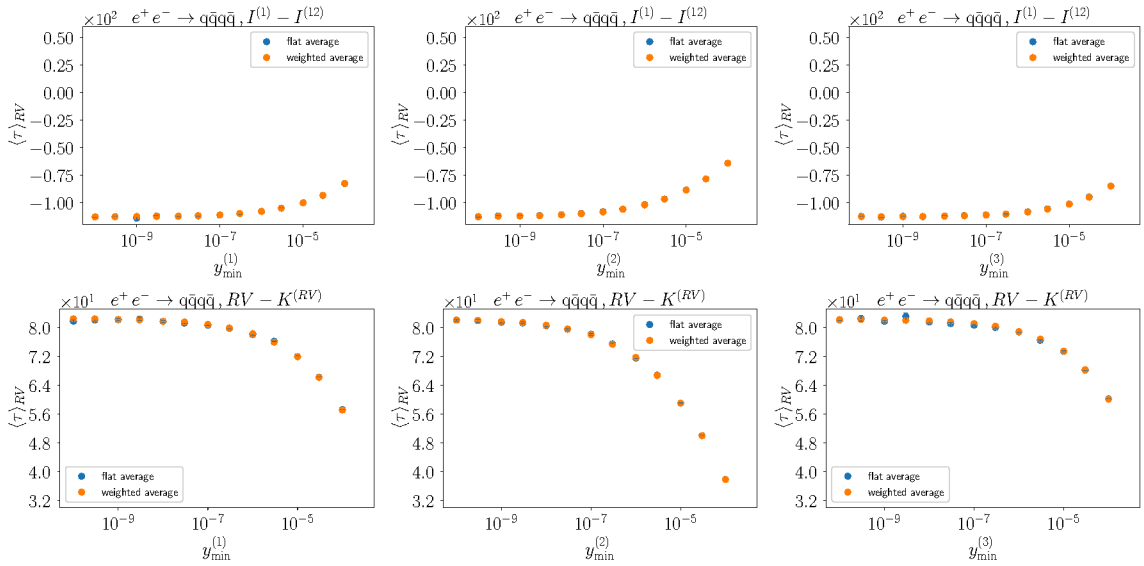


FIGURE 7.11: The saturation plots depict the cross-section for the $e^+e^- \to q\bar{q}q\bar{q}$ process, employing different definitions of the $y_{\min}$ parameter. The top row illustrates the $I^{(1)} - I^{(12)}$ contribution, while the bottom row showcases the $RV - K^{(RV)}$ contribution. The columns correspond to distinct choices of the $y_{\min}$ variable, adhering to the notation specified in Eq. (7.11).

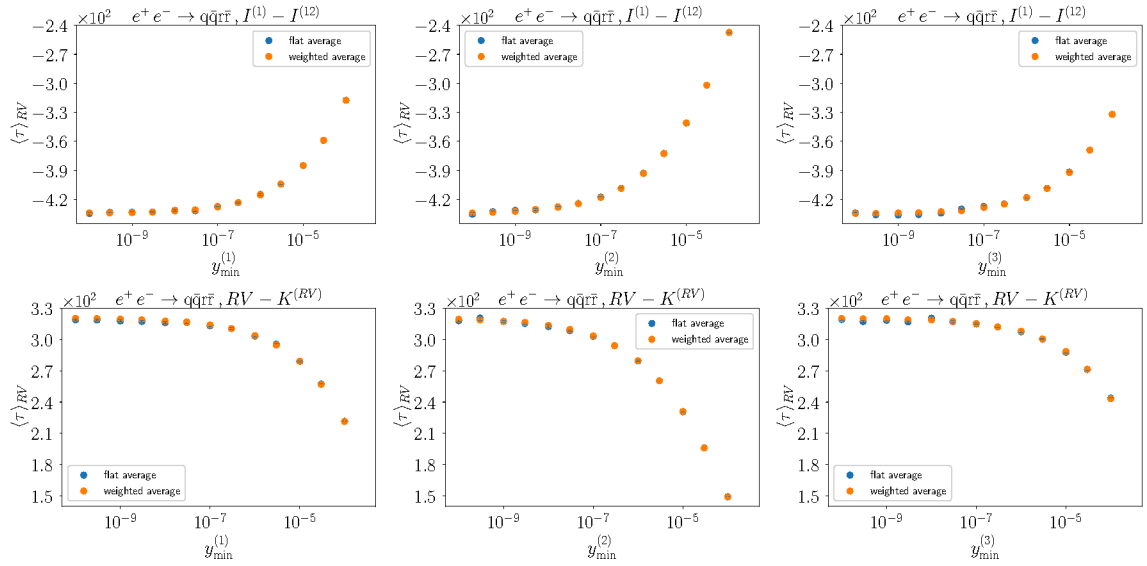


FIGURE 7.12: The saturation plots depict the cross-section for the $e^+e^- \to q\bar{q}r\bar{r}$ process, employing different definitions of the $y_{\min}$ parameter. The top row illustrates the $I^{(\mathbf{1})} - I^{(\mathbf{12})}$ contribution, while the bottom row showcases the $RV - K^{(\mathbf{RV})}$ contribution. The columns correspond to distinct choices of the $y_{\min}$ variable, adhering to the notation specified in Eq. (7.11).

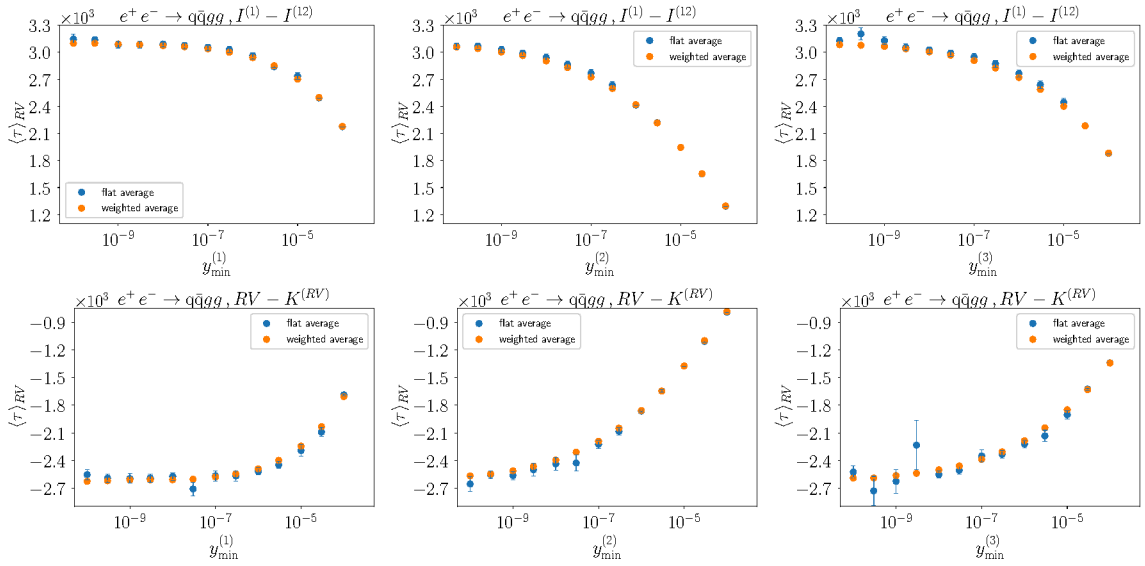


FIGURE 7.13: The saturation plots depict the cross-section for the $e^+e^- \to q\bar{q}gg$ process, employing different definitions of the $y_{\min}$ parameter. The top row illustrates the $I^{(1)} - I^{(12)}$ contribution, while the bottom row showcases the $RV - K^{(RV)}$ contribution. The columns correspond to distinct choices of the $y_{\min}$ variable, adhering to the notation specified in Eq. (7.11).

The results of this study for all the RV subprocesses are depicted in Figs. 7.11 – 7.13. Similar to the study in the previous section, we split the contributions between $I^{(1)} - I^{(12)}$ and $RV - K^{(RV)}$. For convenience, the plots in different columns are plotted with the same fixed horizontal axis, facilitating comparison. Examining these plots, we can see that saturation is indeed achieved for every choice of $y_{\min}$. For $y_{\min}^{(1)}$, this happens earlier than for the other two choices, which is unsurprising as different choices of $y_{\min}$ scale differently.

One can observe that for $e^+e^- \to q\bar{q}q\bar{q}$ and $e^+e^- \to q\bar{q}r\bar{r}$, there is no noticeable difference between the choices of $y_{\min}^{(2)}$ and $y_{\min}^{(3)}$. However, for $e^+e^- \to q\bar{q}gg$, the $y_{\min}^{(2)}$ choice seems superior. This is expected because the former processes have a simpler singularity structure, and the overlap of $e_i$ and $w_{ij}$ does not play an important role, whereas for the latter process, it appears to be significant. In general, based on this study, any choice of the definition of $y_{\min}$ seems safe for the RV contribution.

In the next section, we will produce event shape observables using two different choices of $y_{\min}$ to gain better insights into the impact of fixing this definition on the physical observables.

We note that similar study is also being performed for the $RR$ contributions [121] and it was successfully checked that saturation is achieved using the choice of $y_{\min}^{(1)}$.

## 7.4 Event shape observables

Now that we have confirmed the correct definition and implementation of the LASS subtraction terms and performed the $y_{\min}$ study, we are ready to calculate the actual physical observables. For this purpose, we choose four event shape observables typically studied in $e^+e^- \to 3$ jet processes [130, 133]. The observables of our choice are:

$\tau$-parameter (thrust):

$$T = \max_{\vec{n}} \left( \frac{\sum_i |\vec{n} \cdot \vec{p}_i|}{\sum_i |\vec{p}_i|} \right), \quad \tau \equiv 1 - T. \tag{7.12}$$

The thrust ($T$) is a measure of the longitudinal momentum flow along a particular direction $\vec{n}$, and $\tau$ is the thrust minor, which is sensitive to the distribution of particles transverse to the thrust axis.

$C$-parameter:

$$C_{\text{par}} = \frac{3}{2} \frac{\sum_{i,j} |\vec{p}_i||\vec{p}_j| \sin^2 \theta_{ij}}{(\sum_i |\vec{p}_i|)^2}. \tag{7.13}$$

The $C$-parameter is a measure of the transverse momentum flow with respect to the thrust axis, and it is sensitive to the distribution of particles in the event plane.

Energy-energy correlation:

$$\text{EEC}(\chi) = \frac{1}{\sigma_{\text{had}}} \sum_{i,j} \int \frac{E_i E_j}{Q^2} \mathrm{d}\sigma_{e^+e^- \to i,j+X} \delta(\cos\chi + \cos\theta_{ij}). \tag{7.14}$$

The energy-energy correlation (EEC) is a measure of the angular distribution of the energy flow in the event, and it is sensitive to the multi-jet structure of the final state.

Jet-cone energy fraction:

$$\frac{\mathrm{d}\Sigma_{\text{JCEF}}}{\mathrm{d}\cos\chi} = \sum_i \int \frac{E_i}{Q} \, \mathrm{d}\sigma_{e^+e^- \to i+X} \delta \left( \cos\chi - \frac{\vec{p}_i \cdot \vec{n}_T}{|\vec{p}_i|} \right). \tag{7.15}$$

The jet-cone energy fraction (JCEF) is a measure of the energy flow inside a cone of a given opening angle $\chi$ around the thrust axis, and it is sensitive to the internal structure of jets.

These observables are chosen because they provide complementary information about the event topology and the dynamics of the final-state particles, allowing for a comprehensive study of the underlying QCD processes.

To perform this study, we utilized the integration grid obtained in the previous section. To accelerate the speed of the calculation, the integration was performed 200 times in parallel with different random number seeds, each integrating over 10, 000, 000 events. This means that in every bin of each event shape observable, we have 200 independent estimates. We combine these estimates using weighted average tactics described previously, effectively accumulating the statistics of $2 \times 10^9$ events.

To understand the impact of the particular choice of the definition of $y_{\text{min}}$, we repeat this study for two different choices, $y_{\text{min}}^{(1)}$ and $y_{\text{min}}^{(2)}$, and plot the ratio of the event shape observables obtained with these choices ($y_{\text{min}}^{(1)} = 10^{-8}$, $y_{\text{min}}^{(2)} = 10^{-9}$). This ratio quantifies the residual dependence on the technical cut parameter, providing an estimate of the theoretical uncertainty arising from our formulation. The results for all the subprocesses contributing to $RV$ are depicted in Figs. 7.14 – 7.25, and we split between the contributions coming from $I$-terms and $K$-terms.

We observe that in all cases, for every event shape observable, we obtain numerically smooth and stable distributions. It is important to emphasize that the results presented here are solely the $RV$ contributions to the total NNLO correction; therefore, it is difficult to draw any physical conclusions based on these plots alone. However, these plots already exhibit the typical shape and characteristics of the physical event shape observables. For example, the presence of the integrable singularity in the distribution of $C$-parameter at the value $C_{\text{par}} = 3/4$ is easily visible in Fig. 7.22.

Regarding the impact of the particular choice of $y_{\text{min}}$, we see that in most cases, the effect, if present at all, is covered by the statistical error and hence negligible. One can also clearly see that in some cases, especially for the contributions coming from the $RV - K^{(\mathbf{RV})}$, the ratio plots in certain bins show abnormally large deviations from unity. Even though the deviation is covered by the large uncertainty, it is necessary to better understand whether this effect is purely statistical or if there

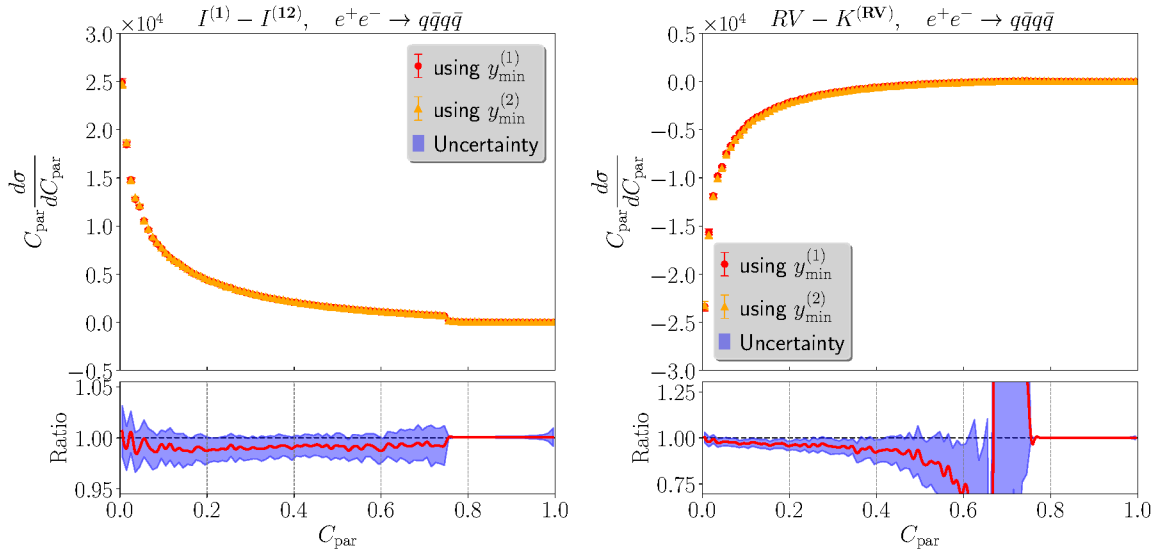


FIGURE 7.14: Real-virtual contributions to the C-parameter for $e^+e^- \to q\bar{q}q\bar{q}$ from $I^{(1)} - I^{(12)}$ (left) and $RV - K^{RV}$ (right) terms. Top: results with two technical cut choices. Bottom: ratio of the two cut choices with uncertainties.

is an underlying issue with the particular definition of $y_{\min}$. An effective method to exclude the statistical effects would be to increase the statistics in MC generation a couple of times and repeat the steps described above, which we save for future work.

In summary, in this Chapter we presented the first robust numerical implementation of the LASS scheme, which can efficiently perform the integration of NNLO observables. We have full analytic control over the $VV$ contribution, but the point raised in Chapter 4 regarding the $\Delta_{ij}$ terms remains to be investigated. A very detailed study was performed to investigate the singular behavior of every subtraction term. In the case of $RV$ radiation, we produce numerically stable results, as demonstrated by the smooth distributions of event-shape observables depicted above. However, to decisively fix the technical cut parameter, it is still necessary to accumulate higher statistics. Moreover, the numeric stability of the $RR$ contribution during the integration requires further investigations, which are currently being actively conducted.

In conclusion, although this project is still ongoing, the preliminary findings are encouraging and highlight the potential of this approach for future research.

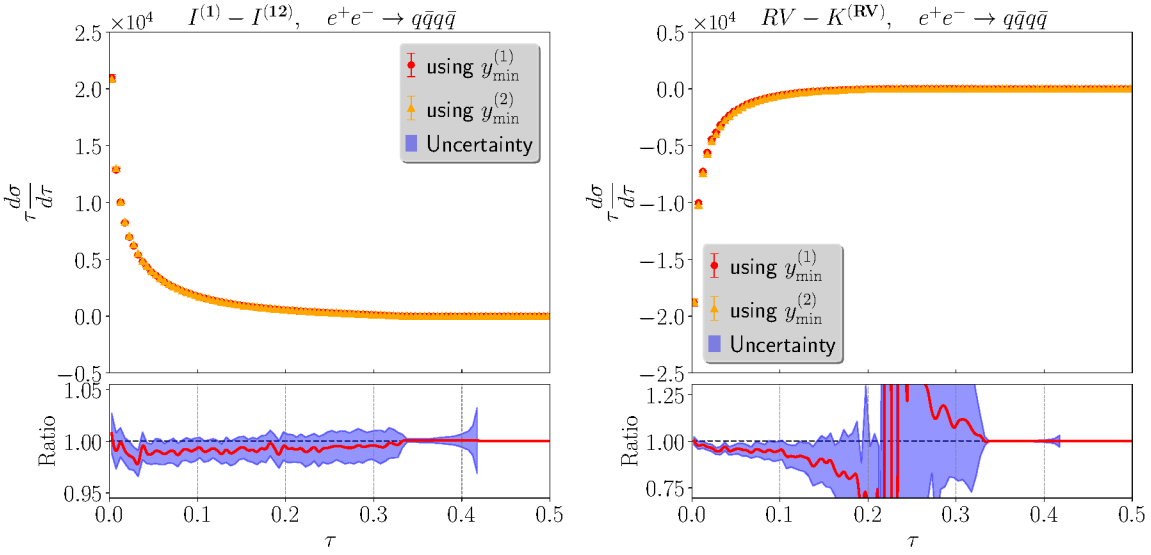


FIGURE 7.15: Real-virtual contributions to the $\tau$-parameter for $e^+e^- \to q\bar{q}q\bar{q}$ from $I^{(1)} - I^{(12)}$ (left) and $RV - K^{RV}$ (right) terms. Top: results with two technical cut choices. Bottom: ratio of the two cut choices with uncertainties.

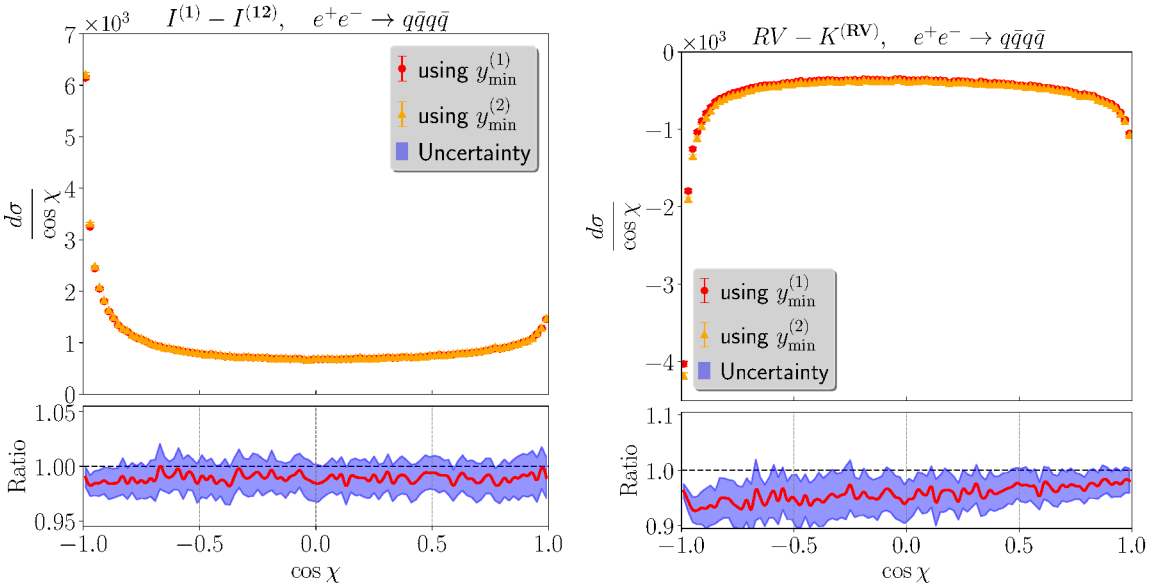


FIGURE 7.16: Real-virtual contributions to the energy-energy correlation for $e^+e^- \to q\bar{q}q\bar{q}$ from $I^{(1)} - I^{(12)}$ (left) and $RV - K^{RV}$ (right) terms. Top: results with two technical cut choices. Bottom: ratio of the two cut choices with uncertainties.

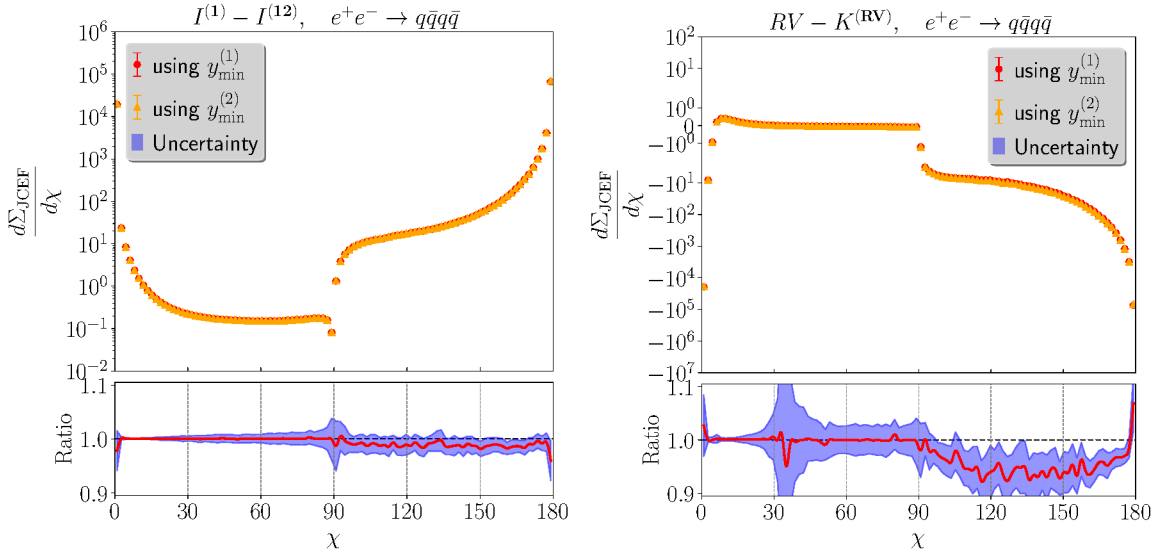


FIGURE 7.17: Real-virtual contributions to the jet cone energy fraction for $e^+e^- \to q\bar{q}q\bar{q}$ from $I^{(1)} - I^{(12)}$ (left) and $RV - K^{RV}$ (right) terms. Top: results with two technical cut choices. Bottom: ratio of the two cut choices with uncertainties.

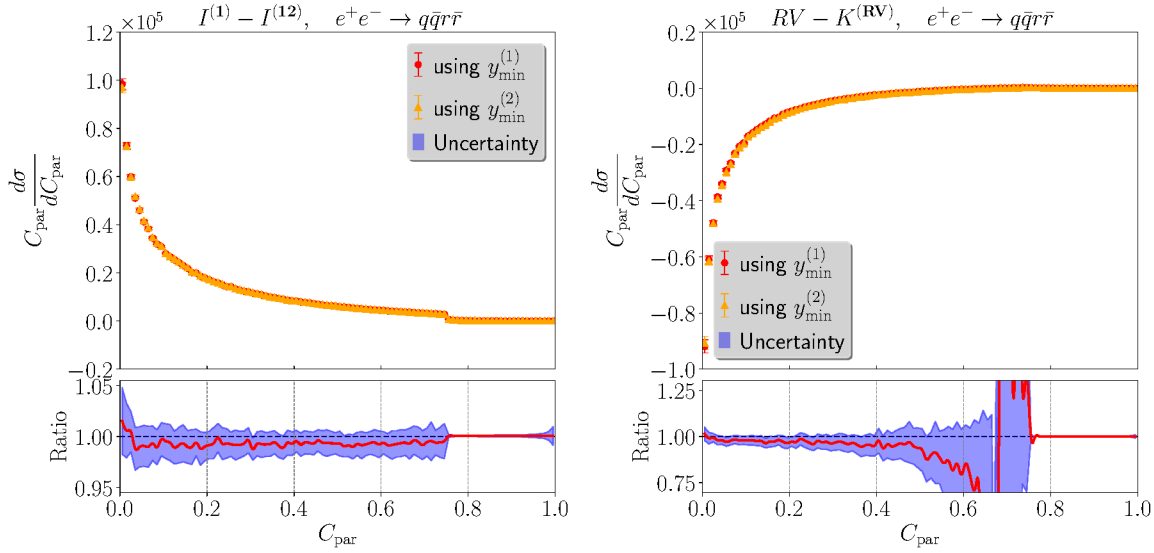


FIGURE 7.18: Real-virtual contributions to the C-parameter for $e^+e^- \to q\bar{q}r\bar{r}$ from $I^{(1)} - I^{(12)}$ (left) and $RV - K^{RV}$ (right) terms. Top: results with two technical cut choices. Bottom: ratio of the two cut choices with uncertainties.

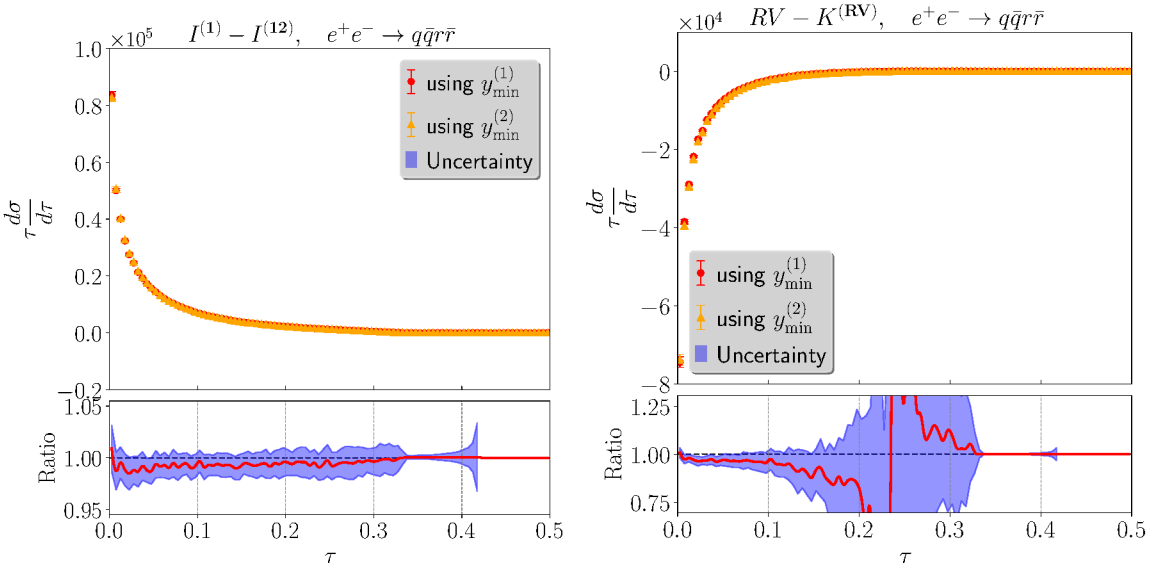


FIGURE 7.19: Real-virtual contributions to the $\tau$-parameter for $e^+e^- \to q\bar{q}r\bar{r}$ from $I^{(1)} - I^{(12)}$ (left) and $RV - K^{RV}$ (right) terms. Top: results with two technical cut choices. Bottom: ratio of the two cut choices with uncertainties.

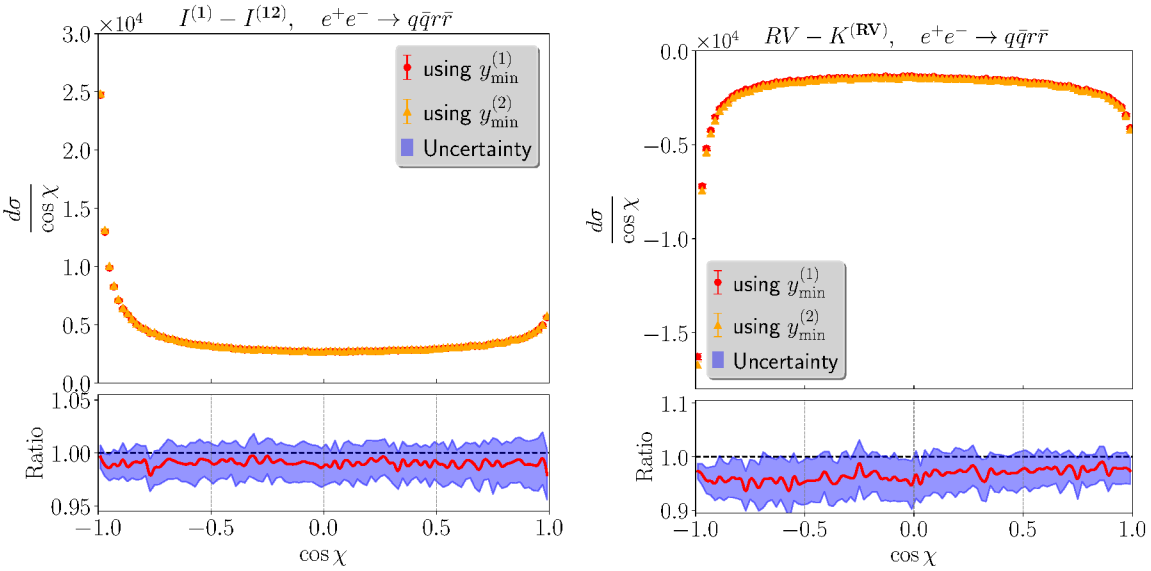


FIGURE 7.20: Real-virtual contributions to the energy-energy correlation for $e^+e^- \to q\bar{q}r\bar{r}$ from $I^{(1)} - I^{(12)}$ (left) and $RV - K^{RV}$ (right) terms. Top: results with two technical cut choices. Bottom: ratio of the two cut choices with uncertainties.

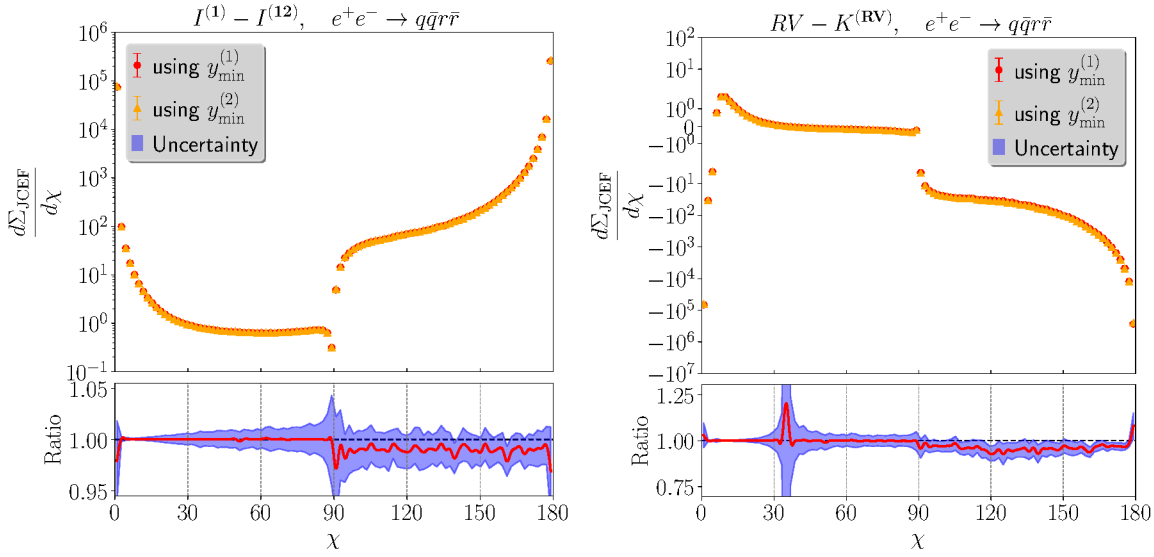


FIGURE 7.21: Real-virtual contributions to the energy-energy correlation for $e^+e^- \to q\bar{q}r\bar{r}$ from $I^{(1)} - I^{(12)}$ (left) and $RV - K^{RV}$ (right) terms. Top: results with two technical cut choices. Bottom: ratio of the two cut choices with uncertainties.

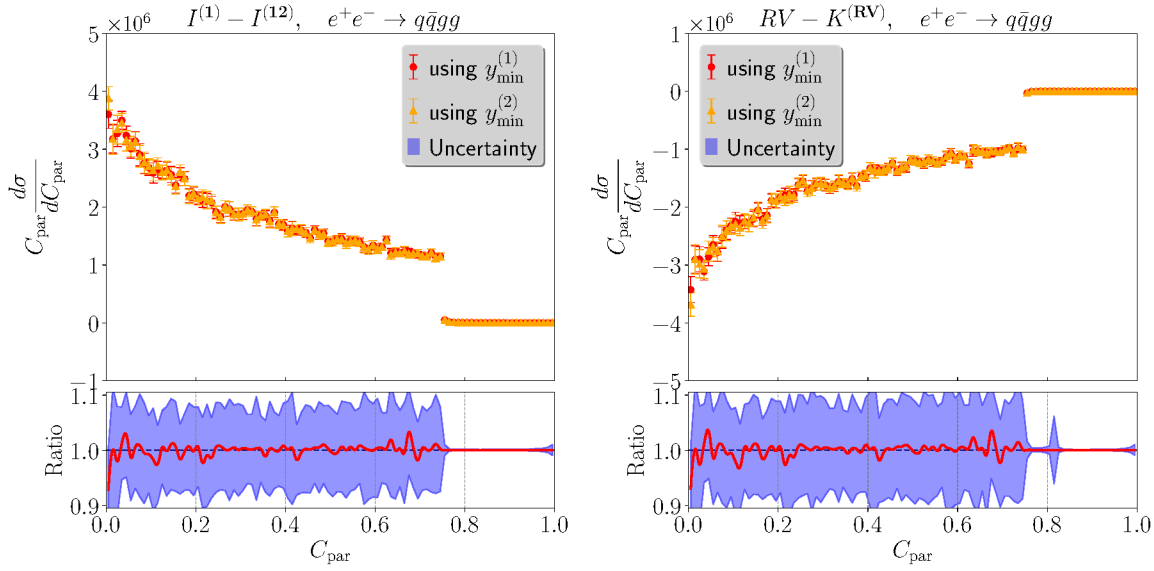


FIGURE 7.22: Real-virtual contributions to the C-parameter for $e^+e^- \to q\bar{q}gg$ from $I^{(1)} - I^{(12)}$ (left) and $RV - K^{RV}$ (right) terms. Top: results with two technical cut choices. Bottom: ratio of the two cut choices with uncertainties.

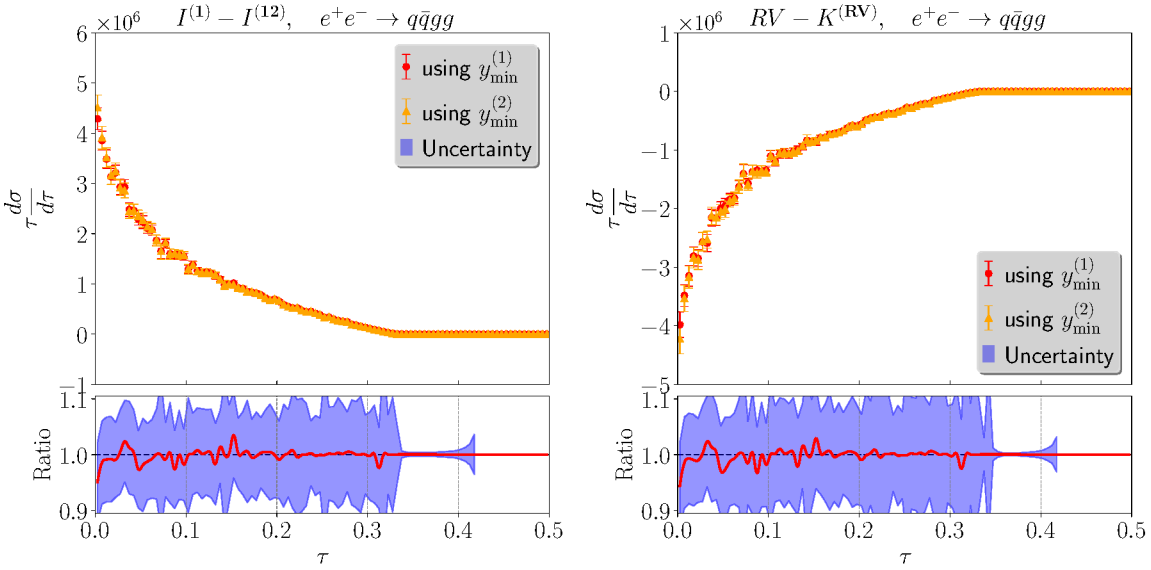


FIGURE 7.23: Real-virtual contributions to the $\tau$-parameter for $e^+e^- \to q\bar{q}gg$ from $I^{(1)} - I^{(12)}$ (left) and $RV - K^{RV}$ (right) terms. Top: results with two technical cut choices. Bottom: ratio of the two cut choices with uncertainties.

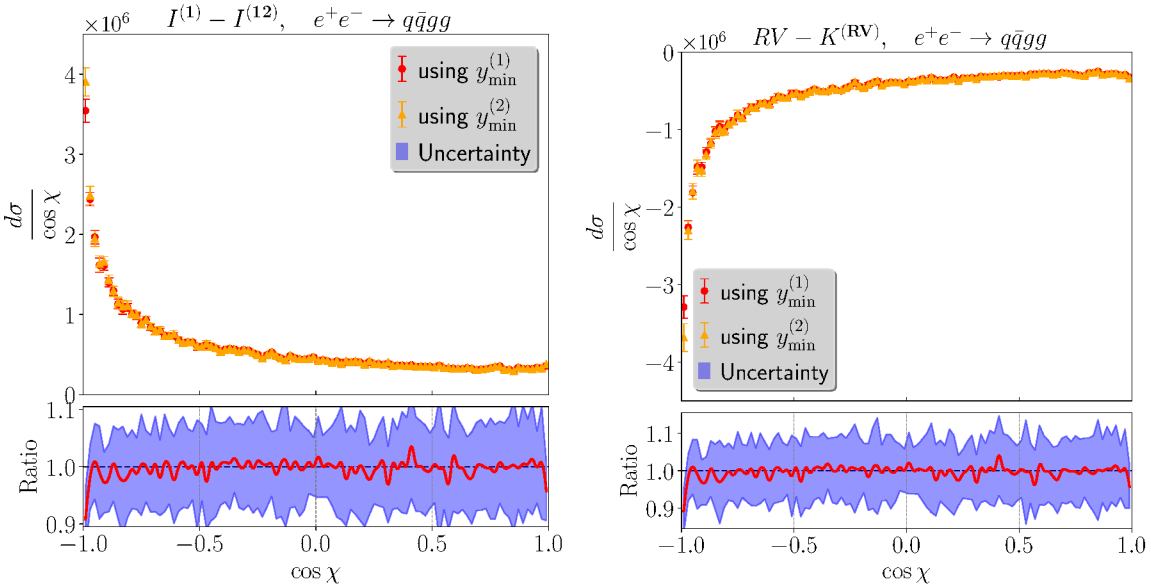


FIGURE 7.24: Real-virtual contributions to the energy-energy correlation for $e^+e^- \to q\bar{q}gg$ from $I^{(1)} - I^{(12)}$ (left) and $RV - K^{RV}$ (right) terms. Top: results with two technical cut choices. Bottom: ratio of the two cut choices with uncertainties.

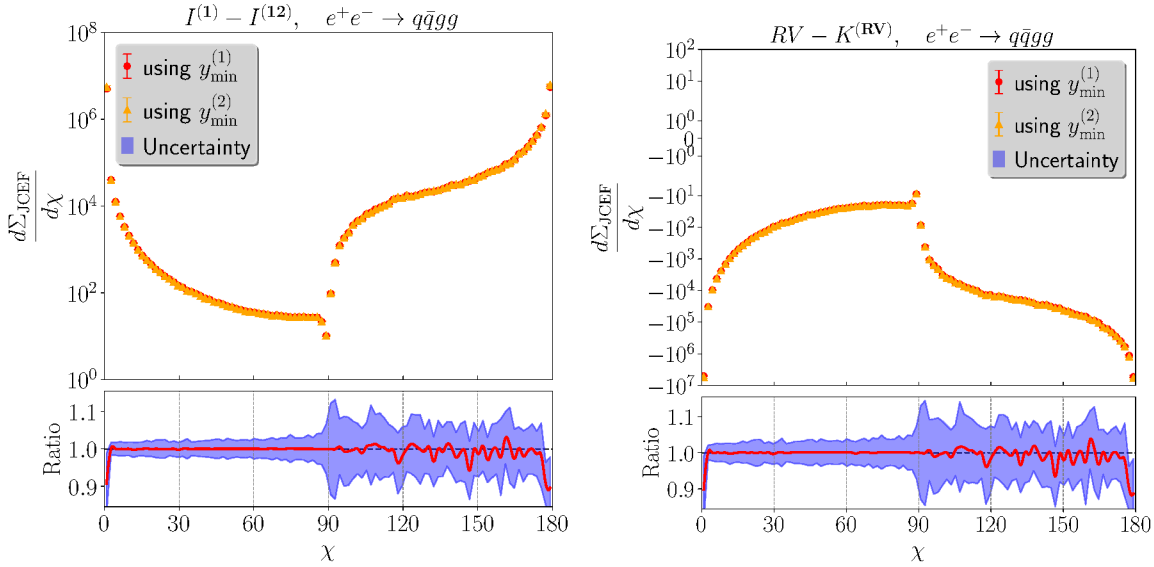


FIGURE 7.25: Real-virtual contributions to the jet cone energy fraction for $e^+e^- \to q\bar{q}gg$ from $I^{(1)} - I^{(12)}$ (left) and $RV - K^{RV}$ (right) terms. Top: results with two technical cut choices. Bottom: ratio of the two cut choices with uncertainties.

# Chapter 8

# Outlook

In this thesis, we have conducted an in-depth analysis of the Local Analytic Sector Subtraction scheme and its application to the NNLO calculation of the electron-positron annihilation into 3 jets. The key aspects of the scheme, including the construction of sector functions, derivation of subtraction counterterms, and analytic integration techniques, have been thoroughly examined. We have developed a powerful approach combining an SMT solver and symbolic manipulation to automatically generate color bases for QCD amplitudes, greatly simplifying the calculation of color-correlated matrix elements.

The numerical implementation of the complete LASS framework has been successfully demonstrated for the 3-jet production process. Extensive checks have been performed to validate the subtraction terms' limiting behavior, the finite remainders of the double-virtual contribution, and the impact of the technical cut parameter. The computation of differential cross sections for various event shape observables has showcased the method's stability and efficiency.

This work represents a significant step towards the development of a fully automated tool for NNLO calculations in QCD using the LASS scheme. The techniques and insights gained from this study can be readily extended to more complex processes involving a larger number of final-state particles and different initial states. The automatic generation of color bases and the efficient numerical implementation provide a solid foundation for tackling these challenging calculations.

Future efforts will focus on refining the technical cut prescription, optimizing the

phase space parametrization, and incorporating the double-real radiation contribution to complete the NNLO calculation for the 3-jet process. Additionally, the extension of the method to handle massive particles and initial-state singularities will be explored to broaden its applicability to a wider range of phenomenologically relevant processes.

The ultimate goal is to develop a robust, flexible, and user-friendly tool that can perform NNLO calculations for arbitrary processes in QCD using the LASS scheme. Such a tool would greatly facilitate precision studies of Standard Model processes and searches for new physics at current and future collider experiments. By providing a fully local and analytic subtraction framework, the LASS scheme has the potential to streamline NNLO calculations and push the frontiers of precision QCD phenomenology.

# Appendix A

# Phase-space in D dimensions

Two particle phase space is given as:

$$\int \mathrm{dPS}^{(2)} = \int \mu^{4-D} \frac{\mathrm{d}^{D-1}p_1}{2E_1(2\pi)^{D-1}} \frac{\mathrm{d}^{D-1}p_2}{2E_2(2\pi)^{D-1}} (2\pi)^D \delta^D(Q - p_1 - p_2)\,, \tag{A.1}$$

where we have introduced a scale $\mu$ to keep the original mass dimensionality of the phase-space in $D = 4$ dimensions ($\mu^{4-D}\mathrm{d}^D p_i \to \mathrm{d}^4 p_i$). For the massless particles, ($p_1^2 = p_2^2 = 0$) following identities holds:

$$\int \frac{\mathrm{d}^{n-1}p_2}{2E} = \int \mathrm{d}^n p_2 \frac{1}{2E} \delta(p_2^0 - E) = \int \mathrm{d}^n p_2 \delta^+(p_2^2)\,, \tag{A.2}$$

where $\delta^+$ distribution has been defined as:

$$\delta^+(p^2 - m^2) = \theta(p_0)\delta(p^2 - m^2)\,. \tag{A.3}$$

Upon substitution of Eq. (A.2) in Eq. (A.1) we get:

$$\begin{aligned} \int \mathrm{dPS}^{(2)} &= \mu^{4-D} \int \frac{\mathrm{d}^{D-1}p_1}{2E_1(2\pi)^{D-1}} \frac{\mathrm{d}^D p_2}{(2\pi)^{D-1}} (2\pi)^D \delta^+(p_2^2) \delta^D(Q - p_1 - p_2) \\ &= \frac{\mu^{4-D}}{(2\pi)^{D-2}} \int \frac{\mathrm{d}^{D-1}p_1}{2E_1} \delta((Q - p_1)^2)\,. \end{aligned} \tag{A.4}$$

In the cms frame we have: $Q^\mu = p_1^\mu + p_2^\mu = (\sqrt{s}, 0, 0, 0)$ and $(Q - p_1)^2 = s - 2E_1\sqrt{s}$. Rewriting Eq. (A.4) in polar coordinates, we obtain:

$$\int \mathrm{dPS}^{(2)} = \frac{\mu^{4-D}}{(2\pi)^{D-2}} \int \mathrm{d}E_1 \frac{E_1^{D-3}}{2} \delta\left(s - 2E_1\sqrt{s}\right) \int \mathrm{d}\Omega_{D-2}\,. \tag{A.5}$$

Recall the definition of the solid angle in D dimensions:

$$\mathrm{d}\Omega_D = \mathrm{d}\phi \mathrm{d}\theta_1 \sin\theta_1 \ldots \mathrm{d}\theta_{D-3} \sin^{D-3}\theta_{D-3}\,. \tag{A.6}$$

By using the integration formula:

$$\int_0^\pi \mathrm{d}\theta \sin^D\theta = \sqrt{\pi} \frac{\Gamma\left(\frac{D+1}{2}\right)}{\Gamma\left(\frac{D+2}{2}\right)}\,, \tag{A.7}$$

we can integrate over all the angles except the last one:

$$\int \mathrm{d}\Omega_{D-2} = \frac{2\pi^{\frac{D-2}{2}}}{\Gamma\left(\frac{D-2}{2}\right)} \int_0^\pi \mathrm{d}\theta_{D-3} \sin^{D-3}\theta_{D-3}\,. \tag{A.8}$$

Equation (A.5) becomes:

$$\begin{aligned}
\int \mathrm{dPS}^{(2)} =& \frac{\mu^{4-D}}{(2\pi)^{D-2}} \frac{2\pi^{(D-2)/2}}{\Gamma\left(\frac{D-2}{2}\right)} \int \mathrm{d}E_1 \frac{E_1^{D-3}}{2} \delta\left(s - 2\sqrt{s}E_1\right) \int_0^\pi \mathrm{d}\theta \sin^{D-3}\theta \\
=& \frac{\mu^{4-D}}{(2\pi)^{D-2}} \frac{1}{2\sqrt{s}} \frac{\pi^{(D-2)/2}}{\Gamma\left(\frac{D-2}{2}\right)} \left(\frac{\sqrt{s}}{2}\right)^{D-3} \int_{-1}^1 \left(1 - \cos^2\theta\right)^{\frac{D-4}{2}} \mathrm{d}\cos\theta \\
\overset{D\to 4-2\epsilon}{=}& \frac{1}{8\pi} \frac{(4\pi\mu^2)^\varepsilon}{\Gamma(1-\varepsilon)} \frac{1}{\sqrt{s}} \left(\frac{\sqrt{s}}{2}\right)^{1-2\varepsilon} \int_{-1}^1 \left(1 - \cos^2\theta\right)^{-\varepsilon} \mathrm{d}\cos\theta\,.
\end{aligned} \tag{A.9}$$

Analogously to Eq. (A.1), the phase-space for $n$-final state particles can be parametrized as:

$$\begin{aligned}
\int \mathrm{dPS}^{(n)} = \int \mu^{4-D} \frac{\mathrm{d}^{D-1}p_1}{2E_1(2\pi)^{D-1}} \frac{\mathrm{d}^{D-1}p_2}{2E_2(2\pi)^{D-1}} \cdots \frac{\mathrm{d}^{D-1}p_n}{2E_n(2\pi)^{D-1}} \\
\times (2\pi)^D \delta^D(Q - p_1 - p_2 - \ldots - p_n)\,.
\end{aligned} \tag{A.10}$$

This expression can be iteratively factorized in terms of the products of the phase-space elements of the lower number particles by picking two particles with momenta $k_1$ and $k_2$, such that $k_1 + k_2 = q$ and by substituting the following identity in Eq. (A.10):

$$\begin{aligned} 1 &= \int \frac{dq^2}{2\pi} \int \frac{d^{n-1}q}{2\pi^{n-1}} \frac{1}{2E_q} (2\pi)^n \delta^n (q - k_1 - k_2) \\ &= \int dq^2 \int d^n q \delta^n (q - k_1 - k_2) \, \delta \left( q^2 - Q^2 \right) = 1 \,, \end{aligned} \tag{A.11}$$

which is just a statement about the energy-momentum conversation.

In this way one can derive Equations like Eq. (3.22).

# Appendix B

# Derivation of the constituent integrals of $I^{(2)}$ and $I^{(\mathrm{RV})}$

In this Appendix, we present the derivation of master integrals essential for completing the integration steps outlined in Chapter 4. This portion of the work is based on Ref. [142]. Each derived master integral is subject to specific constraints on the parameters to ensure convergence. These conditions are derived and highlighted in blue. Before substituting the results, it is crucial to verify that these conditions are satisfied.

## B.1 $I_{A,B,C,D,E}$

In this Section we will derive Eq. (4.14). The expression of $I_{A,B,C,D,E}$ is given as:

$$
\begin{aligned}
I_{A,B,C,D,E} &= \int_0^1 dz \int_0^1 dy' \, (1-y')^A \, (y')^B \, (1-z)^C \, z^D \frac{1}{(z+(1-z)y')^E} \\
&= \frac{\Gamma(A+1)\Gamma(B+1)}{\Gamma(A+B+2)} \, \frac{\Gamma(C+1)\Gamma(B+D+2-E)}{\Gamma(B+C+D+3-E)} \times \\
&\quad \times \; {}_3F_2\left(A+B+2-E, B+1, C+1, A+B+2, B+C+D+3-E, 1\right) \\
&\quad \text{subject to} \qquad \mathrm{Re}(A+1) > 0 \quad \text{and} \quad \mathrm{Re}(B+1) > 0 \,, \\
&\qquad\qquad\qquad\quad \mathrm{Re}(C+1) > 0 \quad \text{and} \quad \mathrm{Re}(D+1) > 0 \,, \\
&\qquad\qquad\qquad\quad E > 0 \quad \text{and} \quad \mathrm{Re}(-E+B+1) < 0 \,.
\end{aligned}
$$

There is the additional condition $\mathrm{Re}(B+D+2-E)>0$ from the $z$-integration, which is being taken care of by the Gamma-function.

## Derivation

The general case with powers $A, B, C, D, E$. We assume $E > 0$, other assumptions will be detailed below.

$$
\begin{aligned}
I &= \int_0^1 dz \int_0^1 dy' \,(1-y')^A\,(y')^B\,(1-z)^C\,z^D \frac{1}{(z+(1-z)y')^E} \\
&= \int_0^1 dz\,(1-z)^C\,z^{D-E} \int_0^1 dy' \,(1-y')^A\,(y')^B \frac{1}{(1+\frac{1-z}{z}y')^E} \\
&= \int_0^1 dz\,(1-z)^C\,z^{D-E} \;\frac{\Gamma(A+1)\Gamma(B+1)}{\Gamma(A+B+2)}\,{}_2F_1\left(E, B+1, A+B+2, -\frac{1-z}{z}\right), \\
&\quad \text{where} \qquad \mathrm{Re}(A+B+2) > \mathrm{Re}(B+1) > 0 \\
&\quad \text{which means} \qquad \mathrm{Re}(A+1)>0 \quad \text{and} \quad \mathrm{Re}(B+1)>0 \\
&= \int_0^1 dz\, z^C\,(1-z)^{D-E} \;\frac{\Gamma(A+1)\Gamma(B+1)}{\Gamma(A+B+2)}\,{}_2F_1\left(E, B+1, A+B+2, -\frac{z}{1-z}\right) \\
&\quad \text{flipping} \qquad z \to (1-z) \\
&= \frac{\Gamma(A+1)\Gamma(B+1)}{\Gamma(A+B+2)} \int_0^1 dz\, z^C\,(1-z)^D \;\; {}_2F_1\left(E, A+1, A+B+2, z\right) \\
&\quad \text{using} \qquad {}_2F_1\left(E, B+1, A+B+2, -\tfrac{z}{1-z}\right) = (1-z)^E\,{}_2F_1\left(E, A+1, A+B+2, z\right) \\
&= \frac{\Gamma(A+1)\Gamma(B+1)}{\Gamma(A+B+2)} \int_0^1 dz\, z^C\,(1-z)^{B+D+1-E} \;\; {}_2F_1\left(A+B+2-E, B+1, A+B+2, z\right) \\
&\quad \text{using} \qquad {}_2F_1\left(E, A+1, A+B+2, z\right) = (1-z)^{B+1-E}\,{}_2F_1\left(A+B+2-E, B+1, A+B+2, z\right) \\
&= \frac{\Gamma(A+1)\Gamma(B+1)}{\Gamma(A+B+2)} \int_0^1 dz\, z^C\,(1-z)^{B+D+1-E} \;\; {}_2F_1\left(A+B+2-E, B+1, A+B+2, z\right) \\
&\quad \text{for convergence of} \quad {}_2F_1 \quad \text{as} \quad z \to 1, \text{the following condition is needed here} \\
&\quad \mathrm{Re}\big((A+B+2-E)+(B+1)-(A+B+2)\big) = \mathrm{Re}(-E+B+1) < 0 \\
&= \frac{\Gamma(A+1)\Gamma(B+1)}{\Gamma(A+B+2)} \;\frac{\Gamma(C+1)\Gamma(B+D+2-E)}{\Gamma(B+C+D+3-E)} \qquad \times
\end{aligned}
$$

$$\times \quad {}_3F_2\left(A+B+2-E, B+1, C+1, A+B+2, B+C+D+3-E, 1\right) ,$$

where the following identity was used:

$$\int_0^1 dz\, z^{n_4}\,(1-z)^{n_5}\,{}_2F_1\left(n_1, n_2, n_3, z\right) = \frac{\Gamma(n_4+1)\Gamma(n_5+1)}{\Gamma(n_4+n_5+2)}\,{}_3F_2\left(n_1, n_2, n_4+1, n_3, n_4+n_5+2, 1\right) ,$$

which introduces the new constraints:

$$\mathrm{Re}(C+1) > 0 \quad \text{and} \quad \mathrm{Re}(B+D+2-E) > 0\,.$$

and for convergence of ${}_3F_2$ with argument 1 the following must be fulfilled:

$$\mathrm{Re}\big((A+B+2)+(B+D+2-E)-(A+B+2-E)-(B+1)\big) = \mathrm{Re}(D+1) > 0\,.$$

## B.2 General case

Before we derive the expressions for the remaining integrals, it is necessary to analyze the general structure of the integrand.

We investigate the following integrand with general powers $A, B, C, D, E, F, G, H$:

$$\begin{aligned} I &= \int_0^1 dy' \int_0^1 dz \int_0^1 dz' \int_0^1 dw' \quad \times \\ &\times \frac{(1-w')^A (w')^B (1-y')^C (y')^D (1-z)^E z^F (1-z')^G (z')^H}{\left[z+(1-z)y'\right]\left[zz'+y'(1-z)(1-z')+2(1-2w')\sqrt{y'}\sqrt{(1-z)z}\sqrt{(1-z')z'}\right]} . \end{aligned} \tag{B.1}$$

Taking the $w'$ integration first, we have with $X = \sqrt{zz'}$ and $Y = \sqrt{y'}\sqrt{(1-z)}\sqrt{(1-z')}$

$$I^{w'} = \int_0^1 dw' \frac{(1-w')^A (w')^B}{\left[(X+Y)^2 - 4w'XY\right]} . \tag{B.2}$$

Although most general, Eq. (B.1) is not the best expression to start from, because many of the parameters $A, B, \ldots$ are restricted and we want to exploit this. For example, due to the azimuthal dependence of the integrand, we will always have $A = B$ in Eq. (B.2).

### Special case

As a special case we start with the azimuthal integral (mapping $z' \leftrightarrow z$ and $z' \leftrightarrow (1-z')$ reversed compared to Eq. (B.1) above):

$$\begin{aligned} I_b &= \int_0^1 dy' \int_0^1 dz \int_0^1 dz' \int_0^1 dw' \quad \times \\ &\times \frac{(1-w')^{1/2-b} (w')^{1/2-b} (1-y')^{-1-2\epsilon} (y')^{2-\epsilon} (1-z)^{-\epsilon} z^{-\epsilon} (1-z')^{-\epsilon} (z')^{-\epsilon}}{\left[1-(1-y')z'\right]\left[z(1-z')+y'(1-z)z'+2(1-2w')\sqrt{y'}\sqrt{(1-z)z}\sqrt{(1-z')z'}\right]} \\ &= \int_0^1 dy' \int_0^1 dz \int_0^1 dz' \int_0^1 dw' \quad \times \\ &\times \frac{(1-w')^{1/2-b} (w')^{1/2-b} (1-y')^{-1-2\epsilon} (y')^{2-\epsilon} (1-z)^{-\epsilon} z^{-\epsilon} (1-z')^{-\epsilon} (z')^{-\epsilon}}{\left[1-(1-y')z'\right]\left[(A+B)^2 - 4w'AB\right]} , \end{aligned} \tag{B.3}$$

where we have abbreviated $A = \sqrt{z}\sqrt{(1-z')}$ and $B = \sqrt{y'}\sqrt{(1-z)}\sqrt{z'}$, cf. Eq. (3.40) in [29]. Typically, $b = 1+\epsilon$ in our applications.

Note, that the $y$-integration is trivial, can be done in terms of Euler Beta-function.

For the $w'$ integration we follow App. B in [29], specifically Eq. (B.3) in [29].

$$\begin{aligned} I^{w'}_{a,b}(A,B) &= \int_0^1 dw' \, \frac{[w'(1-w')]^{1/2-b}}{\left[(A+B)^2 - 4w'AB\right]^a} \\ &= \frac{1}{(A+B)^{2a}} \int_0^1 dw' \, \frac{[w'(1-w')]^{1/2-b}}{\left[1-w'\eta\right]^a} \\ &\qquad \text{where} \qquad \eta = \tfrac{4AB}{(A+B)^2} \\ &= \frac{1}{(A+B)^{2a}} \frac{\Gamma(3/2-b)^2}{\Gamma(3-2b)} \, {}_2F_1\left(a, 3/2-b, 3-2b, \eta\right) . \end{aligned} \tag{B.4}$$

Using Eq. 9.134 (3.) from Ref. [143]:

$${}_2F_1\left(\alpha,\beta,2\beta,\frac{4z}{(1+z)^2}\right) = (1+z)^{2\alpha} \, {}_2F_1\left(\alpha,\alpha+\frac{1}{2}-\beta,\beta+\frac{1}{2},z^2\right) \tag{B.5}$$

In terms of:

$$\eta = \frac{4z}{(1+z)^2} \qquad \longrightarrow \qquad z = \frac{1-\sqrt{1-\eta}}{1+\sqrt{1-\eta}} = \begin{cases} \frac{A}{B} & \text{if} \quad A \le B \\ \frac{B}{A} & \text{if} \quad A \ge B \end{cases} \tag{B.6}$$

As a result we get:

$$I^{w'}_{a,b}(A,B) = \frac{\Gamma(3/2-b)^2}{\Gamma(3-2b)} \begin{cases} \frac{1}{B^{2a}} \, {}_2F_1\left(a, a+b-1, 2-b, \frac{A^2}{B^2}\right) & \text{if} \quad A \le B \\ \frac{1}{A^{2a}} \, {}_2F_1\left(a, a+b-1, 2-b, \frac{B^2}{A^2}\right) & \text{if} \quad A \ge B \end{cases} \tag{B.7}$$

This agrees with Eq. (B.8) in [29].

Recall, that $A^2 = z(1-z')$ and $B^2 = y'(1-z)z'$. Thus, with $a = 1, b = 1+\epsilon$ in Eq. (B.4), we get for Eq. (B.3)

$$\begin{aligned} I_b &= \frac{\Gamma(3/2-b)^2}{\Gamma(3-2b)} \int_0^1 dy' \int_0^1 dz \int_0^1 dz' \quad \times \\ &\times \quad \frac{(1-y')^{-1-2\epsilon} \, (y')^{2-\epsilon} \, (1-z)^{-\epsilon} \, z^{-\epsilon} \, (1-z')^{-\epsilon} \, (z')^{-\epsilon}}{\left[1-(1-y')z'\right]} \quad \times \\ &\times \quad \begin{cases} \frac{1}{B^2} \, {}_2F_1\left(1, b, 2-b, \frac{A^2}{B^2}\right) & \text{if} \quad A \le B \\ \frac{1}{A^2} \, {}_2F_1\left(1, b, 2-b, \frac{B^2}{A^2}\right) & \text{if} \quad A \ge B \end{cases} , \end{aligned} \tag{B.8}$$

where we do the integration over $z$ next. To that end, we have to solve integrals of the type

$$\begin{aligned} I^{z,\leq} &= \int_0^1 dz\,(1-z)^{-\epsilon}\,z^{-\epsilon}\,\frac{1}{B^2}\,{}_2F_1\left(1,b,2-b,\frac{A^2}{B^2}\right) \quad \text{if} \quad A \leq B \\ &= \frac{1}{y'z'}\int_0^1 dz\,(1-z)^{-\epsilon-1}\,z^{-\epsilon}\,{}_2F_1\left(1,b,2-b,\frac{z(1-z')}{(1-z)y'z'}\right), \end{aligned} \tag{B.9}$$

and likewise for $A \geq B$. Such integrals are considered in Eq. (B.10) in [29], which adopts a slightly more general notation for the combined integration of $w'$ and $z$. We abbreviate $C = (1-z')$ and $D = y'z'$ and define:

$$I^{z,w'}_{a,b,\beta,\gamma}(C,D) = \int_0^1 dz \int_0^1 dw' \,\frac{z^\beta\,(1-z)^\gamma\,[w'(1-w')]^{1/2-b}}{\left[zC+(1-z)D+2(1-2w')\sqrt{C}\sqrt{D}\sqrt{(1-z)z}\right]^a}\,.$$

Using Eq. (B.4):

$$I^{z,w'}_{a,b,\beta,\gamma}(C,D) = \int_0^1 dz\,z^\beta\,(1-z)^\gamma\,I^{w'}_{a,b}(\sqrt{C}\sqrt{z},\sqrt{D}\sqrt{(1-z)})$$

$$= \frac{\Gamma(3/2-b)^2}{\Gamma(3-2b)}\int_0^1 dz\,z^\beta\,(1-z)^\gamma \quad \times$$

$$\times \begin{cases} \frac{1}{((1-z)D)^a}\,{}_2F_1\left(a,a+b-1,2-b,\frac{zC}{(1-z)D}\right) & \text{if} \quad zC \leq (1-z)D \\ \frac{1}{(zC)^a}\,{}_2F_1\left(a,a+b-1,2-b,\frac{(1-z)D}{zC}\right) & \text{if} \quad zC \geq (1-z)D \end{cases}$$

using $\quad zC \leq (1-z)D \quad \longrightarrow \quad z \leq \frac{D}{C+D}$

$$= \frac{\Gamma(3/2-b)^2}{\Gamma(3-2b)}\left[\frac{1}{D^a}\int_0^{\frac{D}{C+D}} dz\,z^\beta\,(1-z)^{\gamma-a}\,{}_2F_1\left(a,a+b-1,2-b,\frac{zC}{(1-z)D}\right)\right.$$

$$\left. +\frac{1}{C^a}\int_{\frac{D}{C+D}}^1 dz\,z^{\beta-a}\,(1-z)^\gamma\,{}_2F_1\left(a,a+b-1,2-b,\frac{(1-z)D}{zC}\right)\right]$$

using $\quad z \longrightarrow \frac{v\frac{D}{C}}{1+v\frac{D}{C}}$ ($1^{st}$ integral) $\quad$ and $\quad z \longrightarrow \frac{1}{1+v\frac{C}{D}}$ ($2^{nd}$ integral)

$$= \frac{\Gamma(3/2-b)^2}{\Gamma(3-2b)}\left[C^{\gamma-a+1}\,D^{\beta-a+1}\int_0^1 dv\,v^\beta\,(C+vD)^{a-\beta-\gamma-2}\,{}_2F_1\,(a,a+b-1,2-b,v)\right.$$

$$+C^{\gamma-a+1}\,D^{\beta-a+1}\int_0^1 dv\,v^{\gamma}\,(D+vC)^{a-\beta-\gamma-2}\,{}_2F_1\,(a,a+b-1,2-b,v)\Big]\,, \tag{B.10}$$

which shows manifest symmetry under simultaneous mapping $C \leftrightarrow D$ and $\beta \leftrightarrow \gamma$, as it should. It agrees with Eq. (B.17) in [29]. For the case $a = 1$ Eq. (B.10) then becomes

$$\begin{aligned} I^{z,w'}_{1,b,\beta,\gamma}(C,D) \;&=\; \frac{\Gamma(3/2-b)^2}{\Gamma(3-2b)}\,C^{\gamma}\,D^{\beta}\left[\int_0^1 dv\,v^{\beta}\,(C+vD)^{-\beta-\gamma-1}\,{}_2F_1\,(1,b,2-b,v)\right. \\ &\left. +\int_0^1 dv\,v^{\gamma}\,(D+vC)^{-\beta-\gamma-1}\,{}_2F_1\,(1,b,2-b,v)\right]. \end{aligned} \tag{B.11}$$

For the setting $\beta = \gamma = -\epsilon = 1-b$ in Eq. (B.11) we can use GR 7.512 (9.), which reads:

$$\begin{aligned} &\int_0^1 dx\,x^{\gamma-1}\,(1-x)^{\rho-1}\,(1-xz)^{-\sigma}\,{}_2F_1\,(\alpha,\beta,\gamma,x) \;= \\ &= \frac{\Gamma(\gamma)\Gamma(\rho)\Gamma(\gamma+\rho-\alpha-\beta)}{\Gamma(\gamma+\rho-\alpha)\Gamma(\gamma+\rho-\beta)}\,(1-z)^{-\sigma}\,{}_3F_2\left(\rho,\sigma,\gamma+\rho-\alpha-\beta,\gamma+\rho-\alpha,\gamma+\rho-\beta,\frac{z}{z-1}\right). \\ &\quad \text{where} \quad \mathrm{Re}(\gamma)>0\,, \quad \mathrm{Re}(\rho)>0\,, \quad \mathrm{Re}(\gamma+\rho-\alpha-\beta)>0\,, \quad |\arg(1-z)|<\pi\,. \end{aligned} \tag{B.12}$$

Thus, the first integral in Eq. (B.11) becomes

$$\begin{aligned} &\int_0^1 dv\,v^{1-b}\,(C+vD)^{b-2-\gamma}\,{}_2F_1\,(1,b,2-b,v) \;= \\ &= \frac{\Gamma(2-2b)}{\Gamma(3-2b)}\,(C+D)^{b-2-\gamma}\,{}_3F_2\left(1,2-b+\gamma,2-2b,2-b,3-2b,\frac{D}{C+D}\right), \end{aligned} \tag{B.13}$$

using $\beta = -\epsilon = 1-b$ and

$$\begin{aligned} &\int_0^1 dv\,v^{1-b}\,(C+vD)^{b-2-\gamma}\,{}_2F_1\,(1,b,2-b,v) \;= \\ &= \frac{\Gamma(2-2b)}{\Gamma(3-2b)}\,(C+D)^{2b-3}\,{}_2F_1\left(1,2-2b,2-b,\frac{D}{C+D}\right), \end{aligned} \tag{B.14}$$

using $\gamma = -\epsilon = 1-b$.

Now we collect all terms in Eq. (B.10) for the case $a = 1$ and $\beta = \gamma = -\epsilon = 1-b$ and use Eq. 9.131 (2.) from Ref. [143] for mapping arguments ${}_2F_1(\ldots,z) \rightarrow$

${}_2F_1(\ldots, 1-z)$ on the second ${}_2F_1$ function, getting:

$$\begin{aligned} I^{z,w'}_{1,b,1-b,1-b}(C,D) &= \frac{\Gamma(3/2-b)^2}{\Gamma(3-2b)}\frac{\Gamma(2-2b)}{\Gamma(3-2b)}(C\,D)^{1-b}(C+D)^{2b-3} \quad \times \\ \times &\left[{}_2F_1\left(1,2-2b,2-b,\frac{D}{C+D}\right)+{}_2F_1\left(1,2-2b,2-b,\frac{C}{C+D}\right)\right] \\ &= \frac{\Gamma(3/2-b)^2}{\Gamma(3-2b)}\frac{\Gamma(1-b)\Gamma(2-b)}{\Gamma(3-2b)}\frac{1}{C+D}\,, \end{aligned} \tag{B.15}$$

which agrees with Eq. (B.30) in [29] for the case considered here. The Gamma functions can still be simplified so that,

$$I^{z,w'}_{1,b,1-b,1-b}(C,D) = 2^{4(b-1)}\frac{\pi}{(1-b)}\frac{1}{C+D}\,. \tag{B.16}$$

The special case in Eq. (B.3) thus factorizes nicely (recall $C=(1-z')$ and $D=y'z'$), and (upon mapping $z'\to 1-z'$) is of the type of integrals already computed before, see Eq. (B.1).

$$\begin{aligned} I_b &= \int_0^1 dy' \int_0^1 dz' \frac{(1-y')^{-1-2\epsilon}(y')^{2-\epsilon}(1-z')^{-\epsilon}(z')^{-\epsilon}}{\left[1-(1-y')z'\right]} I^{z,w'}_{1,b,1-b,1-b}(C,D) \\ &\quad \text{where} \qquad \tfrac{1}{(C+D)} = \tfrac{1}{(1-(1-y')z')} \\ &= 2^{4(b-1)}\frac{\pi}{(1-b)}\int_0^1 dy' \int_0^1 dz' \frac{(1-y')^{-1-2\epsilon}(y')^{2-\epsilon}(1-z')^{-\epsilon}(z')^{-\epsilon}}{\left[1-(1-y')z'\right]^2} \\ &\quad \text{where} \qquad z'\to 1-z' \\ &= 2^{4(b-1)}\frac{\pi}{(1-b)}\int_0^1 dy' \int_0^1 dz' \frac{(1-y')^{-1-2\epsilon}(y')^{2-\epsilon}(1-z')^{-\epsilon}(z')^{-\epsilon}}{\left[z'+(1-z')y'\right]^2} \\ &= 2^{4(b-1)}\frac{\pi}{(1-b)} I_{-1-2\epsilon,2-\epsilon,-\epsilon,-\epsilon,2}\,, \end{aligned} \tag{B.17}$$

where care should be taken to match the requirements for convergence of the ${}_3F_2$ in Eq. (B.1). For the case at hand, partial fractioning in $y'/(1-y')$ can be performed, i.e., $I_{-1-2\epsilon,2-\epsilon,-\epsilon,-\epsilon,2} = -I_{-2\epsilon,1-\epsilon,-\epsilon,-\epsilon,2} + I_{-1-2\epsilon,1-\epsilon,-\epsilon,-\epsilon,2}$.

For the case $b = 1 + \epsilon$, we find finally:

$$I_{1+\epsilon} = 4^{2\epsilon}\,\pi \left\{ \frac{1}{2\,\epsilon^2} + \frac{1}{\epsilon} + 4 - \frac{3}{2}\zeta_2 + \epsilon\,(16 - 3\zeta_2 - 8\zeta_3) + \epsilon^2 \left( 64 - 12\zeta_2 - 16\zeta_3 - \frac{177}{20}\zeta_2^2 \right) \right\} .$$

## Summary

We can generalize Eq. (B.3) to the following case (keeping in mind the restrictions in the derivation of the azimuthal integral) and indicating the factorization obtained,

$$\begin{aligned}
I_{b,A,B,C,D,E} &= \int_0^1 dy' \int_0^1 dz \int_0^1 dz' \int_0^1 dw' \quad \times \\
\times \quad & \frac{(w'(1-w'))^{1/2-b}\,(z(1-z))^{1-b}\,(1-y')^A\,(y')^B\,(1-z')^C\,(z')^D}{\left[1-(1-y')z'\right]^{E-1}\left[z(1-z')+y'(1-z)z'+2(1-2w')\sqrt{y'}\sqrt{(1-z)z}\sqrt{(1-z')z'}\right]} \\
&= 2^{4(b-1)}\,\frac{\pi}{(1-b)} \int_0^1 dy' \int_0^1 dz' \,\frac{(1-y')^A\,(y')^B\,(1-z')^C\,(z')^D}{\left[1-(1-y')z'\right]^E} \\
&\qquad \text{where} \qquad\qquad z' \to 1-z' \\
&= 2^{4(b-1)}\,\frac{\pi}{(1-b)} \int_0^1 dy' \int_0^1 dz' \,\frac{(1-y')^A\,(y')^B\,(1-z')^D\,(z')^C}{\left[z'-(1-z')y'\right]^E} \\
&= 2^{4(b-1)}\,\frac{\pi}{(1-b)}\, I_{A,B,D,C,E} \\
&= 2^{4(b-1)}\,\frac{\pi}{(1-b)}\,\frac{\Gamma(A+1)\Gamma(B+1)}{\Gamma(A+B+2)}\,\frac{\Gamma(D+1)\Gamma(B+C+2-E)}{\Gamma(B+C+D+3-E)} \quad \times \\
\times \quad & {}_3F_2\left(A+B+2-E, B+1, D+1, A+B+2, B+C+D+3-E, 1\right) . \qquad \text{(B.18)}
\end{aligned}$$

Note the flipped indices $C$ and $D$ when using Eq. (B.1) and the conditions for the parameters $A, B, C, D, E$ have also been specified in Eq. (B.1).

## B.3 $I_{a,b,A,B,C,D,E}$

We can then generalize eq. (B.18) as follows:

$$
\begin{aligned}
I_{a,b,A,B,C,D,E} &= \int_0^1 dy' \int_0^1 dz \int_0^1 dz' \int_0^1 dw' \quad \times \\
\times \quad & \frac{(w'(1-w'))^{1/2-b}\,(z(1-z))^{1-b}\,(1-y')^A\,(y')^B\,(1-z')^C\,(z')^D}{\left[1-(1-y')z'\right]^{E-1}\left[z(1-z')+y'(1-z)z'+2(1-2w')\sqrt{y'}\sqrt{(1-z)z}\sqrt{(1-z')z'}\right]^a} \\
&= 2^{4(b-1)}\,\pi\,\frac{\Gamma(2-b-a)\Gamma(3-2b)}{\Gamma(2-b)\Gamma(4-2b-a)}\int_0^1 dy' \int_0^1 dz' \frac{(1-y')^A\,(y')^B\,(1-z')^C\,(z')^D}{\left[1-(1-y')z'\right]^{E+a-1}} \\
&\qquad \text{where} \qquad\qquad z' \to 1-z' \\
&= 2^{4(b-1)}\,\pi\,\frac{\Gamma(2-b-a)\Gamma(3-2b)}{\Gamma(2-b)\Gamma(4-2b-a)}\int_0^1 dy' \int_0^1 dz' \frac{(1-y')^A\,(y')^B\,(1-z')^D\,(z')^C}{\left[z'-(1-z')y'\right]^{E+a-1}} \\
&= 2^{4(b-1)}\,\pi\,\frac{\Gamma(2-b-a)\Gamma(3-2b)}{\Gamma(2-b)\Gamma(4-2b-a)}\,I_{A,B,D,C,E+a-1} \\
&= 2^{4(b-1)}\,\pi\,\frac{\Gamma(2-b-a)\Gamma(3-2b)}{\Gamma(2-b)\Gamma(4-2b-a)}\,\frac{\Gamma(A+1)\Gamma(B+1)}{\Gamma(A+B+2)}\,\frac{\Gamma(D+1)\Gamma(B+C+3-E-a)}{\Gamma(B+C+D+4-E-a)} \times \\
\times \quad & {}_3F_2\left(A+B+3-E-a, B+1, D+1, A+B+2, B+C+D+4-E-a, 1\right) . \qquad \text{(B.19)}
\end{aligned}
$$

## B.4 $I_{b,\beta,\gamma,A,B,C,D,E}$

We start off from Eq. (B.10) for a new trial for the special case $a = 1$ but otherwise keep less constraints on $\beta$ and $\gamma$. Recall, we abbreviate $C = (1 - z')$ and $D = y'z'$. We will use (without proof of the general case) eqs. (B.30) and (B.31) in [29].

$$I^{z,w'}_{1,b,\beta,\gamma}(C,D) = \int_0^1 dz \int_0^1 dw' \frac{z^\beta (1-z)^\gamma [w'(1-w')]^{1/2-b}}{[zC + (1-z)D + 2(1-2w')\sqrt{C}\sqrt{D}\sqrt{(1-z)z}]}$$

fixing $\beta = 1 - b$ and using Eq. (B.30)

$$I^{z,w'}_{1,b,1-b,\gamma}(C,D) = \frac{1}{C} \frac{\Gamma(3/2-b)^2}{\Gamma(3-2b)} \frac{\Gamma(1-b)\Gamma(\gamma+1)}{\Gamma(\gamma-b+2)} {}_2F_1\left(1, \gamma+1, 2-b, -\frac{D}{C}\right), \quad \text{(B.20)}$$

and, likewise, with $\gamma = 1 - b$

$$I^{z,w'}_{1,b,\beta,1-b}(C,D) = \frac{1}{D} \frac{\Gamma(3/2-b)^2}{\Gamma(3-2b)} \frac{\Gamma(1-b)\Gamma(\beta+1)}{\Gamma(\beta-b+2)} {}_2F_1\left(1, \beta+1, 2-b, -\frac{C}{D}\right). \quad \text{(B.21)}$$

Now, we will assume in Eq. (B.20) and (B.21), that either $\beta + b = n$ or $\gamma + b = n$ with $n \geq 0$ a natural number. Recall, $b = 1 + \epsilon$ in our applications. This implies basically the same dependence on the fractional powers of $\epsilon$ for $\sim [w'(1-w')]^{-\epsilon}$ and $\sim [z(1-z)]^{-\epsilon}$, which is the case for the phase space of two unresolved partons, cf. Eq. (A.22) for $d\Phi^{(abcd)}_{\text{rad},2}$ in [29]. Then, we can apply Eq. (3.50) in [29], which can be proven with the help of Eq. 9.132 (1.) from Ref. [143]. For integer $n \geq 0$ we have

$${}_2F_1(1, c+n, c, x) = (c-1) \sum_{k=0}^{n} \frac{\Gamma(n+1)\Gamma(c+n-k-1)}{\Gamma(n-k+1)\Gamma(c+n)} \frac{1}{(1-x)^{k+1}}, \quad \text{(B.22)}$$

so that the hypergeometric function can be expressed in terms of simple powers, as in the special case in eqs. (B.15) and (B.16). We start off with Eq. (B.20) and set $\gamma = n + 1 - b$, so that

$$I^{z,w'}_{1,b,1-b,n+1-b}(C,D) = \frac{1}{C} \frac{\Gamma(3/2-b)^2}{\Gamma(3-2b)} \frac{\Gamma(1-b)\Gamma(n+2-b)}{\Gamma(n+3-2b)} {}_2F_1\left(1, n+2-b, 2-b, -\frac{D}{C}\right)$$

and using Eq. (B.22)

$$= \frac{\Gamma(3/2-b)^2}{\Gamma(3-2b)} \frac{\Gamma(2-b)\Gamma(n+1)}{\Gamma(n+3-2b)} \sum_{k=0}^{n} \frac{\Gamma(n-k-b+1)}{\Gamma(n-k+1)} \frac{C^k}{(C+D)^{k+1}}$$

$$= 2^{4(b-1)}\,\pi\,\frac{\Gamma(3-2b)\Gamma(n+1)}{\Gamma(2-b)\Gamma(n+3-2b)}\sum_{k=0}^{n}\frac{\Gamma(n-k-b+1)}{\Gamma(n-k+1)}\,\frac{C^k}{(C+D)^{k+1}}\,, \tag{B.23}$$

which agrees for $n = 0$ with eqs. (B.15) and (B.16). Likewise, Eq. (B.21) for $\beta = n+1-b$ simplifies as

$$\begin{aligned} I^{z,w'}_{1,b,n+1-b,1-b}(C,D) \;&=\; 2^{4(b-1)}\,\pi\,\frac{\Gamma(3-2b)\Gamma(n+1)}{\Gamma(2-b)\Gamma(n+3-2b)}\,\times \\ &\quad\times\sum_{k=0}^{n}\frac{\Gamma(n-k-b+1)}{\Gamma(n-k+1)}\,\frac{D^k}{(C+D)^{k+1}}\,. \end{aligned} \tag{B.24}$$

With these preparations, we can generalize Eq. (B.18) as follows:

$$\begin{aligned} I_{b,\beta,\gamma,A,B,C,D,E} \;&=\; \int_0^1 dy'\int_0^1 dz\int_0^1 dz'\int_0^1 dw'\quad\times \\ &\times\quad\frac{\left(w'(1-w')\right)^{1/2-b}\,z^{\beta}\,(1-z)^{\gamma}\,(1-y')^{A}\,(y')^{B}\,(1-z')^{C}\,(z')^{D}}{\left[1-(1-y')z'\right]^{E-1}\mathcal{D}}\,, \end{aligned} \tag{B.25}$$

and we will be considering the two cases $\beta = n+1-b, \gamma = 1-b$ and $\beta = 1-b, \gamma = n+1-b$. It is always possible to reach these settings by repeated partial fractioning in $z$. Let us start off with $\beta = 1-b$, $\gamma = n+1-b$ and use Eq. (B.23), so that:

$$\begin{aligned} I_{b,1-b,n+1-b,A,B,C,D,E} \;&=\; 2^{4(b-1)}\,\pi\,\frac{\Gamma(3-2b)\Gamma(n+1)}{\Gamma(2-b)\Gamma(n+3-2b)}\sum_{k=0}^{n}\frac{\Gamma(n-k-b+1)}{\Gamma(n-k+1)}\quad\times \\ \times\quad&\int_0^1 dy'\int_0^1 dz'\,\frac{(1-y')^{A}\,(y')^{B}\,(1-z')^{C+k}\,(z')^{D}}{\left[1-(1-y')z'\right]^{E+k}} \\ =\;& 2^{4(b-1)}\,\pi\,\frac{\Gamma(3-2b)\Gamma(n+1)}{\Gamma(2-b)\Gamma(n+3-2b)}\sum_{k=0}^{n}\frac{\Gamma(n-k-b+1)}{\Gamma(n-k+1)}\,I_{A,B,D,C+k,E+k} \\ =\;& 2^{4(b-1)}\,\pi\,\frac{\Gamma(3-2b)\Gamma(n+1)}{\Gamma(2-b)\Gamma(n+3-2b)}\sum_{k=0}^{n}\frac{\Gamma(n-k-b+1)}{\Gamma(n-k+1)}\quad\times \\ \times\quad&\frac{\Gamma(A+1)\Gamma(B+1)}{\Gamma(A+B+2)}\,\frac{\Gamma(D+1)\Gamma(B+C+2-E)}{\Gamma(B+C+D+3-E)}\quad\times \\ \times\quad&{}_3F_2\left(A+B+2-E-k,B+1,D+1,A+B+2,B+C+D+3-E,1\right)\,, \end{aligned} \tag{B.26}$$

where we have used Eq. (B.1) and the conditions for the parameters $A, B, C, D, E$ have been specified there.

The other case, $\beta = n+1-b$, $\gamma = 1-b$, follows from Eq. (B.24), and reads

$$I_{b,n+1-b,1-b,A,B,C,D,E} = 2^{4(b-1)}\,\pi\,\frac{\Gamma(3-2b)\Gamma(n+1)}{\Gamma(2-b)\Gamma(n+3-2b)}\sum_{k=0}^{n}\frac{\Gamma(n-k-b+1)}{\Gamma(n-k+1)} \quad \times$$

$$\times \quad \int_0^1 dy' \int_0^1 dz' \,\frac{(1-y')^A\,(y')^{B+k}\,(1-z')^C\,(z')^{D+k}}{\left[1-(1-y')z'\right]^{E+k}}$$

$$= \quad 2^{4(b-1)}\,\pi\,\frac{\Gamma(3-2b)\Gamma(n+1)}{\Gamma(2-b)\Gamma(n+3-2b)}\sum_{k=0}^{n}\frac{\Gamma(n-k-b+1)}{\Gamma(n-k+1)}\,I_{A,B+k,D+k,C,E+k}$$

$$= \quad 2^{4(b-1)}\,\pi\,\frac{\Gamma(3-2b)\Gamma(n+1)}{\Gamma(2-b)\Gamma(n+3-2b)}\sum_{k=0}^{n}\frac{\Gamma(n-k-b+1)}{\Gamma(n-k+1)} \quad \times$$

$$\times \quad \frac{\Gamma(A+1)\Gamma(B+k+1)}{\Gamma(A+B+k+2)}\;\frac{\Gamma(D+k+1)\Gamma(B+C+2-E)}{\Gamma(B+C+D+3+k-E)} \quad \times$$

$$\times \quad {}_3F_2\left(A+B+2-E, B+k+1, D+k+1, A+B+k+2, B+C+D+3+k-E, 1\right) .$$

## B.5 Last special cases

We start from

$$I_{\text{last}} = \int_0^1 dy' \int_0^1 dz \int_0^1 dz' \int_0^1 dw' \quad \times$$
$$\times \quad \frac{(w'(1-w'))^{1/2-b}\, z^{-b}(1-z)^{-b}\,(1-y')^A\,(y')^B\,(1-z')^{1-b}\,(z')^\delta}{\big[C+D\big]\big[zC+(1-z)D+2(1-2w')\sqrt{C}\sqrt{D}\sqrt{(1-z)z}\big]}\,, \tag{B.27}$$

where $b = 1+\epsilon$ and we can use

$$z^{-b}(1-z)^{-b} = z^{1-b}(1-z)^{-b} + z^{-b}(1-z)^{1-b}\,. \tag{B.28}$$

The first case we have done already, the second case leads to an integral (note that we abbreviate $C = (1-z')$ and $D = y'z'$)

$$\begin{aligned} I_{\text{last}} &= \int_0^1 dy' \int_0^1 dz \int_0^1 dz' \int_0^1 dw' \quad \times \\ &\qquad \times \quad \frac{(w'(1-w'))^{1/2-b}\, z^{-b}(1-z)^{1-b}\,(1-y')^A\,(y')^B\,(1-z')^{1-b}\,(z')^\delta}{\big[C+D\big]\big[zC+(1-z)D+2(1-2w')\sqrt{C}\sqrt{D}\sqrt{(1-z)z}\big]} \\ &= \int_0^1 dy' \int_0^1 dz \int_0^1 dz' \int_0^1 dw' \quad \times \\ &\qquad \times \quad \frac{(w'(1-w'))^{1/2-b}\, z^{1-b}(1-z)^{-b}\,(1-y')^A\,(y')^B\,(1-z')^{1-b}\,(z')^\delta}{\big[C+D\big]\big[zD+(1-z)C+2(1-2w')\sqrt{C}\sqrt{D}\sqrt{(1-z)z}\big]} \end{aligned} \tag{B.29}$$

i.e., the same, but with $C$ and $D$ interchanged.

With $b = 1+\epsilon$ the powers of the exponents are $A = 2-2b$, $B = -b+m$ with $m = 1,2,3,4$ and $\delta = 4-b$. Therefore, we use $A$, $B = -b+m$ with $m \geq 1$ and $\delta = -b+n$ with $n = 4$.

This evaluates for $C = (1 - z')$ and $D = y'z'$ to

$$
\begin{aligned}
I_{\text{last}} &= \int_0^1 dy' \int_0^1 dz \int_0^1 dz' \int_0^1 dw' \quad \times \\
&\quad \times \frac{(w'(1-w'))^{1/2-b}\, z^{1-b}(1-z)^{-b}\,(1-y')^A\,(y')^{-b+m}\,(1-z')^{1-b}\,(z')^{-b+n}}{[C+D]\,[zD+(1-z)C+2(1-2w')\sqrt{C}\sqrt{D}\sqrt{(1-z)z}]} \\
&= 2^{4(b-1)}\,\pi\,\frac{\Gamma(1-b)^2\Gamma(3-2b)}{\Gamma(2-b)^2\,\Gamma(2-2b)} \int_0^1 dy' \int_0^1 dz'\,(1-y')^A\,(y')^{-b+m}\,(1-z')^{1-b}\,(z')^{-b+n} \quad \times \\
&\quad \times \frac{1}{C+D}\,\frac{1}{D}\,{}_2F_1\left(1, 1-b, 2-b, -\frac{C}{D}\right) \\
&= 2^{4(b-1)}\,\pi\,\frac{\Gamma(1-b)^2\Gamma(3-2b)}{\Gamma(2-b)^2\,\Gamma(2-2b)} \int_0^1 dy' \int_0^1 dz'\,(1-y')^A\,(y')^{-b+m}\,(1-z')^{1-b}\,(z')^{-b+n} \quad \times \\
&\quad \times \frac{1}{C+D}\left\{\frac{\Gamma(-b)\Gamma(2-b)}{\Gamma(1-b)^2}\,\frac{1}{C}\,{}_2F_1\left(1, b, 1+b, -\frac{D}{C}\right) + \Gamma(b)\Gamma(2-b)\,C^{-1+b}\,D^{-b}\right\} \\
&= 2^{4(b-1)}\,(2\,\pi) \int_0^1 dy' \int_0^1 dz'\,(1-y')^A\,(y')^{-b+m}\,(1-z')^{1-b}\,(z')^{-b+n} \quad \times \\
&\quad \times \left\{-\frac{1}{C+D}\int_0^1 dt\, t^{-1+b}\,\frac{1}{C+tD} + \Gamma(b)\Gamma(1-b)\,\frac{C^{-1+b}\,D^{-b}}{C+D}\right\} \\
&= 2^{4(b-1)}\,(2\,\pi) \int_0^1 dt \int_0^1 dy' \int_0^1 dz'\,(1-y')^A\,(y')^{-b+m}\,(1-z')^{-b}\,(z')^{-b+n} \quad \times \\
&\quad \times \left(-\frac{t^{-1+b}}{1-t}\,\frac{1}{1-(1-y')z'} + \frac{t^b}{1-t}\,\frac{1}{1-(1-ty')z'}\right) \\
&\quad + 2^{4(b-1)}\,(2\,\pi)\,\Gamma(b)\Gamma(1-b) \int_0^1 dy' \int_0^1 dz'\,(1-y')^A\,(y')^{-2b+m}\,(z')^{-2b+n}\,\frac{1}{1-(1-y')z'} \\
&= 2^{4(b-1)}\,(2\,\pi)\,\frac{\Gamma(1-b)\Gamma(1-b+n)}{\Gamma(2-2b+n)} \int_0^1 dt \int_0^1 dy'\,(1-y')^A\,(y')^{-b+m} \quad \times \\
&\times \left(-\frac{t^{-1+b}}{1-t}\,{}_2F_1\left(1, 1-b+n, 2-2b+n, 1-y'\right) + \frac{t^b}{1-t}\,{}_2F_1\left(1, 1-b+n, 2-2b+n, 1-ty'\right)\right) \\
&\quad + 2^{4(b-1)}\,(2\,\pi)\,\Gamma(b)\Gamma(1-b) \int_0^1 dy' \int_0^1 dz'\,(1-y')^A\,(y')^{-2b+m}\,(z')^{-2b+n}\,\frac{1}{1-(1-y')z'}\,. \qquad \text{(B.30)}
\end{aligned}
$$

The first term is in the category of integrals done before, the last term with the double integral over $y'$ and $z'$ can be integrated directly.

Depending on the values of $m$, we interchage the order of integration for $y'$ and $z'$. We have for $m = 1, 2, 3$

$$
2^{4(b-1)}\,(2\,\pi)\,\Gamma(b)\Gamma(1-b) \int_0^1 dy' \int_0^1 dz'\,(1-y')^A\,(y')^{-2b+m}\,(z')^{-2b+n}\,\frac{1}{1-(1-y')z'}
$$

$$
\begin{aligned}
&= 2^{4(b-1)}\,(2\,\pi)\,\Gamma(b)\Gamma(1-b)\Gamma(2b-m)\Gamma(1-2b+m)\int_0^1 dz'\,(1-z')^{-2b+m}\,(z')^{-1-A-m+n} \\
&\quad +2^{4(b-1)}\,(2\,\pi)\,\frac{\Gamma(b)\Gamma(1-b)\Gamma(1+A)\Gamma(m-2b)}{\Gamma(1+A+m-2b)}\int_0^1 dz'\,(z')^{-2b+n}\;{}_2F_1\left(1,1+A,1+2b-m,1-z'\right) \\
&= 2^{4(b-1)}\,(2\,\pi)\,\frac{\Gamma(b)\Gamma(1-b)\Gamma(2b-m)\Gamma(1-2b+m)^2\Gamma(-A-m+n)}{\Gamma(1-2b-A+n)} \\
&\quad +2^{4(b-1)}\,(2\,\pi)\,\frac{\Gamma(b)\Gamma(1-b)\Gamma(1+A)\Gamma(m-2b)\Gamma(1-2b+n)}{\Gamma(2-2b+n)\Gamma(1+A+m-2b)}\times \\
&\qquad \times\;\; {}_3F_2\left(1,1,1+A,1+2b-m,2-2b+n,1\right)\,.
\end{aligned}
$$

For $m = 2, 3, 4$ we have

$$
\begin{aligned}
&2^{4(b-1)}\,(2\,\pi)\,\Gamma(b)\Gamma(1-b)\int_0^1 dy'\int_0^1 dz'\,(1-y')^A\,(y')^{-2b+m}\,(z')^{-2b+n}\,\frac{1}{1-(1-y')z'} \\
&= 2^{4(b-1)}\,(2\,\pi)\,\frac{\Gamma(b)\Gamma(1-b)\Gamma(1-2b+n)}{\Gamma(2-2b+n)}\times \\
&\qquad \times\;\; \int_0^1 dy'\,(1-y')^A\,(y')^{-2b+m}\;{}_2F_1\left(1,1-2b+n,2-2b+n,1-y'\right) \\
&= 2^{4(b-1)}\,(2\,\pi)\,\frac{\Gamma(b)\Gamma(1-b)\Gamma(1-2b+n)}{\Gamma(2-2b+n)}\times \\
&\qquad \times\;\; \int_0^1 dy'\,(y')^A\,(1-y')^{-2b+m}\;{}_2F_1\left(1,1-2b+n,2-2b+n,y'\right) \\
&= 2^{4(b-1)}\,(2\,\pi)\,\frac{\Gamma(b)\Gamma(1-b)\Gamma(1-2b+n)}{\Gamma(2-2b+n)} \quad\times \\
&\qquad \times\;\; \frac{\Gamma(A+1)\Gamma(-2b+m+1)}{\Gamma(A-2b+m+2)}\;{}_3F_2\left(1,1-2b+n,A+1,2-2b+n,A-2b+m+2,1\right)\,.
\end{aligned}
$$

With these results we obtain the following results (the notation $\mathrm{Int}_i$ corresponds to $m = i+1$). Note, that we omit an overall factor $2^{4(b-1)}\,\pi\; = 4^{2\epsilon}\pi$ in the expressions below:

```
Int0=
   +ep^(-3)*(-1/2)
   +ep^(-2)*(-3/2)
   +ep^(-1)*(-6+1/2*z2)
   +ep*(-63/2-21*z3+21*z2-399/20*z2^2)
   +ep^2*(-60-199*z5+61*z3+285/4*z2+7*z2*z3-1197/20*z2^2)
   -63/4-7*z3+3/2*z2;

Int1=
```

```
   +ep^(-1)*(-3/2)
   +ep*(-14-18*z3+1/2*z2)
   +ep^2*(-53/2-24*z3+95/4*z2-153/5*z2^2)
   -25/4-2*z2;

Int2=
   +ep^(-1)*(-1/2)
   +ep*(-24+18*z3-9/2*z2)
   +ep^2*(-149/2-46*z3+55/4*z2+153/5*z2^2)
   -25/4+2*z2;

Int3=
   +ep^(-1)*(3-2*z2)
   +ep*(47/8+75*z3-12*z2-153/5*z2^2)
   +ep^2*(125/16-316*z5-53*z3-21*z2+40*z2*z3+594/5*z2^2)
   +5-18*z3+9*z2;
```

In the expressions above, the values z2, z3, and z5 correspond to the Riemann zeta function evaluated at 2, 3, and 5, respectively, denoted as $\zeta(2)$, $\zeta(3)$, and $\zeta(5)$.

Another special case which needs to be analyzed has a following form:

$$\begin{aligned} I &= \int_0^1 dy' \int_0^1 dz \int_0^1 dz' \int_0^1 dw' \quad \times \\ &\times \frac{(w'(1-w'))^{1/2-b}\, z^{1-b}(1-z)^{-b}\,(1-y')^A\,(y')^B\,(1-z')^{1-b}\,(z')^\delta}{\big[C+D\big]\big[zC+(1-z)D+2(1-2w')\sqrt{C}\sqrt{D}\sqrt{(1-z)z}\big]}\,. \end{aligned} \tag{B.31}$$

The power $(1-z')^{1-b}$ is always the same. We allow for $(z')^\delta$ with $\delta = -1-\epsilon, -\epsilon, 1-\epsilon, \ldots, 5-\epsilon$, which is $\delta = -b, 1-b, 2-b, \ldots, 6-b$, or, more generally $\delta = -b+n$ with $n \geq 0$. Also $A = -1-2\epsilon = 1-2b$ or $A = -2\epsilon = 2-2b$ in all cases. Finally, we have $B = -b+m$ with with $m \geq 0$.

The case $A = -1-2\epsilon$ can be decomposed with partial fractioning

$$\begin{aligned} \frac{1}{(1-y')}\frac{1}{\big[C+D\big]} &= \frac{1}{(1-y')}\frac{1}{1-(1-y')z'} \\ &= \frac{1}{(1-y')} + \frac{z'}{1-(1-y')z'} \\ &= \frac{1}{(1-y')} + \frac{z'}{\big[C+D\big]}\,. \end{aligned} \tag{B.32}$$

The integral in the first case is of simpler type, the one in the second case is treated here as well. Also, we have relations between $A$ and $B = -b + m$ as

$$\frac{1}{y'(1-y')} \;=\; \frac{1}{y'} + \frac{1}{(1-y')}\,. \tag{B.33}$$

We use the relations in eqs. (B.32) and (B.33) as checks.

We start from eq. (B.31)

$$\begin{aligned}
I \;=\;& \int_0^1 dy' \int_0^1 dz \int_0^1 dz' \int_0^1 dw' \quad \times \\
& \times \; \frac{(w'(1-w'))^{1/2-b}\, z^{1-b}(1-z)^{-b}\,(1-y')^A\,(y')^{-b+m}\,(1-z')^{1-b}\,(z')^{-b+n}}{[C+D]\,[zC+(1-z)D+2(1-2w')\sqrt{C}\sqrt{D}\sqrt{(1-z)z}]} \\
=\;& 2^{4(b-1)}\,(2\,\pi) \int_0^1 dy' \int_0^1 dz'\,(1-y')^A\,(y')^{-b+m}\,(1-z')^{1-b}\,(z')^{-b+n}\,\frac{1}{C+D} \int_0^1 dt\, t^{-b}\,\frac{1}{C+tD} \\
=\;& 2^{4(b-1)}\,(2\,\pi) \int_0^1 dt \int_0^1 dy' \int_0^1 dz'\,(1-y')^A\,(y')^{-b+m}\,(1-z')^{-b}\,(z')^{-b+n} \quad \times \\
& \times \; \left(\frac{t^{-b}}{1-t}\,\frac{1}{1-(1-y')z'} - \frac{t^{1-b}}{1-t}\,\frac{1}{1-(1-ty')z'}\right) \\
=\;& 2^{4(b-1)}\,(2\,\pi)\,\frac{\Gamma(1-b)\Gamma(1-b+n)}{\Gamma(2-2b+n)} \int_0^1 dt \int_0^1 dy'\,(1-y')^A\,(y')^{-b+m} \quad \times \\
\times \;& \left(\frac{t^{-b}}{1-t}\,{}_2F_1\left(1,1-b+n,2-2b+n,1-y'\right) - \frac{t^{1-b}}{1-t}\,{}_2F_1\left(1,1-b+n,2-2b+n,1-ty'\right)\right)
\end{aligned}$$

partial fractioning in $t$ and re-grouping

$$\begin{aligned}
=\;& 2^{4(b-1)}\,(2\,\pi)\,\frac{\Gamma(1-b)\Gamma(1-b+n)}{\Gamma(2-2b+n)} \int_0^1 dt\, t^{-b} \int_0^1 dy'\,(1-y')^A\,(y')^{-b+m} \quad \times \\
\times \;& \left({}_2F_1\left(1,1-b+n,2-2b+n,1-ty'\right)\right. \\
& \left. + \left\{\frac{{}_2F_1\left(1,1-b+n,2-2b+n,1-y'\right)}{1-t} - \frac{{}_2F_1\left(1,1-b+n,2-2b+n,1-ty'\right)}{1-t}\right\}\right)\,.
\end{aligned} \tag{B.34}$$

- This expression can be dealt with for $n = 0, 1$, using Eq. 9.131-2 from Ref. [143] to map the argument from $1 - y'$ to $y'$ or $1 - ty'$ to $ty'$ and to integrate subsequently, which we will work out below.
- But it needs additional work for higher $n$. For these cases ($n \geq 2$) we can shift recursively using Eq. 9.137-17 from Ref. [143] until we reach some hypergeometric function of the type ${}_2F_1\left(1,1-b,2-2b+l,1-y'\right)$ or

${}_2F_1\,(1, 1-b, 2-2b+l, 1-ty')$, where $l \leq 0$, we apply Eq. 9.131-2 from Ref. [143] to map the argument from $1-y'$ to $y'$ or $1-ty'$ to $ty'$ in case of $l = 0, 1$. For $l \geq 2$ the series expansion of the hypergeometric function is fully convergent and we can integrate term-wise.

- The procedure for the reduction and solution of the integrals is coded up in a `FORM` routine. We work out the first case below.

We abbreviate $C = (1-z')$ and $D = y'z'$ and we have (from Bakar's notes) the last special integral ($b = 1+\epsilon$ in our applications)

$$\begin{aligned}
I_\gamma &= \int_0^1 dy' \int_0^1 dz \int_0^1 dz' \int_0^1 dw' \quad \times \\
&\quad \times \frac{\left(w'(1-w')\right)^{1/2-b} z^{1-b}(1-z)^\gamma \,(1-y')^A \,(y')^B \,(1-z')^{1-b}\,(z')^{-b}}{\left[C+D\right]\left[zC+(1-z)D+2(1-2w')\sqrt{C}\sqrt{D}\sqrt{(1-z)z}\right]} \\
&= \int_0^1 dy' \int_0^1 dz' \,\frac{(1-y')^A \,(y')^B \,(1-z')^{1-b}\,(z')^{-b}}{\left[C+D\right]}\, I^{z,w'}_{1,b,1-b,\gamma}(C,D) \\
&= \int_0^1 dy' \int_0^1 dz' \,(1-y')^A \,(y')^B \,(1-z')^{1-b}\,(z')^{-b}\,\frac{1}{\left[C+D\right]} \quad \times \\
&\quad \times \frac{1}{C}\,\frac{\Gamma(3/2-b)^2}{\Gamma(3-2b)}\,\frac{\Gamma(1-b)\Gamma(\gamma+1)}{\Gamma(\gamma-b+2)}\,{}_2F_1\left(1, \gamma+1, 2-b, -\frac{D}{C}\right), \qquad \text{(B.35)}
\end{aligned}$$

which simplifies for the special case $\gamma = -b$ as

$$\begin{aligned}
I_{-b} &= \int_0^1 dy' \int_0^1 dz \int_0^1 dz' \int_0^1 dw' \quad \times \\
&\quad \times \frac{\left(w'(1-w')\right)^{1/2-b} z^{1-b}(1-z)^{-b} \,(1-y')^A \,(y')^B \,(1-z')^{1-b}\,(z')^{-b}}{\left[C+D\right]\left[zC+(1-z)D+2(1-2w')\sqrt{C}\sqrt{D}\sqrt{(1-z)z}\right]} \\
&= 2^{4(b-1)}\,\pi\,\frac{\Gamma(1-b)^2\Gamma(3-2b)}{\Gamma(2-b)^2\,\Gamma(2-2b)} \int_0^1 dy' \int_0^1 dz' \,(1-y')^A \,(y')^B \,(1-z')^{1-b}\,(z')^{-b} \quad \times \\
&\quad \times \frac{1}{C+D}\,\frac{1}{C}\,{}_2F_1\left(1, 1-b, 2-b, -\frac{D}{C}\right) \\
&= 2^{4(b-1)}\,\pi\,\frac{\Gamma(1-b)\Gamma(3-2b)}{\Gamma(2-b)\Gamma(2-2b)} \int_0^1 dy' \int_0^1 dz' \,(1-y')^A \,(y')^B \,(1-z')^{1-b}\,(z')^{-b} \quad \times \\
&\quad \times \frac{1}{C+D} \int_0^1 dt\, t^{-b}\,\frac{1}{C+tD}
\end{aligned}$$

$$= 2^{4(b-1)}(2\pi)\int_0^1 dy'\int_0^1 dz'\,(1-y')^A\,(y')^B\,(1-z')^{1-b}\,(z')^{-b}\,\frac{1}{C+D}\times \\ \times\int_0^1 dt\,t^{-b}\,\frac{1}{C+tD}\,. \tag{B.36}$$

Doing a partial fractioning in $D$, which is equivalent to $y'$, we find

$$\frac{1}{C+D}\,\frac{1}{C+tD} = \frac{1}{1-t}\,\frac{1}{C}\,\frac{1}{C+D}-\frac{t}{1-t}\,\frac{1}{C}\,\frac{1}{C+tD} \\ = \frac{1}{1-t}\,\frac{1}{1-z'}\,\frac{1}{1-(1-y')z'}-\frac{t}{1-t}\,\frac{1}{1-z'}\,\frac{1}{1-(1-ty')z'}\,,$$

where we have substituted $C$ and $D$. The right hand side has a spurious singularity for $t\to 1$, to be kept in mind.

Then the $z'$ integration can be done (for the special case we have $A=2-2b$ and $B=1-b$)

$$I_{\text{last}} = 2^{4(b-1)}(2\pi)\int_0^1 dt\int_0^1 dy'\int_0^1 dz'\,(1-y')^A\,(y')^B\,(1-z')^{-b}\,(z')^{-b} \quad\times \\ \times\quad\left(\frac{t^{-b}}{1-t}\,\frac{1}{1-(1-y')z'}-\frac{t^{1-b}}{1-t}\,\frac{1}{1-(1-ty')z'}\right) \\ = 2^{4(b-1)}(2\pi)\,\frac{\Gamma(1-b)^2}{\Gamma(2-2b)}\int_0^1 dt\int_0^1 dy'\,(1-y')^A\,(y')^B \quad\times \\ \times\quad\left(\frac{t^{-b}}{1-t}\,{}_2F_1\left(1,1-b,2-2b,1-y'\right)-\frac{t^{1-b}}{1-t}\,{}_2F_1\left(1,1-b,2-2b,1-ty'\right)\right) \\ = 2^{4(b-1)}(2\pi)\,\Gamma(1-b)\int_0^1 dt\int_0^1 dy'\,(1-y')^A\,(y')^B \quad\times \\ \times\quad\left(\frac{t^{-b}}{1-t}\,\frac{\Gamma(-b)}{\Gamma(1-2b)}\,{}_2F_1\left(1,1-b,1+b,y'\right)+\frac{t^{-b}}{1-t}\,\Gamma(b)\,(y')^{-b}\,(1-y')^{-1+2b}\right. \\ \left.-\frac{t^{1-b}}{1-t}\,\frac{\Gamma(-b)}{\Gamma(1-2b)}\,{}_2F_1\left(1,1-b,1+b,ty'\right)-\frac{t^{1-b}}{1-t}\,\Gamma(b)\,(ty')^{-b}\,(1-ty')^{-1+2b}\right)$$

partial fractioning in $t$ and re-grouping

$$= 2^{4(b-1)}(2\pi)\,\Gamma(1-b)\int_0^1 dt\,t^{-b}\int_0^1 dy'\,(1-y')^A\,(y')^B \quad\times \\ \times\quad\left(\frac{\Gamma(-b)}{\Gamma(1-2b)}\,{}_2F_1\left(1,1-b,1+b,ty'\right)+\Gamma(b)\,(ty')^{-b}\,(1-ty')^{-1+2b}\right. \\ \left.+\frac{\Gamma(-b)}{\Gamma(1-2b)}\left\{\frac{{}_2F_1\left(1,1-b,1+b,y'\right)}{1-t}-\frac{{}_2F_1\left(1,1-b,1+b,ty'\right)}{1-t}\right\}\right.$$

$$+\,\Gamma(b)\,\left\{\frac{(y')^{-b}\,(1-y')^{-1+2b}}{1-t}\,-\,\frac{(ty')^{-b}\,(1-ty')^{-1+2b}}{1-t}\,\right\}\Bigg)\,. \tag{B.37}$$

For a hypergeometric function ${}_2F_1(\alpha,\beta,\gamma,x)$ the series converges (absolutely) throughout the entire unit circle, if $\mathrm{Re}(\alpha+\beta-\gamma)<0$. In all other integrals we can use the the geometric series

$$\frac{1}{(1-x)^\alpha} \;=\; \sum_{i=0}^{\infty}\binom{i+\alpha-1}{i}\,x^i\,. \tag{B.38}$$

We have ${}_2F_1\,(1,1-b,1+b,y')$ that $\mathrm{Re}(1+1-b-1-b)=1-2b<0$. For $b=1+\epsilon$ this is $-1-2\epsilon<0$. This allows to interchange summation and integration.

The differences $\{\dots\}$ in the second line and third are regular as $t\;\to\;1$, which can be seen using the geometric series and the series representation of ${}_2F_1\,(1,1-b,1+b,y')$. In terms of Pochhammer symbols $(a)_n=\Gamma(a+n)/\Gamma(a)$ we have

$${}_2F_1\left(1,1-b,1+b,y'\right) \;=\; \sum_{i=0}^{\infty}\frac{(1)_i\,(1-b)_i}{(1+b)_i}\,\frac{(y')^i}{i!}\,. \tag{B.39}$$

Thus,

$$\begin{aligned}\frac{{}_2F_1\,(1,1-b,1+b,y')}{1-t}\,-\,\frac{{}_2F_1\,(1,1-b,1+b,ty')}{1-t} \;=\\ =\;\sum_{i=0}^{\infty}\frac{(1)_i\,(1-b)_i}{(1+b)_i}\,\frac{(y')^i}{i!}\,\frac{1-t^i}{1-t}\,,\end{aligned} \tag{B.40}$$

and

$$\begin{aligned}\frac{(y')^{-b}\,(1-y')^{-1+2b}}{1-t}\,-\,\frac{(ty')^{-b}\,(1-ty')^{-1+2b}}{1-t} \;=\\ =\;\sum_{i=0}^{\infty}\binom{i-2b}{i}\,(y')^{i-b}\,\frac{1-t^{i-b}}{1-t}\,,\end{aligned} \tag{B.41}$$

we can exchange integration and summation and integrate term-wise.

Putting everthing together, we have

$$I \;=\; 2^{4(b-1)}\,(2\,\pi)\,\Gamma(1-b)\,\int_0^1 dt\,t^{-b}\,\int_0^1 dy'\,(1-y')^A\,(y')^B \quad\times$$

$$
\begin{aligned}
&\times \quad \left( \frac{\Gamma(-b)}{\Gamma(1-2b)}\, {}_2F_1\left(1, 1-b, 1+b, ty'\right) + \Gamma(b)\,(ty')^{-b}\,(1-ty')^{-1+2b} \right. \\
&\quad + \frac{\Gamma(-b)}{\Gamma(1-2b)} \left\{ \frac{{}_2F_1\left(1, 1-b, 1+b, y'\right)}{1-t} - \frac{{}_2F_1\left(1, 1-b, 1+b, ty'\right)}{1-t} \right\} \\
&\quad \left. + \Gamma(b) \left\{ \frac{(y')^{-b}\,(1-y')^{-1+2b}}{1-t} - \frac{(ty')^{-b}\,(1-ty')^{-1+2b}}{1-t} \right\} \right) \\
= \;& 2^{4(b-1)}\,(2\,\pi)\,\Gamma(1-b) \int_0^1 dt\, t^{-b} \int_0^1 dy'\,(1-y')^A\,(y')^B \quad \times \\
&\times \quad \left( \frac{\Gamma(-b)}{\Gamma(1-2b)} \sum_{i=0}^{\infty} \frac{(1)_i\,(1-b)_i}{(1+b)_i} \frac{(ty')^i}{i!} + \Gamma(b)\,(ty')^{-b} \sum_{i=0}^{\infty} \binom{i-2b}{i} (ty')^i \right. \\
&\quad + \frac{\Gamma(-b)}{\Gamma(1-2b)} \sum_{i=0}^{\infty} \frac{(1)_i\,(1-b)_i}{(1+b)_i} \frac{(y')^i}{i!} \frac{1-t^i}{1-t} \\
&\quad \left. + \Gamma(b) \sum_{i=0}^{\infty} \binom{i-2b}{i} (y')^{i-b} \frac{1-t^{i-b}}{1-t} \right) \qquad \text{(B.42)}
\end{aligned}
$$

Here, all integrals can be done. The $t$-integral is regularized as $t \to 1$.

$$
\begin{aligned}
I \;=\; & 2^{4(b-1)}\,(2\,\pi)\,\Gamma(1-b) \quad \times \\
&\times \quad \left( \frac{\Gamma(-b)}{\Gamma(1-2b)} \sum_{i=0}^{\infty} \frac{(1)_i\,(1-b)_i}{(1+b)_i} \frac{1}{i!} \frac{1}{(i+1-b)} \frac{\Gamma(A+1)\Gamma(B+i+1)}{\Gamma(A+B+i+2)} \right. \\
&\quad + \Gamma(b) \sum_{i=0}^{\infty} \binom{i-2b}{i} \frac{1}{(i+1-2b)} \frac{\Gamma(A+1)\Gamma(B+i+1-b)}{\Gamma(A+B+i+2-b)} \\
&\quad + \frac{\Gamma(-b)}{\Gamma(1-2b)} \sum_{i=0}^{\infty} \frac{(1)_i\,(1-b)_i}{(1+b)_i} \frac{1}{i!} \frac{\Gamma(A+1)\Gamma(B+i+1)}{\Gamma(A+B+i+2)} \int_0^1 dt\, t^{-b} \left\{ \frac{1}{1-t} - \frac{t^i}{1-t} \right\} \\
&\quad \left. + \Gamma(b) \sum_{i=0}^{\infty} \binom{i-2b}{i} \frac{\Gamma(A+1)\Gamma(B+i+1-b)}{\Gamma(A+B+i+2-b)} \int_0^1 dt\, t^{-b} \left\{ \frac{1}{1-t} - \frac{t^{i-b}}{1-t} \right\} \right) \\
=\; & 2^{4(b-1)}\,(2\,\pi)\,\Gamma(1-b) \quad \times \\
&\times \quad \left( \frac{\Gamma(-b)}{\Gamma(1-2b)} \sum_{i=0}^{\infty} \frac{(1)_i\,(1-b)_i}{(1+b)_i} \frac{1}{i!} \frac{1}{(i+1-b)} \frac{\Gamma(A+1)\Gamma(B+i+1)}{\Gamma(A+B+i+2)} \right. \\
&+ \Gamma(b) \sum_{i=0}^{\infty} \binom{i-2b}{i} \frac{1}{(i+1-2b)} \frac{\Gamma(A+1)\Gamma(B+i+1-b)}{\Gamma(A+B+i+2-b)} \\
&+ \frac{\Gamma(-b)}{\Gamma(1-2b)} \sum_{i=0}^{\infty} \frac{(1)_i\,(1-b)_i}{(1+b)_i} \frac{1}{i!} \frac{\Gamma(A+1)\Gamma(B+i+1)}{\Gamma(A+B+i+2)} \sum_{j=0}^{\infty} \left\{ \frac{1}{-b+1+j} - \frac{1}{-b+1+i+j} \right\}
\end{aligned}
$$

$$+\Gamma(b)\sum_{i=0}^{\infty}\binom{i-2b}{i}\frac{\Gamma(A+1)\Gamma(B+i+1-b)}{\Gamma(A+B+i+2-b)}\sum_{j=0}^{\infty}\left\{\frac{1}{-b+1+j}-\frac{1}{-2b+1+i+j}\right\}\Bigg). \quad \text{(B.43)}$$

This can be used as input to `XSummer` [74]. Here, sums in the last two lines are individually divergent, but properly regularized in `XSummer` with `Sinf`, which cancels to all orders in $\epsilon$ in the final result. For the case $A = -2\epsilon$, $B = -b+m = -\epsilon$, i.e., $m = 1$ and $b = 1+\epsilon$, we find finally,

$$\begin{aligned} I_{\text{last}} &= 4^{2\epsilon}\,\pi\left\{-\frac{1}{2\epsilon^3}+\frac{2}{\epsilon^2}+\frac{1}{\epsilon}\left(4+\frac{1}{2}\zeta_2\right)+8-8\zeta_2-3\zeta_3+\epsilon\left(16-16\zeta_2-30\zeta_3-\frac{147}{20}\zeta_2^2\right)\right. \\ &\quad \left.+\epsilon^2\left(32-32\zeta_2-60\zeta_3-\frac{123}{5}\zeta_2^2-69\zeta_5+9\zeta_2\zeta_3\right)\right\}. \end{aligned} \quad \text{(B.44)}$$

In `XSummer` this integral is denoted as `[general(-2*ep,1,0)]`.

```
[general(-2*ep,1,0)]=
   +ep^(-3)*(-1/2)
   +ep^(-2)*(2)
   +ep^(-1)*(4+1/2*z2)
   +ep*(16-30*z3-16*z2-147/20*z2^2)
   +ep^2*(32-69*z5-60*z3-32*z2+9*z2*z3-123/5*z2^2)
   +8-3*z3-8*z2;
```

# Bibliography


[1] J. Baglio, C. Duhr, B. Mistlberger, and R. Szafron, "Inclusive production cross sections at $N^3LO$," *JHEP*, vol. 12, p. 066, 2022. DOI: 10.1007/JHEP12(2022)066. arXiv: 2209.06138 [hep-ph].

[2] W. T. Giele, E. W. N. Glover, and D. A. Kosower, "Higher order corrections to jet cross-sections in hadron colliders," *Nucl. Phys. B*, vol. 403, pp. 633–670, 1993. DOI: 10.1016/0550-3213(93)90365-V. arXiv: hep-ph/9302225.

[3] W. T. Giele, E. W. N. Glover, and D. A. Kosower, "The inclusive two jet triply differential cross-section," *Phys. Rev. D*, vol. 52, pp. 1486–1499, 1995. DOI: 10.1103/PhysRevD.52.1486. arXiv: hep-ph/9412338.

[4] S. Frixione, Z. Kunszt, and A. Signer, "Three jet cross-sections to next-to-leading order," *Nucl. Phys. B*, vol. 467, pp. 399–442, 1996. DOI: 10.1016/0550-3213(96)00110-1. arXiv: hep-ph/9512328.

[5] S. Catani and M. H. Seymour, "A General algorithm for calculating jet cross-sections in NLO QCD," *Nucl. Phys. B*, vol. 485, pp. 291–419, 1997, [Erratum: Nucl.Phys.B 510, 503–504 (1998)]. DOI: 10.1016/S0550-3213(96)00589-5. arXiv: hep-ph/9605323.

[6] S. Catani, S. Dittmaier, M. H. Seymour, and Z. Trocsanyi, "The Dipole formalism for next-to-leading order QCD calculations with massive partons," *Nucl. Phys. B*, vol. 627, pp. 189–265, 2002. DOI: 10.1016/S0550-3213(02)00098-6. arXiv: hep-ph/0201036.

[7] Z. Nagy and D. E. Soper, "General subtraction method for numerical calculation of one loop QCD matrix elements," *JHEP*, vol. 09, p. 055, 2003. DOI: 10.1088/1126-6708/2003/09/055. arXiv: hep-ph/0308127.

[8] G. Bevilacqua, M. Czakon, M. Kubocz, and M. Worek, "Complete Nagy-Soper subtraction for next-to-leading order calculations in QCD," *JHEP*, vol. 10, p. 204, 2013. DOI: 10.1007/JHEP10(2013)204. arXiv: 1308.5605 [hep-ph].

[9] J. M. Campbell and R. K. Ellis, "An Update on vector boson pair production at hadron colliders," *Phys. Rev. D*, vol. 60, p. 113 006, 1999. DOI: 10.1103/PhysRevD.60.113006. arXiv: hep-ph/9905386.

[10] T. Gleisberg and F. Krauss, "Automating dipole subtraction for QCD NLO calculations," *Eur. Phys. J. C*, vol. 53, pp. 501–523, 2008. DOI: 10.1140/epjc/s10052-007-0495-0. arXiv: 0709.2881 [hep-ph].

[11] R. Frederix, T. Gehrmann, and N. Greiner, "Automation of the Dipole Subtraction Method in MadGraph/MadEvent," *JHEP*, vol. 09, p. 122, 2008. DOI: 10.1088/1126-6708/2008/09/122. arXiv: 0808.2128 [hep-ph].

[12] K. Hasegawa, S. Moch, and P. Uwer, "AutoDipole: Automated generation of dipole subtraction terms," *Comput. Phys. Commun.*, vol. 181, pp. 1802–1817, 2010. DOI: 10.1016/j.cpc.2010.06.044. arXiv: 0911.4371 [hep-ph].

[13] S. Alioli, P. Nason, C. Oleari, and E. Re, "A general framework for implementing NLO calculations in shower Monte Carlo programs: the POWHEG BOX," *JHEP*, vol. 06, p. 043, 2010. DOI: 10.1007/JHEP06(2010)043. arXiv: 1002.2581 [hep-ph].

[14] S. Platzer and S. Gieseke, "Dipole Showers and Automated NLO Matching in Herwig++," *Eur. Phys. J. C*, vol. 72, p. 2187, 2012. DOI: 10.1140/epjc/s10052-012-2187-7. arXiv: 1109.6256 [hep-ph].

[15] S. Frixione and M. Grazzini, "Subtraction at NNLO," *JHEP*, vol. 06, p. 010, 2005. DOI: 10.1088/1126-6708/2005/06/010. arXiv: hep-ph/0411399.

[16] C. Anastasiou, K. Melnikov, and F. Petriello, "A new method for real radiation at NNLO," *Phys. Rev. D*, vol. 69, p. 076 010, 2004. DOI: 10.1103/PhysRevD.69.076010. arXiv: hep-ph/0311311.

[17] R. Boughezal, C. Focke, W. Giele, X. Liu, and F. Petriello, "Higgs boson production in association with a jet at NNLO using jettiness subtraction," *Phys. Lett. B*, vol. 748, pp. 5–8, 2015. DOI: 10.1016/j.physletb.2015.06.055. arXiv: 1505.03893 [hep-ph].

[18] J. Gaunt, M. Stahlhofen, F. J. Tackmann, and J. R. Walsh, "N-jettiness Subtractions for NNLO QCD Calculations," *JHEP*, vol. 09, p. 058, 2015. DOI: 10.1007/JHEP09(2015)058. arXiv: 1505.04794 [hep-ph].

[19] A. Gehrmann-De Ridder, T. Gehrmann, and E. W. N. Glover, "Antenna subtraction at NNLO," *JHEP*, vol. 09, p. 056, 2005. DOI: 10.1088/1126-6708/2005/09/056. arXiv: hep-ph/0505111.

[20] J. Currie, E. W. N. Glover, and S. Wells, "Infrared Structure at NNLO Using Antenna Subtraction," *JHEP*, vol. 04, p. 066, 2013. DOI: 10.1007/JHEP04(2013)066. arXiv: 1301.4693 [hep-ph].

[21] M. Czakon, "A novel subtraction scheme for double-real radiation at NNLO," *Phys. Lett. B*, vol. 693, pp. 259–268, 2010. DOI: 10.1016/j.physletb.2010.08.036. arXiv: 1005.0274 [hep-ph].

[22] M. Czakon, A. Mitov, and R. Poncelet, "Next-to-Next-to-Leading Order Study of Three-Jet Production at the LHC," *Phys. Rev. Lett.*, vol. 127, no. 15, p. 152 001, 2021, [Erratum: Phys.Rev.Lett. 129, 119901 (2022), Erratum: Phys.Rev.Lett. 129, 119901 (2022)]. DOI: 10.1103/PhysRevLett.127.152001. arXiv: 2106.05331 [hep-ph].

[23] G. Somogyi, Z. Trocsanyi, and V. Del Duca, "Matching of singly- and doubly-unresolved limits of tree-level QCD squared matrix elements," *JHEP*, vol. 06, p. 024, 2005. DOI: 10.1088/1126-6708/2005/06/024. arXiv: hep-ph/0502226.

[24] G. Somogyi, Z. Trocsanyi, and V. Del Duca, "A Subtraction scheme for computing QCD jet cross sections at NNLO: Regularization of doubly-real emissions," *JHEP*, vol. 01, p. 070, 2007. DOI: 10.1088/1126-6708/2007/01/070. arXiv: hep-ph/0609042.

[25] G. Somogyi and Z. Trocsanyi, "A Subtraction scheme for computing QCD jet cross sections at NNLO: Regularization of real-virtual emission," *JHEP*, vol. 01, p. 052, 2007. DOI: 10.1088/1126-6708/2007/01/052. arXiv: hep-ph/0609043.

[26] F. Caola, K. Melnikov, and R. Röntsch, "Nested soft-collinear subtractions in NNLO QCD computations," *Eur. Phys. J. C*, vol. 77, no. 4, p. 248, 2017. DOI: 10.1140/epjc/s10052-017-4774-0. arXiv: 1702.01352 [hep-ph].

[27] L. Magnea, E. Maina, G. Pelliccioli, C. Signorile-Signorile, P. Torrielli, and S. Uccirati, "Local analytic sector subtraction at NNLO," *JHEP*, vol. 12, p. 107, 2018, [Erratum: JHEP 06, 013 (2019)]. DOI: 10.1007/JHEP12(2018)107. arXiv: 1806.09570 [hep-ph].

[28] G. Bertolotti *et al.*, "NNLO subtraction for any massless final state: a complete analytic expression," *JHEP*, vol. 07, p. 140, 2023. DOI: 10.1007/JHEP07(2023)140. arXiv: 2212.11190 [hep-ph].

[29] L. Magnea, G. Pelliccioli, C. Signorile-Signorile, P. Torrielli, and S. Uccirati, "Analytic integration of soft and collinear radiation in factorised QCD cross

sections at NNLO," *JHEP*, vol. 02, p. 037, 2021. DOI: 10.1007/JHEP02(2021)037. arXiv: 2010.14493 [hep-ph].

[30] D. J. Gross, "Twenty five years of asymptotic freedom," *Nucl. Phys. B Proc. Suppl.*, vol. 74, S. Narison, Ed., pp. 426–446, 1999. DOI: 10.1016/S0920-5632(99)00208-X. arXiv: hep-th/9809060.

[31] M. E. Peskin and D. V. Schroeder, *An Introduction to quantum field theory*. Reading, USA: Addison-Wesley, 1995, ISBN: 978-0-201-50397-5.

[32] M. D. Schwartz, *Quantum Field Theory and the Standard Model*. Cambridge University Press, Mar. 2014, ISBN: 978-1-107-03473-0.

[33] G. F. Sterman, *An Introduction to quantum field theory*. Cambridge University Press, Aug. 1993, ISBN: 978-0-521-31132-8.

[34] J. Collins, *Foundations of perturbative QCD*. Cambridge University Press, Nov. 2013, vol. 32, ISBN: 978-1-107-64525-7, 978-1-107-64525-7, 978-0-521-85533-4, 978-1-139-09782-6.

[35] Super-Kamiokande Collaboration, Y. Fukuda *et al.*, "Evidence for oscillation of atmospheric neutrinos," *Phys. Rev. Lett.*, vol. 81, pp. 1562–1567, 1998. DOI: 10.1103/PhysRevLett.81.1562. arXiv: hep-ex/9807003.

[36] Z. Maki, M. Nakagawa, and S. Sakata, "Remarks on the unified model of elementary particles," *Prog. Theor. Phys.*, vol. 28, pp. 870–880, 1962. DOI: 10.1143/PTP.28.870.

[37] L. D. Faddeev and V. N. Popov, "Feynman Diagrams for the Yang-Mills Field," *Phys. Lett. B*, vol. 25, J.-P. Hsu and D. Fine, Eds., pp. 29–30, 1967. DOI: 10.1016/0370-2693(67)90067-6.

[38] M. Srednicki, *Quantum field theory*. Cambridge University Press, Jan. 2007, ISBN: 978-0-521-86449-7, 978-0-511-26720-8.

[39] C. Becchi, A. Rouet, and R. Stora, "Renormalization of the Abelian Higgs-Kibble Model," *Commun. Math. Phys.*, vol. 42, pp. 127–162, 1975. DOI: 10.1007/BF01614158.

[40] I. V. Tyutin, "Gauge Invariance in Field Theory and Statistical Physics in Operator Formalism," 1975. arXiv: 0812.0580 [hep-th].

[41] A. A. Slavnov, "Ward Identities in Gauge Theories," *Theor. Math. Phys.*, vol. 10, pp. 99–107, 1972. DOI: 10.1007/BF01090719.

[42] J. C. Taylor, "Ward Identities and Charge Renormalization of the Yang-Mills Field," *Nucl. Phys. B*, vol. 33, pp. 436–444, 1971. DOI: 10.1016/0550-3213(71)90297-5.

[43] H. Lehmann, K. Symanzik, and W. Zimmermann, "Zur formulierung quantisierter feldtheorien," *Il Nuovo Cimento (1955-1965)*, vol. 1, no. 1, pp. 205–225, Jan. 1955, ISSN: 1827-6121. DOI: 10.1007/BF02731765.

[44] G. 't Hooft and M. J. G. Veltman, "Regularization and Renormalization of Gauge Fields," *Nucl. Phys. B*, vol. 44, pp. 189–213, 1972. DOI: 10.1016/0550-3213(72)90279-9.

[45] CMS Collaboration, V. Khachatryan *et al.*, "Measurement and QCD analysis of double-differential inclusive jet cross sections in pp collisions at $\sqrt{s} = 8$ TeV and cross section ratios to 2.76 and 7 TeV," *JHEP*, vol. 03, p. 156, 2017. DOI: 10.1007/JHEP03(2017)156. arXiv: 1609.05331 [hep-ex].

[46] D. J. Gross and F. Wilczek, "Ultraviolet Behavior of Nonabelian Gauge Theories," *Phys. Rev. Lett.*, vol. 30, J. C. Taylor, Ed., pp. 1343–1346, 1973. DOI: 10.1103/PhysRevLett.30.1343.

[47] W. Furmanski and R. Petronzio, "Lepton - Hadron Processes Beyond Leading Order in Quantum Chromodynamics," *Z. Phys. C*, vol. 11, p. 293, 1982. DOI: 10.1007/BF01578280.

[48] E. B. Zijlstra and W. L. van Neerven, "Order $\alpha_s^2$ QCD corrections to the deep inelastic proton structure functions F2 and F(L)," *Nucl. Phys. B*, vol. 383, pp. 525–574, 1992. DOI: 10.1016/0550-3213(92)90087-R.

[49] T. Matsuura, R. Hamberg, and W. L. van Neerven, "The Contribution of the Gluon-gluon Subprocess to the Drell-Yan *K* Factor," *Nucl. Phys. B*, vol. 345, pp. 331–368, 1990. DOI: 10.1016/0550-3213(90)90391-P.

[50] K. Long, "QCD at high-energy (experiments)," *Nucl. Phys. B Proc. Suppl.*, vol. 117, S. Bentvelsen, P. de Jong, J. Koch, and E. Laenen, Eds., pp. 242–259, 2003. DOI: 10.1016/S0920-5632(03)01421-X. arXiv: hep-ex/0212008.

[51] C. G. Callan Jr. and D. J. Gross, "High-energy electroproduction and the constitution of the electric current," *Phys. Rev. Lett.*, vol. 22, pp. 156–159, 1969. DOI: 10.1103/PhysRevLett.22.156.

[52] G. Altarelli and G. Parisi, "Asymptotic Freedom in Parton Language," *Nucl. Phys. B*, vol. 126, pp. 298–318, 1977. DOI: 10.1016/0550-3213(77)90384-4.

[53] Gudrun Heinrich, *Colourful loops: Introduction to quantum chromodynamics and loop calculations*, 2018. [Online]. Available: https://wwwth.mpp.mpg.de/members/gudrun/members_gudrun__files/teaching/SS2018/QCD.pdf.

[54] G. Falcioni, F. Herzog, S. Moch, and A. Vogt, "Four-loop splitting functions in QCD – The quark-quark case," *Phys. Lett. B*, vol. 842, p. 137 944, 2023. DOI: 10.1016/j.physletb.2023.137944. arXiv: 2302.07593 [hep-ph].

[55] G. Falcioni, F. Herzog, S. Moch, and A. Vogt, "Four-loop splitting functions in QCD – The gluon-to-quark case," *Phys. Lett. B*, vol. 846, p. 138 215, 2023. DOI: 10.1016/j.physletb.2023.138215. arXiv: 2307.04158 [hep-ph].

[56] G. Falcioni, F. Herzog, S. Moch, A. Pelloni, and A. Vogt, "Four-loop splitting functions in QCD – The quark-to-gluon case," Apr. 2024. arXiv: 2404.09701 [hep-ph].

[57] G. P. Korchemsky, "Asymptotics of the Altarelli-Parisi-Lipatov Evolution Kernels of Parton Distributions," *Mod. Phys. Lett. A*, vol. 4, pp. 1257–1276, 1989. DOI: 10.1142/S0217732389001453.

[58] Y. L. Dokshitzer, "Calculation of the Structure Functions for Deep Inelastic Scattering and $e^+e^-$ Annihilation by Perturbation Theory in Quantum Chromodynamics.," *Sov. Phys. JETP*, vol. 46, pp. 641–653, 1977.

[59] V. N. Gribov and L. N. Lipatov, "Deep inelastic e p scattering in perturbation theory," *Sov. J. Nucl. Phys.*, vol. 15, pp. 438–450, 1972.

[60] S. D. Drell and T.-M. Yan, "Massive Lepton Pair Production in Hadron-Hadron Collisions at High-Energies," *Phys. Rev. Lett.*, vol. 25, pp. 316–320, 1970, [Erratum: Phys.Rev.Lett. 25, 902 (1970)]. DOI: 10.1103/PhysRevLett.25.316.

[61] J. H. Christenson, G. S. Hicks, L. M. Lederman, P. J. Limon, B. G. Pope, and E. Zavattini, "Observation of massive muon pairs in hadron collisions," *Phys. Rev. Lett.*, vol. 25, pp. 1523–1526, 1970. DOI: 10.1103/PhysRevLett.25.1523.

[62] C. Duhr and B. Mistlberger, "Lepton-pair production at hadron colliders at $N^3LO$ in QCD," *JHEP*, vol. 03, p. 116, 2022. DOI: 10.1007/JHEP03(2022)116. arXiv: 2111.10379 [hep-ph].

[63] B. Chargeishvili, "Perturbative QCD corrections for $t\bar{t}$+jet production," M.S. thesis, Universität Hamburg, Hamburg, 2021.

[64] G. Altarelli, R. K. Ellis, and G. Martinelli, "Large Perturbative Corrections to the Drell-Yan Process in QCD," *Nucl. Phys. B*, vol. 157, pp. 461–497, 1979. DOI: 10.1016/0550-3213(79)90116-0.

[65] J. Kuipers, T. Ueda, J. A. M. Vermaseren, and J. Vollinga, "FORM version 4.0," *Comput. Phys. Commun.*, vol. 184, pp. 1453–1467, 2013. DOI: 10.1016/j.cpc.2012.12.028. arXiv: 1203.6543 [cs.SC].

[66] T. Kinoshita, "Mass singularities of Feynman amplitudes," *J. Math. Phys.*, vol. 3, pp. 650–677, 1962. DOI: 10.1063/1.1724268.

[67] T. D. Lee and M. Nauenberg, "Degenerate Systems and Mass Singularities," *Phys. Rev.*, vol. 133, G. Feinberg, Ed., B1549–B1562, 1964. DOI: 10.1103/PhysRev.133.B1549.

[68] CTEQ Collaboration, R. Brock *et al.*, "Handbook of perturbative QCD: Version 1.0," *Rev. Mod. Phys.*, vol. 67, pp. 157–248, 1995. DOI: 10.1103/RevModPhys.67.157.

[69] S. Catani, "The Singular behavior of QCD amplitudes at two loop order," *Phys. Lett. B*, vol. 427, pp. 161–171, 1998. DOI: 10.1016/S0370-2693(98)00332-3. arXiv: hep-ph/9802439.

[70] S. Catani and M. Grazzini, "Infrared factorization of tree level QCD amplitudes at the next-to-next-to-leading order and beyond," *Nucl. Phys. B*, vol. 570, pp. 287–325, 2000. DOI: 10.1016/S0550-3213(99)00778-6. arXiv: hep-ph/9908523.

[71] B. Ruijl, T. Ueda, and J. Vermaseren, "FORM version 4.2," Jul. 2017. arXiv: 1707.06453 [hep-ph].

[72] M. Tentyukov and J. A. M. Vermaseren, "The Multithreaded version of FORM," *Comput. Phys. Commun.*, vol. 181, pp. 1419–1427, 2010. DOI: 10.1016/j.cpc.2010.04.009. arXiv: hep-ph/0702279.

[73] J. A. M. Vermaseren, "Harmonic sums, Mellin transforms and integrals," *Int. J. Mod. Phys. A*, vol. 14, pp. 2037–2076, 1999. DOI: 10.1142/S0217751X99001032. arXiv: hep-ph/9806280.

[74] S. Moch and P. Uwer, "XSummer: Transcendental functions and symbolic summation in form," *Comput. Phys. Commun.*, vol. 174, pp. 759–770, 2006. DOI: 10.1016/j.cpc.2005.12.014. arXiv: math-ph/0508008.

[75] T. Huber and D. Maitre, "HypExp: A Mathematica package for expanding hypergeometric functions around integer-valued parameters," *Comput. Phys. Commun.*, vol. 175, pp. 122–144, 2006. DOI: 10.1016/j.cpc.2006.01.007. arXiv: hep-ph/0507094.

[76] G. Bevilacqua, *Private work*, Private communications, 2020-2024.

[77] E. Gardi and L. Magnea, "Factorization constraints for soft anomalous dimensions in QCD scattering amplitudes," *JHEP*, vol. 03, p. 079, 2009. DOI: 10.1088/1126-6708/2009/03/079. arXiv: 0901.1091 [hep-ph].

[78] T. Becher, A. Broggio, and A. Ferroglia, *Introduction to Soft-Collinear Effective Theory*. Springer, 2015, vol. 896. DOI: 10.1007/978-3-319-14848-9. arXiv: 1410.1892 [hep-ph].

[79] T. Becher and M. Neubert, "On the Structure of Infrared Singularities of Gauge-Theory Amplitudes," *JHEP*, vol. 06, p. 081, 2009, [Erratum: JHEP 11, 024 (2013)]. DOI: 10.1088/1126-6708/2009/06/081. arXiv: 0903.1126 [hep-ph].

[80] L. W. Garland, T. Gehrmann, E. W. N. Glover, A. Koukoutsakis, and E. Remiddi, "The Two loop QCD matrix element for e+ e- —> 3 jets," *Nucl. Phys. B*, vol. 627, pp. 107–188, 2002. DOI: 10.1016/S0550-3213(02)00057-3. arXiv: hep-ph/0112081.

[81] B. Chargeishvili, M. V. Garzelli, and S. Moch, "One-loop soft anomalous dimension matrices for $t\bar{t}j$ hadroproduction," Jun. 2022. arXiv: 2206.10977 [hep-ph].

[82] P. Cvitanovic, "Group theory for Feynman diagrams in non-Abelian gauge theories," *Phys. Rev. D*, vol. 14, pp. 1536–1553, 1976. DOI: 10.1103/PhysRevD.14.1536.

[83] M. L. Mangano, "The Color Structure of Gluon Emission," *Nucl. Phys. B*, vol. 309, pp. 461–475, 1988. DOI: 10.1016/0550-3213(88)90453-1.

[84] F. Maltoni, K. Paul, T. Stelzer, and S. Willenbrock, "Color Flow Decomposition of QCD Amplitudes," *Phys. Rev. D*, vol. 67, p. 014026, 2003. DOI: 10.1103/PhysRevD.67.014026. arXiv: hep-ph/0209271.

[85] M. Sjodahl, "ColorFull – a C++ library for calculations in SU($N_c$) color space," *Eur. Phys. J. C*, vol. 75, no. 5, p. 236, 2015. DOI: 10.1140/epjc/s10052-015-3417-6. arXiv: 1412.3967 [hep-ph].

[86] J. Alwall *et al.*, "The automated computation of tree-level and next-to-leading order differential cross sections, and their matching to parton shower simulations," *JHEP*, vol. 07, p. 079, 2014. DOI: 10.1007/JHEP07(2014)079. arXiv: 1405.0301 [hep-ph].

[87] A. J. MacFarlane, A. Sudbery, and P. H. Weisz, "On Gell-Mann's lambda-matrices, $d$- and $f$-tensors, octets, and parametrizations of SU(3)," *Commun. Math. Phys.*, vol. 11, pp. 77–90, 1968. DOI: 10.1007/BF01654302.

[88] P. Cvitanovic, *Group Theory: Birdtracks, Lie's, and Exceptional Groups*. Princeton University Press, May 2020, ISBN: 978-0-691-20298-3.

[89] Y. L. Dokshitzer and G. Marchesini, "Soft gluons at large angles in hadron collisions," *JHEP*, vol. 01, p. 007, 2006. DOI: 10.1088/1126-6708/2006/01/007. arXiv: hep-ph/0509078.

[90] S. Keppeler and M. Sjodahl, "Orthogonal multiplet bases in SU(Nc) color space," *JHEP*, vol. 09, p. 124, 2012. DOI: 10.1007/JHEP09(2012)124. arXiv: 1207.0609 [hep-ph].

[91] S. Keppeler, S. Plätzer, and M. Sjodahl, "Wigner 6j symbols with gluon lines: completing the set of 6j symbols required for color decomposition," Dec. 2023. arXiv: 2312.16688 [hep-ph].

[92] Particle Data Group Collaboration, R. L. Workman *et al.*, "Review of Particle Physics," *PTEP*, vol. 2022, p. 083C01, 2022. DOI: 10.1093/ptep/ptac097.

[93] R. Feger, T. W. Kephart, and R. J. Saskowski, "LieART 2.0 – A Mathematica application for Lie Algebras and Representation Theory," *Comput. Phys. Commun.*, vol. 257, p. 107 490, 2020. DOI: 10.1016/j.cpc.2020.107490. arXiv: 1912.10969 [hep-th].

[94] T. Nutma, "xTras : A field-theory inspired xAct package for mathematica," *Comput. Phys. Commun.*, vol. 185, pp. 1719–1738, 2014. DOI: 10.1016/j.cpc.2014.02.006. arXiv: 1308.3493 [cs.SC].

[95] L. de Moura and N. Bjørner, "Z3: An efficient SMT solver," in *Tools and Algorithms for the Construction and Analysis of Systems*, C. R. Ramakrishnan and J. Rehof, Eds., Berlin, Heidelberg: Springer Berlin Heidelberg, 2008, pp. 337–340, ISBN: 978-3-540-78800-3.

[96] J. Marques-Silva and K. Sakallah, "GRASP: A search algorithm for propositional satisfiability," *IEEE Transactions on Computers*, vol. 48, no. 5, pp. 506–521, 1999. DOI: 10.1109/12.769433.

[97] M. Davis and H. Putnam, "A computing procedure for quantification theory," *J. ACM*, vol. 7, no. 3, pp. 201–215, Jul. 1960, ISSN: 0004-5411. DOI: 10.1145/321033.321034.

[98] M. Davis, G. Logemann, and D. Loveland, "A machine program for theorem-proving," *Commun. ACM*, vol. 5, no. 7, pp. 394–397, Jul. 1962, ISSN: 0001-0782. DOI: 10.1145/368273.368557.

[99] G. B. Dantzig, "Programming in a linear structure," *Econometrica: Journal of the Econometric Society*, vol. 17, pp. 73–74, 1949. DOI: 10.2307/1907526.

[100] G. Nelson and D. C. Oppen, "Congruence closure," *Journal of the ACM (JACM)*, vol. 27, no. 2, pp. 356–364, 1980. DOI: 10.1145/322186.322198.

[101] J. Fourier, "The elimination form of the covariational criterion and allied topics in the calculus of variations," in *Trans. Amer. Math. Soc*, vol. 3, 1902, pp. 439–469. DOI: 10.1090/S0002-9904-1902-00888-X.

[102] L. de Moura and N. Bjørner, "E-matching for SMT solving," in *International Workshop on Satisfiability Modulo Theories*, Springer, 2007, pp. 37–48. DOI: 10.1007/978-3-540-72788-0_4.

[103] G. Nelson and D. C. Oppen, "Fast decision procedures based on congruence closure," *Journal of the ACM (JACM)*, vol. 27, no. 2, pp. 356–364, 1980. DOI: 10.1145/322186.322198.

[104] N. Bjørner, L. de Moura, L. Nachmanson, and C. M. Wintersteiger, "Programming z3," in *Engineering Trustworthy Software Systems: 4th International School, SETSS 2018, Chongqing, China, April 7–12, 2018, Tutorial Lectures*, J. P. Bowen, Z. Liu, and Z. Zhang, Eds. Cham: Springer International Publishing, 2019, pp. 148–201, ISBN: 978-3-030-17601-3. DOI: 10.1007/978-3-030-17601-3_4.

[105] E. Gabriel *et al.*, "Open MPI: Goals, Concept, and Design of a Next Generation MPI Implementation," in *Proceedings, 11th European PVM/MPI Users' Group Meeting*, Budapest, Hungary, Sep. 2004, pp. 97–104.

[106] L. Dalcín, R. Paz, and M. Storti, "MPI for Python," *Journal of Parallel and Distributed Computing*, vol. 65, no. 9, pp. 1108–1115, 2005, ISSN: 0743-7315. DOI: 10.1016/j.jpdc.2005.03.010.

[107] L. Dalcin and Y.-L. L. Fang, "Mpi4py: Status update after 12 years of development," *Computing in Science & Engineering*, vol. 23, no. 4, pp. 47–54, 2021. DOI: 10.1109/MCSE.2021.3083216.

[108] *z3-solver - an efficient SMT solver library*, https://pypi.org/project/z3-solver.

[109] *Open MPI - A High Performance Message Passing Library*, https://www.open-mpi.org.

[110] *mpi4py - Python bindings for MPI*, https://pypi.org/project/mpi4py.

[111] G. P. Lepage, "Adaptive multidimensional integration: VEGAS enhanced," *J. Comput. Phys.*, vol. 439, p. 110 386, 2021. DOI: 10.1016/j.jcp.2021.110386. arXiv: 2009.05112 [physics.comp-ph].

[112] R. E. Caflisch, *Monte Carlo and quasi-Monte Carlo methods*. Cambridge University Press, 1998, vol. 7, pp. 1–49. DOI: 10.1017/S0962492900002804.

[113] D. P. Kroese, T. Taimre, and Z. I. Botev, *Handbook of Monte Carlo methods*. John Wiley & Sons, 2011. DOI: 10.1002/9781118014967.

[114] C. Lemieux, *Monte Carlo and Quasi-Monte Carlo sampling*. Springer Science & Business Media, 2009. DOI: 10.1007/978-0-387-78165-5.

[115] J. S. Liu, *Monte Carlo strategies in scientific computing*. Springer Science & Business Media, 2008. DOI: 10.1007/978-0-387-76371-2.

[116] H. Niederreiter, *Random number generation and quasi-Monte Carlo methods*. SIAM, 1992. DOI: 10.1137/1.9781611970081.

[117] W. H. Press, S. A. Teukolsky, W. T. Vetterling, and B. P. Flannery, *Numerical recipes 3rd edition: The art of scientific computing*. Cambridge University Press, 2007.

[118] C. P. Robert and G. Casella, *Monte Carlo statistical methods*. Springer Science & Business Media, 2004. DOI: 10.1007/978-1-4757-4145-2.

[119] R. Y. Rubinstein and D. P. Kroese, *Simulation and the Monte Carlo method*, 3rd. John Wiley & Sons, 2016. DOI: 10.1002/9781118631972.

[120] G. P. Lepage, "A New Algorithm for Adaptive Multidimensional Integration," *J. Comput. Phys.*, vol. 27, p. 192, 1978. DOI: 10.1016/0021-9991(78)90004-9.

[121] A. Kardos, *Private work*, Private communications, 2020-2024.

[122] W. G. Horner, "XXI. a new method of solving numerical equations of all orders, by continuous approximation," *Philosophical Transactions of the Royal Society of London*, pp. 308–335, [Online]. Available: https://api.semanticscholar.org/CorpusID:186210512.

[123] J. Kuipers, T. Ueda, and J. A. M. Vermaseren, "Code Optimization in FORM," *Comput. Phys. Commun.*, vol. 189, pp. 1–19, 2015. DOI: 10.1016/j.cpc.2014.08.008. arXiv: 1310.7007 [cs.SC].

[124] J. Vermaseren, J. Kulpers, and T. Ueada, "Compactifying formulas with FORM," *PoS*, vol. RADCOR2013, p. 015, 2013. DOI: 10.22323/1.197.0015.

[125] S. K. Park and K. W. Miller, "Random number generators: Good ones are hard to find," *Communications of the ACM*, vol. 31, no. 10, pp. 1192–1201, 1988. DOI: 10.1145/63039.63042.

[126] D. P. Barber *et al.*, "Discovery of Three Jet Events and a Test of Quantum Chromodynamics at PETRA Energies," *Phys. Rev. Lett.*, vol. 43, p. 830, 1979. DOI: 10.1103/PhysRevLett.43.830.

[127] ALEPH Collaboration, A. Heister *et al.*, "Studies of QCD at e+ e- centre-of-mass energies between 91-GeV and 209-GeV," *Eur. Phys. J. C*, vol. 35, pp. 457–486, 2004. DOI: 10.1140/epjc/s2004-01891-4.

[128] OPAL Collaboration, G. Abbiendi *et al.*, "Measurement of event shape distributions and moments in e+ e- —> hadrons at 91-GeV - 209-GeV and a determination of alpha(s)," *Eur. Phys. J. C*, vol. 40, pp. 287–316, 2005. DOI: 10.1140/epjc/s2005-02120-6. arXiv: hep-ex/0503051.

[129] J. M. Butterworth, J. R. Forshaw, and M. H. Seymour, "Multiparton interactions in photoproduction at HERA," *Z. Phys. C*, vol. 72, pp. 637–646, 1996. DOI: 10.1007/s002880050286. arXiv: hep-ph/9601371.

[130] S. Weinzierl, "Event shapes and jet rates in electron-positron annihilation at NNLO," *JHEP*, vol. 06, p. 041, 2009. DOI: 10.1088/1126-6708/2009/06/041. arXiv: 0904.1077 [hep-ph].

[131] A. Gehrmann-De Ridder, T. Gehrmann, E. W. N. Glover, and G. Heinrich, "NNLO corrections to event shapes in e+ e- annihilation," *JHEP*, vol. 12, p. 094, 2007. DOI: 10.1088/1126-6708/2007/12/094. arXiv: 0711.4711 [hep-ph].

[132] V. Del Duca *et al.*, "Jet production in the CoLoRFulNNLO method: event shapes in electron-positron collisions," *Phys. Rev. D*, vol. 94, no. 7, p. 074 019, 2016. DOI: 10.1103/PhysRevD.94.074019. arXiv: 1606.03453 [hep-ph].

[133] V. Del Duca, C. Duhr, A. Kardos, G. Somogyi, and Z. Trócsányi, "Three-Jet Production in Electron-Positron Collisions at Next-to-Next-to-Leading Order Accuracy," *Phys. Rev. Lett.*, vol. 117, no. 15, p. 152 004, 2016. DOI: 10.1103/PhysRevLett.117.152004. arXiv: 1603.08927 [hep-ph].

[134] N. K. Falck, D. Graudenz, and G. Kramer, "Cross-section for Five Jet Production in $e^+e^-$ Annihilation," *Nucl. Phys. B*, vol. 328, pp. 317–341, 1989. DOI: 10.1016/0550-3213(89)90331-3.

[135] K. Hagiwara and D. Zeppenfeld, "Amplitudes for Multiparton Processes Involving a Current at e+ e-, e+- p, and Hadron Colliders," *Nucl. Phys. B*, vol. 313, pp. 560–594, 1989. DOI: 10.1016/0550-3213(89)90397-0.

[136] F. A. Berends, W. T. Giele, and H. Kuijf, "Exact Expressions for Processes Involving a Vector Boson and Up to Five Partons," *Nucl. Phys. B*, vol. 321, pp. 39–82, 1989. DOI: 10.1016/0550-3213(89)90242-3.

[137] Z. Bern, L. J. Dixon, and D. A. Kosower, "One loop corrections to five gluon amplitudes," *Phys. Rev. Lett.*, vol. 70, pp. 2677–2680, 1993. DOI: 10.1103/PhysRevLett.70.2677. arXiv: hep-ph/9302280.

[138] D. H. Bailey, *The MP portable multiprecision transcendental function library*, Software library available at https://www.davidhbailey.com/dhbsoftware/, The latest version of this software is mpfun20, released on 2020-03-26, 2020.

[139] N. J. Higham, *Accuracy and Stability of Numerical Algorithms*. Society for Industrial and Applied Mathematics, 2002. DOI: 10.1137/1.9780898718027.

[140] D. Goldberg, "What every computer scientist should know about floating-point arithmetic," *ACM Computing Surveys*, vol. 23, no. 1, pp. 5–48, 1991. DOI: 10.1145/103162.103163.

[141] A. Kardos, A. Larkoski, and Z. Trócsányi, "Soft-Dropped Observables with CoLoRFuLNNLO," *Acta Phys. Polon. B*, vol. 50, pp. 1891–1899, 2019. DOI: 10.5506/APhysPolB.50.1891.

[142] S. Moch, *Private work*, Private communications, 2020-2024.

[143] I. S. Gradshteyn and I. M. Ryzhik, *Table of Integrals, Series, and Products*. 1943, ISBN: 978-0-12-294757-5, 978-0-12-294757-5.

# *Acknowledgements*

I would like to express my sincere gratitude to Sven-Olaf Moch for the valuable opportunity to collaborate with him. His professionalism and expertise were truly remarkable, and I am grateful for the chance to learn from an accomplished scientist like him. Working with him was not only a privilege but also a thoroughly enjoyable experience, as he combined his professional excellence with a welcoming and personable manner.

I extend my sincere gratitude to the group of people with whom I had the pleasure of collaborating on this project. In particular, I thank to Giuseppe Bevilacqua, our thorough examination of each step in our calculations was not only enjoyable, but also highly productive.

I am deeply grateful to Adam Kardos for his exceptional expertise in this field, which proved to be immensely helpful and motivating throughout our collaboration. Furthermore, I would like to express my appreciation for his warm hospitality during my visits to Hungary, which made my stays truly memorable.

I wish to thank Zoltán Trócsányi for his encouragement and for generously sharing his expertise, which played an important role in bringing this project to its current state.

My gratitude also goes to Maria Vittoria Garzelli for the many insightful discussions we had throughout my doctoral career.

I am grateful to the secretary of our institute, Elizabeth Monteiro Duarte, for her professionalism and for creating a pleasant working environment.

My appreciation goes to Martin Stieben from PHYSnet for his readiness to help and for accommodating my special requests regarding the computing infrastructure.

I am thankful to my inspirational friends and colleagues, Sergey Alekhin, Mrigankamauli Chakraborty, Levente Fekésházy, Marco Klann, Vitaly Magerya, Alexander Manashov, Oliver Schnetz, Leonid Shumilov, Sam Van Thurenhout, Oleksandr Zenaiev, whose support and intellectual stimulation were valuable assets during this endeavor.

Finally, I would like to express my profound gratitude to my parents and sister for their love, support, and encouragement, which have helped me reach this point. They have always been a constant source of strength and motivation.

# Eidesstattliche Versicherung

Hiermit versichere ich an Eides statt, die vorliegende Dissertationsschrift selbst verfasst und keine anderen als die angegebenen Hilfsmittel und Quellen benutzt zu haben.

Ort, Datum: Hamburg, 23.05.2024

Unterschrift: B. Chargeishcili